UNIVERSITY OF CALIFORNIA, SAN DIEGO

Robust source localization using the generalized array invariant and a vertical array

A dissertation submitted in partial satisfaction of the
requirements for the degree
Doctor of Philosophy

in

Oceanography

by

Chomgun Cho

Committee in charge:

Hee Chun Song, Chair
William S. Hodgkiss, Co-Chair
William A. Coles
Leroy M. Dorman
William A. Kuperman
Aaron M. Thode

2017

The dissertation of Chomgun Cho is approved, and it is acceptable in quality and form for publication on microfilm and electronically:

_____

_____

_____

_____

_____
Co-Chair

_____
Chair

University of California, San Diego

2017

DEDICATION

To my lovely family–my wife, Sunhyung; my daughter, Youngeun; my son, Junho–for their love, care, support, and encouragement.

TABLE OF CONTENTS

LIST OF FIGURES

LIST OF TABLES

ACKNOWLEDGEMENTS

I would like to express my deepest gratitude to my committee chair Dr. Hee Chun Song, who has always passionate to his research, encouraging and supporting my research during my PhD period. Therefore, I always count on him. Without his help, this dissertation would not have been come into the world. I am grateful for Professor William S. Hodgkiss, who is very cheerful and happy, spreading his happiness and giving me the insight of signal processing: specifically, beamforming. I am also thankful to my dissertation committee members Professors William A. Kuperman, William A. Coles, Leroy M. Dorman, and Dr. Aaron M. Thode for giving me constructive feedback and invaluable comments to improve my dissertation.

This PhD work is supported by Agency for Defense Development (ADD) in South Korea and the office of Naval Research Grant No. N00014-13-1-0510, so I would like to express my profound thanks for their financial support.

Also, I would like to thank everyone at Marine Physical Laboratory (MPL) in friendly atmosphere that everyone is willing to help each other.

Last but not least, my family: My wife, Sunhyung Kim; my daughter, Youngeun Cho; my son, Junho Cho. They are always encouraging and supporting me with all their heart.

This dissertation is a collection of papers that were published in the Journal of Acoustical Society of Americas. Chapter 2, in full, is a reprint of the material as it appears in the Journal of Acoustical Society of Americas: H.C. Song and Chomgun Cho, "The relation between the waveguide invariant and array invariant," *J. Acoust. Soc. Am*, 138 (2), 899-903, 2015. The dissertation author was a primary investigator and author of this material.

Chapter 3, in full, is a reprint of the material as it appears in the Journal of Acoustical Society of Americas: Chomgun Cho, H.C. Song, and W. S. Hodgkiss, "Robust source-range estimation using the array/waveguide invariant and a vertical array," *J. Acoust. Soc. Am*, 139 (1), 63-69, 2016. The dissertation author was a primary investigator and author of this material.

Chapter 4, in full, is a reprint of the material as it appears in the Journal of

Acoustical Society of Americas: Chomgun Cho and H.C. Song, P. Hursky, and S. M. Jesus, "Iterative range estimation in a sloping-bottom shallow-water waveguide using the generalized array invariant," *J. Acoust. Soc. Am*, 142 (1), 55-60, 2017. The dissertation author was a primary investigator and author of this material.

Chapter 5, in full, is a reprint of the material as it appears in the Journal of Acoustical Society of Americas: H.C. Song and Chomgun Cho, "Array invariant-based source localization in shallow water using a sparse vertical array," *J. Acoust. Soc. Am*, 141 (1), 183-188, 2017. The dissertation author was a primary investigator and author of this material.

Chapter 6, in full, is a reprint of the material as it appears in the Journal of Acoustical Society of Americas: Chomgun Cho and H.C. Song, "Impact of array tilt on source-range estimation in shallow water using the array invariant," *J. Acoust. Soc. Am*, 141 (4), 2849-2856, 2017. The dissertation author was a primary investigator and author of this material.

VITA

1999	B. S. in Electronic Engineering, Yonsei University, Seoul, South Korea
2001	M. S. in Electrical and Electronic Engineering, Yonsei University, Seoul, South Korea
2017	Ph. D. in Oceanography, University of California, San Diego, La Jolla, California
2001-2006	Researcher, Agency for Defense Development, South Korea
2007-Present	Senior researcher, Agency for Defense Development, South Korea

PUBLICATIONS

C. Cho, H.C. Song, P. Hursky, and S. M. Jesus, "Iterative range estimation in a sloping-bottom shallow-water waveguide using the generalized array invariant," *J. Acoust. Soc. Am.*, 142 (1), pp. 55-60, 2017.

C. Cho and H.C. Song, "Impact of array tilt on source-range estimation in shallow water using the array invariant," *J. Acoust. Soc. Am.*, 141 (4), pp. 2849-2856, 2017.

C. Cho, H.C. Song, and W. S. Hodgkiss, "Robust source-range estimation using the array/waveguide invariant and a vertical array," *J. Acoust. Soc. Am.*, 139 (1), pp. 63-69, 2016.

C. Cho, S. Nam, and H.C. Song, "Seasonal variation of speed and width from kinematic parameters of mode-1 nonlinear internal waves in the northeastern East China Sea," *J. Geophys. Res. Oceans*, 121, pp. 5942-5958, 2016.

H.C. Song, C. Cho, G. Byun, and J.S. Kim, "Cascade of blind deconvolution and array invariant for robust source-range estimation (L)," *J. Acoust. Soc. Am.*, 141 (5), pp. 3270-3273, 2017.

H.C. Song and C. Cho, "Array invariant-based source localization in shallow water using a sparse vertical array," *J. Acoust. Soc. Am.*, 141 (1), pp. 183-188, 2017.

H.C. Song and C. Cho, "The relation between the waveguide invariant and array invariant," *J. Acoust. Soc. Am.*, 138 (2), pp. 899-903, 2015.

ABSTRACT OF THE DISSERTATION

Robust source localization using the generalized array invariant and a vertical array

by

Chomgun Cho

Doctor of Philosophy in Oceanography

University of California, San Diego, 2017

Hee Chun Song, Chair
William S. Hodgkiss, Co-Chair

The array invariant approach for passive localization utilizes multiple arrivals separated in beam angle and travel time via conventional plane-wave beamforming using either a horizontal or vertical array in shallow-water. Since this approach does not require precise knowledge of the environment and an acoustic propagation model, it is robust to environmental fluctuations. In addition, the approach is essentially equivalent to the waveguide invariant β based on the dispersion relationship between the group and phase speeds when $\beta = 1$, a generic value in ideal waveguides. However, the array invariant can be applicable to many shallow-water environments where the surface-bottom reflected arrivals behave similarly

to those in ideal waveguides, simply using $\beta = 1$. By incorporating the waveguide invariant, the array invariant can be extended to general waveguides, referred to as generalized array invariant that is fully supported by the waveguide invariant physics. This dissertation presents the relationship between the waveguide invariant and array invariant, demonstrations with several experimental data using the generalized array invariant with a short- or long-aperture vertical array, and an impact of array tilt on the array invariant-based source-range estimation.

- HF97 (High Frequency 1997) experiment: Demonstration of the robustness of source-range estimation using a 12-m vertical array for a source (2–3 kHz) at 6-km range in ∼100-m deep water in a fluctuating ocean environment over a day.

- RADAR07 (Random Array of Drifting Acoustic Receivers 2007) experiment: Range-dependent environment with a sloping bottom using a 2.8-m vertical array for a moving source (2–3.5 kHz) between 0.5 and 5 km in range with the water depth varying from 80 to 50 m.

- SAVEX15 (Shallow-water Acoustic Variability EXperiment 2015) experiment: Range-independent environment using a large-aperture (about 56 m) sparse vertical array for a moving source (0.5–2 kHz) between 1.5 and 3.5 km in range in ∼100-m deep water.

- KAM11 (The Kauai Acomms MURI 2011) experiment: Impact of array tilt on source range using a 1.2-m vertical array for a moored source (7–19 kHz) at 3-km range in ∼100-m deep water.

Chapter 1

Introduction

For more than four decades, vertical line arrays have played key roles such as acoustic source localization, detection, noise measuring, and passive fathometer to exploit the ocean through sound. One important key role is the acoustic source localization for military and civilian applications to track marine mammals or objects in underwater for analysis of their behaviors, and well-known localization techniques are matched-field processing (MFP) [1–4], waveguide invariant (WI) [4, 5], and array invariant (AI) [6–8, 11].

The MFP first introduced by Bucker [1] has been remarkable interests and extensively studied for passive source localization in ocean waveguide using a vertical array. The MFP can be considered the generalized plane-wave beamforming and requires an acoustic propagation model to generate the replicas, i.e., steering vectors from the solution of the wave equation in the ocean environment [3]. After correlating them with the data from a receiver array, this processing finds the highest correlation in all possible source locations. This computationally intensive array processing requires accurate knowledge of the acoustic propagation environment in order to exploit the unique spatial field structure of signals propagating in an ocean waveguide. Subsequent studies [2–4] showed that the MFP performs well and provides the range and depth for low frequency (e.g. < 1 kHz). For broadband signals, this approach can be utilized by either coherently or incoherently averaging over the frequency band. However, the MFP is very sensitive to mismatch in the propagation environments (sound speeds, bottom density and attenuation, etc)

and/or receiver array geometry such as array tilt and position. Recently, in order to mitigate environmental mismatch for the high frequency, a nonlinear signal processing technique called frequency difference MFP (FDMFP) [12] was developed for a broadband source localization; however, this FDMFP is also computationally intensive.

The waveguide invariant introduced by Chuprov and described by β is the fundamental descriptor of acoustic wave propagations in ocean waveguide, which characterizes the interference structure observed in the range-frequency plane and this structure that relates group speed to phase speed (equivalently group and phase slowness) [4, 5]. The isovelocity waveguide has a canonical value of $\beta = 1$, which is also applicable to many shallow water environments. However, for an arbitrary sound speed profile, the propagating modes can be divided into distinct groups of modes that behave similarly, and each group can have a different value of β. Waveguide invariant β also can be range-dependent if the waveguide has a range-dependent bathymetry and sound speed [13, 14] and internal waves [15]. Waveguide invariant theory has been utilized for various applications in the ocean: Time-reversal focusing [16, 17], sonar array processing [18], and source localization [19–23]. For source localization, Thode et al. demonstrated that the Bartlett MFP sidelobe interference structures converge to the source range in the range-frequency plane where the source is fixed [19]. Moreover, Sostrand [21] showed that an impulsive source is localized at 10 to 115 km range using the end-fire of a bottom-mounted horizontal array and waveguide invariant. Also, Cockrell and Schmidt [23] reported that a range estimate accuracy is approximately 25% up to around 2 km from a fixed source to a moving underwater vehicle using waveguide invariant.

Array invariant (AI) proposed by Lee and Makris [6] and denoted by χ utilizes multiple arrivals separated in beam angle and travel time for instantaneous source-range estimation via conventional plane-wave beamforming for either a horizontal or vertical array in a horizontally stratified ocean waveguide. This method was demonstrated using both simulations and data for source range estimation in shallow water using a towed horizontal array, providing a reasonable source-range

estimate with little computational effort and the full array gain. Furthermore, no environmental knowledge is required except that the received field should not be dominated by waterborne propagation. Although this approach was based on the relationship between the group speed and phase speed, the authors claimed that the AI is different from the waveguide invariant because this approach does not rely on model interference. However, this dissertation will show the relationship between the two invariants in Chapter 2.

The remainder of this dissertation is organized as follows.

Chapter 2 derives the relation between the waveguide invariant and array invariant for a horizontal and vertical array [7]. After examining the relationship, two examples are illustrated as two typical acoustic environments with opposite signs of β: ideal waveguide ($\beta \approx +1$) and n^2-linear waveguide ($\beta \approx -3$).

Chapter 3 demonstrates robust source-range estimation using a vertical array in shallow water [8]. The High Frequency 1997 (HF97) experiment data was analyzed to show that the array invariant using a 12-m long vertical array robustly estimates a range for a broadband source (2–3 kHz) at 6-km range in $\sim$ 100-m deep water in a fluctuating ocean environment over a one-day period.

Chapter 4 derives iterative range estimation for a moving source in a sloping-bottom shallow-water waveguide using the generalized array invariant [9]. This chapter demonstrates the iterative source-range estimation in range-dependent bathymetry where the Random Array of Drifting Acoustic Receivers 2007 (RADAR 07) experiment was performed. The receiver array with a 2.8-m long deployed at 70-m depth captured a broadband source (2–3.5 kHz) about 6-m depth towed at a speed of about 3 knots (1.4 m/s) between 0.5 to 5 km in range with the corresponding water depth constantly decreasing 80 and 50 m along a sloping environment.

Chapter 5 demonstrates array-invariant-based source localization in shallow water using a sparse vertical array [10]. To do this, the Shallow-water Acoustic Variability EXperiment (SAVEX15) data was analyzed using a sparse 56-m long vertical array (16-element) in approximately 100-m deep shallow water. A broadband source (0.5–2 kHz) was at various ranges (1.5–3.5 km) from the vertical array. This chapter shows the array invariant approach can be applied to a long sparse

vertical array in range-independent environments where the sound speed variation across the array was 12 m/s.

Chapter 6 presents impact of array tilt on source-range estimation using a vertical array in shallow water [11]. To do this, theoretical analysis, simulated data analysis, and the experimental data analysis were conducted using a 1.2-m vertical array in ∼100-m deep water. The experimental data was acquired from Kauai Acomms MURI 2011 (KAM11) experiment, where both a high-frequency broadband (7–19 kHz) source and a vertical array were deployed at about 15-m deep near surface.

Lastly, this dissertation presents conclusions and suggests future work.

Bibliography

[1] H. P. Bucker, "Use of calculated sound fields and matched-field detection to locate sound sources in shallow water," J. Acoust.Soc. Am. **59**, 368–373 (1976).

[2] A. Tolstoy, *Matched field processing for underwater acoustics* (World Scientific Publishing Co.) (1993), Chap. 2.

[3] A. B. Baggeroer, W. A. Kuperman, and P. N. Mikhalevsky, "An overview of matched field methods in ocean acoustics," IEEE J. Oceanic Eng. **18**, 401–424 (1993).

[4] F. B. Jensen, W. A. Kuperman, M. B. Porter, and H. Schmidt, *Computational Ocean Acoustics* (Springer, New York) (2011), Chs. 2 and 10.

[5] S. D. Chuprov, "Interference structure of a sound field in a layered ocean", in *Acoustics of the Ocean*, 71–91 (Nauka, Moscow) (1982), edited by L. M. Breakhovskikh and I. B. Andreevoi.

[6] S. Lee and N. C. Makris, "The array invariant", J. Acoust. Soc. Am. **119**, 336–351 (2006).

[7] H. C. Song and C. Cho, "The relation between the waveguide invariant and array invariant (L)," J. Acoust. Soc. Am. **138**, 899–903 (2015).

[8] C. Cho, H. C. Song, and W. S. Hodgkiss, "Robust source-range estimation using the array/waveguide invariant and a vertical array", J. Acoust. Soc. Am. **139**, 63–69 (2016).

[9] C. Cho, H. C. Song, P. Hursky, and S. M. Jesus, "Iterative range estimation in a sloping-bottom shallow-water waveguide using the generalized array invariant," J. Acoust. Soc. Am. **142**, 55–60 (2017).

[10] H. C. Song and C. Cho, "Array invariant-based source localization in shallow water using a sparse vertical array," J. Acoust. Soc. Am. **141**, 183–188 (2017).

[11] C. Cho and H. C. Song, "Impact of array tilt on source-range estimation in shallow water using the array invariant," J. Acoust. Soc. Am. **141**, 2849–2856 (2017).

[12] B. M. Worthmann, H. C. Song, and D. R. Dowling, "High frequency source localization in a shallow ocean sound channel using frequency difference matched field processing," J. Acoust. Soc. Am. **138**, 3549–3562 (2015).

[13] S. V. Burenkov, "Distinctive features of the interference structure of sound field in a two-dimensionally inhomogeneous waveguide", Sov. Phys. Acoust. **35**, 465–467 (1989).

[14] G. L. D'Spain and W. A. Kuperman, "Application of waveguide invariants to analysis of spectrograms from shallow water environments that vary in range and azimuth", J. Acoust.Soc. Am. **106**, 2454–2468 (1999).

[15] D. Rouseff and R. C. Spindel, "Modeling the waveguide invariant as a distribution", Ocean Acoustic Interference Phenomena and Signal Processing **621**, 137–150 (2002).

[16] H. C. Song, W. A. Kuperman, and W. S. Hodgkiss, "A time-reversal mirror with variable range focusing", J. Acoust. Soc. Am. **103**, 3234–3240 (1998).

[17] S. Kim, W. A. Kuperman, W. S. Hodgkiss, H. C. Song, G. F. Edelmann, and T. Akal, "Robust time reversal focusing in the ocean", J. Acoust. Soc. Am. **114**, 145–157 (2003).

[18] H. Tao and J. L. Krolik, "Waveguide invariant focusing for broadband beamforming in an oceanic waveguide", J. Acoust. Soc. Am. **123**, 1338–1346 (2008).

[19] A. M. Thode, "Localization uisng Bartlett matched-field processor sidelobes", J. Acoust. Soc. Am. **107**, 278–286 (2000).

[20] A. M. Thode, "Source ranging with minimal environmental information using a virtual receiver and waveguide invariant theory", J. Acoust. Soc. Am. **108**, 1582–1594 (2000).

[21] K. A. Sostrand, "Range localization of 10-100 km explosions by means of an endfire array and a waveguide invariant", IEEE J. Ocean. Eng. **30**, 207–212 (2005).

[22] A. Turgut, M. Orr, and D. Rouseff, "Broadband source localization using horizontal-beam acoustic intensity striations", J. Acoust. Soc. Am. **127**, 73–83 (2010).

[23] K. L. Cockrell and H. Schmidt, "Robust passive ranging estimation using the waveguide invariant," J. Acoust. Soc. Am. **127**, 2780–2789 (2010).

Chapter 2

The relation between the waveguide invariant and array invariant

Authors:
H.C. Song
Chomgun Cho

2.1 Abstract

The waveguide invariant β is based on the dependence of group speed on phase speed and summarizes the robust interference phenomenon in the range-frequency plane. Over the last decade the elegant approach has been utilized for various applications including passive source ranging. Separately, the array invariant approach [Lee and Makris, J. Acoust. Soc. Am. 119, 336-351 (2006)] has been proposed for a robust source-range estimator from beam-time intensity data using either a horizontal or vertical array. In this letter, it is shown that the array invariant can be derived from the waveguide invariant theory assuming $\beta = 1$.

2.2 Introduction

The *waveguide invariant*, denoted by β, is based on the dependence of group speed on phase speed in an acoustic waveguide and summarizes the interference striations observed in the plot of acoustic intensity versus range and frequency [1,2]. It has been generalized by Grachev [3] to include other acoustic parameters such as sound speed and water depth. It is commonly derived using normal modes of the waveguide [2,4,5], while recently a complementary interpretation has been provided through the behavior of impulse response [6]. In many cases, the waveguide invariant within a group of modes is a scalar parameter (e.g., $\beta \approx 1$), approximately independent of range, frequency, mode numbers, and even details of the sound speed profiles. As a result, the elegant and robust property of β has been utilized over the last decade for various applications in underwater acoustics [7–11], including passive range localization [12–17].

Separately, the *array invariant*, denoted by χ, has been proposed by Lee and Makris [18] for instantaneous source-range estimation in a horizontally stratified ocean waveguide from passive beam-time intensity data after conventional plane-wave beamforming using either a horizontal or vertical array. While the approach was generally based on the relationship between the group speed and phase speed, the authors claimed that the array invariant is distinguished from the waveguide invariant because it does not rely on modal interference, providing a better estimate in real time with little computational effort and the full array gain. Further, no knowledge of the environment is required except that the received field should not be dominated by purely waterborne propagation. The method was successfully demonstrated using both simulations and experimental data for source range estimation in shallow water using a towed horizontal array. On the other hand, a similar beam-time diagram was introduced for range localization by Søstrand [15] using an endfire bottom-moored horizontal array, but invoking the waveguide invariant theory.

The objective of this letter is to show that indeed the array invariant can be derived from the waveguide invariant theory and is a special case of $\beta = 1$, applicable to many shallow-water waveguides where surface/bottom reflected paths

are dominant with $\beta \approx 1$. This explains why waterborne (refracted) rays or modes, characterized by a different group of modes with a negative β, should be excluded from the array invariant processing. Since the parameter χ includes β in our derivation, the array invariant approach potentially can be extended to the case when $\beta \neq 1$ (e.g., -3), provided that a similar group of modes is utilized for range estimation.

Section 2.3 reformulates the waveguide invariant theory in the beam-time plane and derives an elliptic equation for vertical arrays and a simple linear equation for horizontal arrays, consistent with the array invariant approach. Section 2.4 then makes a specific connection between the two invariants. Section 2.5 analyzes two different waveguides with opposite signs of β to illustrate how the waveguide invariant affects the beam-time migration pattern utilized for range estimation, followed by a summary in Sec. 2.6.

2.3 Waveguide invariant

For simplicity, we assume a range-independent waveguide while the waveguide invariant theory can be extended to mildly range-dependent environments [2, 4, 5]. As depicted in Fig. 2.1, two common arrays are considered: (a) vertical array and (b) horizontal array aligned with the source (i.e., endfire) which can be easily generalized to the case with an azimuth angle ϕ_0 in the horizontal plane.

2.3.1 Vertical array

The waveguide invariant β is defined from a functional relationship between the group and phase velocities, V_g and V_p (or, equivalently the group and phase slowness, S_g and S_p). We can then express individual group and phase velocities as a Taylor expansion around the average group and phase velocities of a set of modes (or eigen rays). It is shown by Jensen et al. [5] that

$$\frac{1}{\beta} = -\frac{d(1/V_g)}{d(1/V_p)} = -\frac{d(S_g)}{d(S_p)}. \tag{2.1}$$

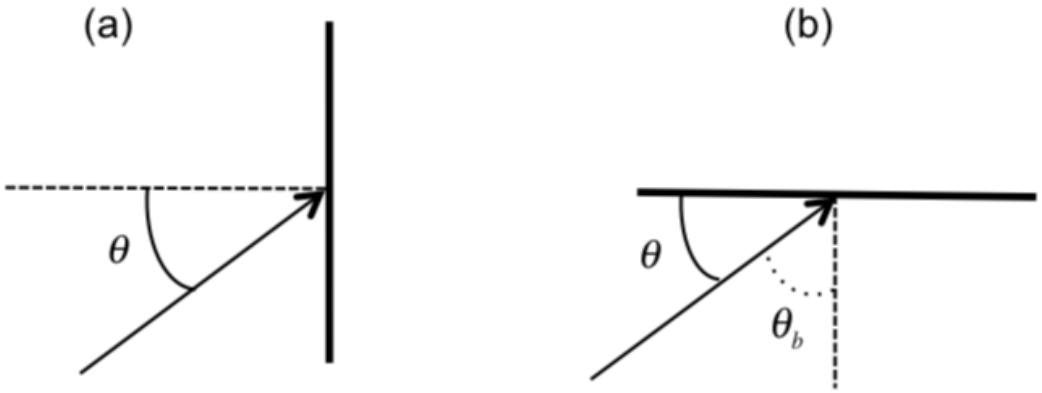

Figure 2.1: The geometry of two common arrays (thick lines): (a) vertical array and (b) endfire horizontal array. θ is the grazing angle of the ray arrival. In (b), θ_b is the elevation angle defined with respect to the broadside of the horizontal array. In general, the horizontal array will have an azimuth angle ϕ_0 in the horizontal plane from the source (i.e., source bearing) while $\phi_0 = \pi/2$ corresponds to the endfire in (b).

The group velocity can be calculated as the source range R divided by the travel time t

$$V_g = \frac{R}{t}. \tag{2.2}$$

The phase velocity V_p is the ratio of the local sound speed c to the cosine of the incident grazing angle θ at a receiver as shown in Fig. 2.1a

$$V_p = \frac{c}{\cos\theta} = \frac{c}{\sqrt{1-\sin^2\theta}} = \frac{c}{\sqrt{1-s^2}}, \tag{2.3}$$

where $s \equiv \sin\theta$ and $0 \leq s < 1$. The conversion to $\sin\theta$ in Eq. (2.3) is necessary because the beamforming output using a vertical array will be provided as a function of $\sin\theta$. The local sound speed c should be replaced by an average sound speed used for plane-wave beamforming, assuming that the sound speed variation is minimal across the aperture [18].

The waveguide invariant formula in Eq. (2.1) then can be rewritten as

$$\frac{1}{\beta} = -\frac{d(t/R)}{d(\sqrt{1-s^2}/c)} = \left(\frac{c}{R}\right)\frac{dt/ds}{s/\sqrt{1-s^2}}. \tag{2.4}$$

Let's define a parameter b_v such that

$$b_v \equiv \left(\frac{R}{c}\right)\frac{1}{\beta}. \tag{2.5}$$

Note that b_v has a dimension of time since β is a dimensionless scalar parameter (e.g., $\beta = 1$). In addition, b_v has the same sign as β. The above differential equation is simplified to

$$dt = b_v \frac{s}{\sqrt{1-s^2}} ds. \tag{2.6}$$

Now we assume β is constant and thus b_v is constant. Integrating in t and s respectively yields

$$t - t_0 = b_v \int_{s_0}^{s} \frac{s}{\sqrt{1-s^2}} ds = -b_v \sqrt{1-s^2}\Big|_{s_0}^{s} = -b_v\sqrt{1-s^2} + b_v\sqrt{1-s_0^2}, \tag{2.7}$$

where t_0 and s_0 are arbitrary constants. Rearranging the equation, we have

$$t = -b_v\sqrt{1-s^2} + t_c, \tag{2.8}$$

where

$$t_c = t_0 + b_v\sqrt{1-s_0^2}. \tag{2.9}$$

This equation has the form of an ellipse whose minor and major axes coincide with the Cartesian coordinates (s, t) assuming $|b_v| > 1$

$$s^2 + \frac{(t-t_c)^2}{b_v^2} = 1, \tag{2.10}$$

whose center is located on the t-axis at $(0, t_c)$ and b_v is the vertical semi-major axis.

2.3.2 Horizontal array

Let's first consider a horizontal array aligned to the source (i.e., endfire) as depicted in Fig. 2.1b. In this case, the phase velocity V_p in Eq. (2.3) is written simply as

$$V_p = \frac{c}{\cos\theta} = \frac{c}{\sin\theta_b} = \frac{c}{s_b}, \tag{2.11}$$

where $s_b \equiv \sin\theta_b$ with θ_b defined with respect to the broadside of the horizontal array (i.e., elevation angle), consistent with the vertical array case and c is the local sound speed at the depth of the horizontal array.

The waveguide invariant formula in Eq. (2.1) then becomes

$$\frac{1}{\beta} = -\frac{d(t/R)}{d(s_b/c)} = -\left(\frac{c}{R}\right)\frac{dt}{ds_b}. \tag{2.12}$$

In contrast with an elliptic equation derived for a vertical array, we now have a simple linear equation in the beam-time coordinates (s_b, t) having a slope

$$\frac{dt}{ds_b} = -\left(\frac{R}{c}\right)\frac{1}{\beta} = -b_h. \tag{2.13}$$

where b_h is equivalent to b_v defined in Eq. (2.5) for a vertical array.

In general, the horizontal array is not in the endfire with an azimuth angle of ϕ_0 in the horizontal plane from the source. In this case, we can employ a spherical coordinate geometry to understand the effect of the azimuth angle [18]. Alternatively, the process of rotating the horizontal array to the endfire is equivalent to replacing the local sound speed c with an apparent sound speed, $(c \times \sin\phi_0)$. Now a more general definition of b_h can be introduced for a horizontal array with source bearing ϕ_0

$$b_h = \left(\frac{R}{c\sin\phi_0}\right)\frac{1}{\beta} = \frac{b_v}{\sin\phi_0}. \tag{2.14}$$

This expression reduces to the endfire case when $\phi_0 = \pi/2$.

2.4 Relating the waveguide invariant to array invariant

In the previous section, the functional relationship of the waveguide invariant between the phase and group velocities (V_p, V_g) is mapped into the functional relationship between the sine of the arrival angle (i.e., beam) with respect to the broadside of the array and the travel time, (s, t) and (s_b, t), respectively. Our results are compared with those described in the array invariant approach [18], leading to a few important observations:

- The parameters b_v and b_h defined in Sec. 2.3 during the transformation correspond to the array invariants χ_v and χ_l defined in Eqs. (19) and (16) of Ref. [18], respectively, except that the waveguide invariant β is absent in

χ_v and χ_l. Recall that the source range R contained in these parameters is estimated for passive range localization from the beam-time intensity data.

- When $\beta = 1$, b_v and b_h are equivalent to the reciprocal of χ_v and χ_l, respectively, i.e., $b_v = 1/\chi_v$ and $b_h = -1/\chi_l$. Since $\beta \approx 1$ for most bottom-interacting shallow-water environments [5], the array invariant approach can be applied without explicitly invoking the waveguide invariant. Note that a small deviation from $\beta = 1$ can be easily translated to range estimation errors or to the uncertainty in the local sound speed c since they are all glued together.

- Not surprisingly, the array invariant approach excludes waterborne (or refracted) paths which are typically characterized by a negative β, as opposed to the surface-bottom reflected paths with a positive $\beta \approx 1$. This is because for reflection-dominated paths, group speed decreases with increasing phase speed, whereas for refracting paths, group speed increases with increasing phase speed [5]. In addition, modes near cut-off are excluded in the array/waveguide invariant.

- Since the array invariant is directly linked to the waveguide invariant, the array invariant approach can be extended to the case when $\beta \neq 1$, provided that a similar group of modes is utilized for range estimation. Specifically, an example of upward-refracting environment with $\beta = -3$ will be illustrated in Section 2.5.

2.5 Illustrative examples

Two acoustic environments with opposite signs of β displayed in Fig. 2.2 are analyzed to illustrate how the beam-time migration (elliptic or linear) is utilized for range localization: (a) ideal waveguide (isovelocity) and (b) n^2-linear waveguide where $n^2(z) = c_0^2/c^2(z) = 1 - 2az$ with $a = 8 \times 10^{-6}$ m^{-1}. Both waveguides have analytic expressions for the waveguide invariant: (a) $\beta = \cos^2\theta$ and (b) $\beta = -3/(1 - \tan^2\theta)$. By limiting the range of grazing angles (or modes), however,

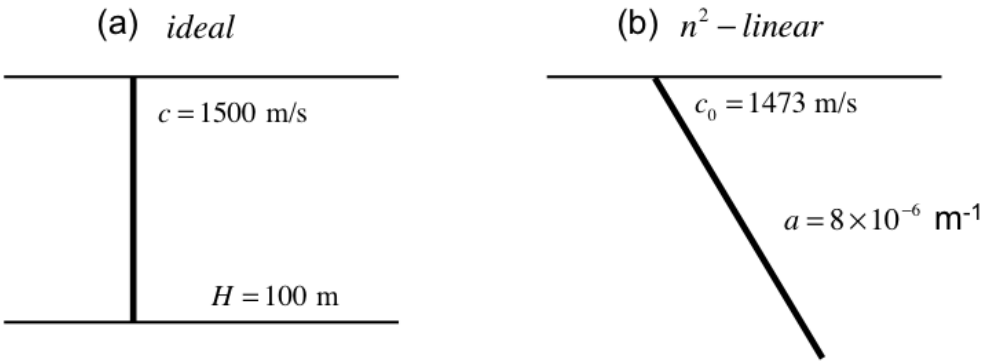

Figure 2.2: Schematic of two waveguides: (a) ideal ($\beta = 1$) and (b) n^2-linear ($\beta = -3$) where $n^2(z) = c_0^2/c^2(z) = 1 - 2az$ with $c_0 = 1473$ m/s and $a = 8 \times 10^{-6}$ m^{-1}. The source-receiver distance is 5 km. The phase and group speeds that generate the beam-time migration together are evaluated at 500 Hz.

we can assume $\beta = 1$ and $\beta = -3$, respectively [5, 6]. In the Appendix, the beam-time migration for the isovelocity case is derived using $\beta = \cos^2\theta$ to validate this assumption.

Despite its simplification, the ideal waveguide with $\beta = 1$ represents many realistic shallow-water environments when surface/bottom reflected paths are dominant. Similarly, the n^2-linear waveguide with $\beta = -3$ represents propagation environments dominant with refracted paths. The source frequency is set to 500 Hz and the distance between a source and a receive array is 5 km. Both the source and receive depth (center of the array) are chosen 50 m in Fig. 2.2a whereas in Fig. 2.2b the source is at the surface and the receiver is at 200 m depth.

2.5.1 Vertical array

The beam-time migration that can be generated by a vertical array is illustrated in Fig. 2.3. The solid lines are the theoretical ellipses in (s, t) coordinates derived in Eq. (2.10) (only right-half shown due to symmetry). Superimposed (crosses) are the beam-time migration where each mark (+) denotes the travel

time (t) based on the individual group speed and range versus the corresponding phase speed in beam angle (s). In the ideal waveguide with a positive β, the first 26 modes are shown in Fig. 2.3a along the ellipse in the *lower* quadrant, constrained by the sign of b_v in Eq. (2.8) that has the same sign as β, consistent with Fig. 10b of Ref. [18]. The beam-time migration curve using $\beta = \cos^2\theta$ (refer to the Appendix) is also displayed in Fig. 2.3a (dashed line), which is almost identical to the ellipse assuming $\beta = 1$ for the low-order modes with small grazing angles (i.e., $s < 0.4$). The beam-time migration with a vertical array requires minimal 3 modes to fit the ellipses although more modes would provide a robust and better estimate.

In contrast, the beam-time migration in the n^2-linear waveguide is captured by the ellipse in the *upper* quadrant due to the negative β as shown in Fig. 2.3b. The densely-populated first 77 modes (+) are displayed whose turning depth is less than 1000 m, indicating that the array invariant approach for passive range localization is applicable to the refracting paths with a negative β. For convenience, the Cartesian coordinates (s, t) have a different scale to show the entire half of the ellipses (i.e., stretched in s-axis).

2.5.2 Horizontal array

Similarly, the beam-time migration that can be generated by a horizontal array is shown in Fig. 2.4 assuming the azimuth angle of $\phi_0 = 80°$ (almost the endfire). In comparison with ellipses for a vertical array, the solid lines indicate a simple linear equation with a slope derived in Eq. (2.13) in (s_b, t) coordinates. Superimposed (+) are the pair of group and phase speeds transformed into the pair of travel time (t) and beam angle (s_b). As expected, the beam-time migration for the ideal waveguide in Fig. 2.4a is consistent with Fig. 7b of [18]. In addition, the beam-time migration curve derived using $\beta = \cos^2\theta$ (refer to the Appendix) is displayed in Fig. 2.4a (dashed line), which is almost identical to the linear line assuming $\beta = 1$ for the low-order modes with small grazing angles (i.e., $s_b > 0.95$). The high-order modes (e.g., > 20) deviate from the linear line that can be excluded from the array invariant processing or whose contribution would be negligible due to attenuation.

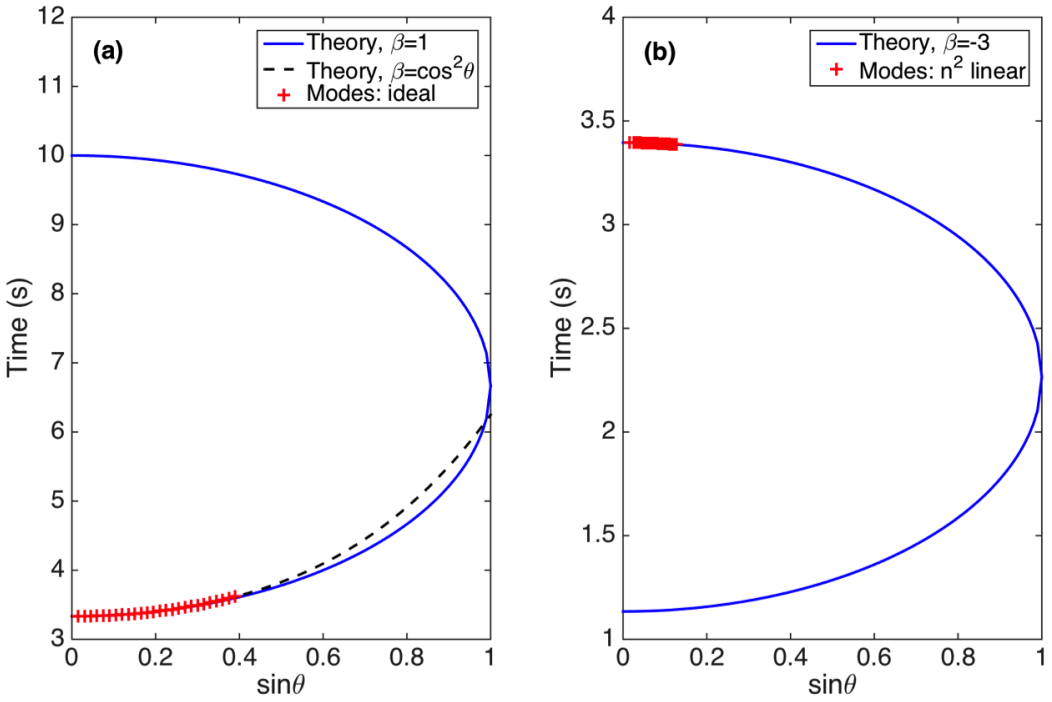

Figure 2.3: (Color online) Beam-time migration generated by a vertical array: (a) ideal and (b) n^2-linear. The solid lines are the theoretical ellipses derived in Eq. (2.10) in (s,t) coordinates (only right-half shown due to symmetry). Superimposed are the beam-time migration where each mark (+) denotes the travel time (t) based on the group speed and range versus the phase speed in beam angle (s). The selection of quadrants, either lower or upper, depends on the sign of b_v or β. For the ideal waveguide in (a), the beam-time migration curve based on $\beta = \cos^2\theta$ is also displayed (dashed line). For convenience, the Cartesian coordinates (s,t) have a different scale (i.e., stretched in s-axis).

On the other hand, the slope is reversed from negative to positive in Fig. 2.4b for the n^2-linear waveguide with a negative β. The beam-time migration with a horizontal array requires minimal 2 modes to fit the straight line while more modes would lead to a better estimate.

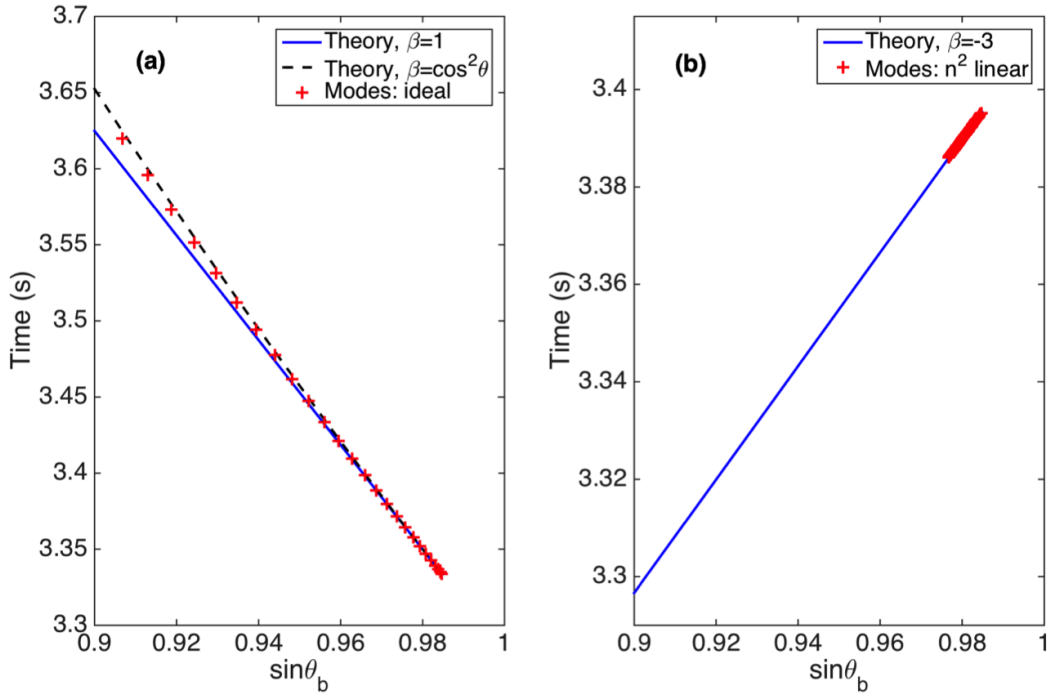

Figure 2.4: (Color online) Beam-time migration generated by a horizontal array with the azimuth angle of $\phi_0 = 80°$: (a) ideal and (b) n^2-linear. The linear equations derived in Eq. (2.13) are drawn in (s_b, t) coordinates. Superimposed are the beam-time migration where each mark (+) denotes the travel time (t) based on the group speed and range versus the corresponding phase speed in beam angle (s_b). The slope, either negative or positive, depends on the sign of b_h or β. For the ideal waveguide in (a), the beam-time migration curve based on $\beta = \cos^2\theta$ is also displayed (dashed line).

2.6 Summary

The array invariant proposed for passive range localization was shown fundamentally equivalent to the waveguide invariant theory when $\beta = 1$. Specifically, the functional relationship between the group and phase speeds was converted into the functional relationship between the travel time and beam angle, i.e., beam-time migration. Since many shallow-water environments are characterized by $\beta \approx 1$, the array invariant approach could be applied without explicitly invoking the waveguide invariant. It was found that the beam-time migration follows ellipses for vertical arrays and lines for horizontal arrays. The potential generalization of the array/wavguide invariant approach was illustrated using an upward-refracting

environment with $\beta = -3$.

2.7 Appendix: Derivation of beam-time migration for ideal waveguide using $\beta = \cos^2\theta$

The analytic expression for the waveguide invariant in ideal waveguide (i.e., isoveloctity) is $\beta = \cos^2\theta$, which depends on the grazing angle θ. For small grazing angles (low-order modes), however, the dependence is negligible and β can be assumed approximately unity. Here we derive the beam-time migration curve using $\beta = \cos^2\theta$ in Sec. 2.3 to validate the approximation.

2.7.1 Vertical array

Introducing $\beta = \cos^2\theta = 1 - s^2$ into Eq. (2.4), we obtain

$$dt = \frac{R}{c}\frac{sds}{(1-s^2)^{\frac{3}{2}}}. \tag{2.15}$$

With the substitution $(1-s^2) = u^{\frac{2}{3}}$ and $sds = -\frac{1}{3}u^{-\frac{1}{3}}du$, the equation takes the form

$$dt = -\left(\frac{R}{3c}\right)u^{-\frac{4}{3}}du. \tag{2.16}$$

We next integrate both sides of the equation to obtain

$$t - t_0 = -\left(\frac{R}{3c}\right)\frac{1}{-\frac{4}{3}+1}u^{-\frac{4}{3}+1}\Big|_{u_0}^{u} = \frac{R}{c}\left(u^{-\frac{1}{3}} - u_0^{-\frac{1}{3}}\right). \tag{2.17}$$

Since $u^{\frac{1}{3}} = \sqrt{1-s^2}$, there follows

$$t - t_0 = \frac{R}{c}\left(\frac{1}{\sqrt{1-s^2}} - \frac{1}{\sqrt{1-s_0^2}}\right). \tag{2.18}$$

Using the Taylor series expansion, we can rewrite the above equation

$$t - t_c = \frac{R}{c}\left(1 + \frac{1}{2}s^2 + \frac{3}{8}s^4 + O(s^6)\right), \tag{2.19}$$

where

$$t_c = t_0 - \frac{R}{c}\frac{1}{\sqrt{1-s_0^2}}. \tag{2.20}$$

This equation is not in the form of an ellipse in (s,t) coordinates as depicted in Fig. 2.3a (dashed line). For small grazing angles (i.e., $s < 0.4$), however, this curve is almost identical to the ellipse derived assuming $\beta = 1$.

2.7.2 Horizontal array

Substituting $\beta = \cos^2\theta = s_b^2$ in Eq. (2.12), we obtain

$$dt = -\frac{R}{c}\frac{ds_b}{s_b^2}. \tag{2.21}$$

Integrating both sides gives

$$t - t_0 = \frac{R}{c}\left.\frac{1}{s_b}\right|_{s_{b0}}^{s_b} = \frac{R}{c}\left(\frac{1}{s_b} - \frac{1}{s_{b0}}\right) \tag{2.22}$$

or, equivalently,

$$t - t_c = \left(\frac{R}{c}\right)\frac{1}{s_b}, \tag{2.23}$$

where

$$t_c = t_0 - \frac{R}{c}\frac{1}{s_{b0}}. \tag{2.24}$$

The beam-time migration in (s_b,t) coordinates is not a straight line as depicted in Fig. 2.4a (dashed line). For small grazing angles (i.e., $s_b > 0.95$), however, this curve is almost identical to the straight line based on $\beta = 1$.

Acknowledgment

Chapter 2, in full, is a reprint of the material as it appears in the Journal of Acoustical Society of Americas: H.C. Song and Chomgun Cho, "The relation between the waveguide invariant and array invariant," *J. Acoust. Soc. Am*, 138 (2), 899-903, 2015. The dissertation author was a primary investigator and author of this material.

Bibliography

[1] D. E. Weston and K. J. Stevens, "Interference of wide-band sound in shallow water", J. Sound and Vibration **21**, 57–64 (1972).

[2] S. D. Chuprov, "Interference structure of a sound field in a layered ocean", in *Acoustics of the Ocean*, 71–91 (Nauka, Moscow) (1982), edited by L. M. Breakhovskikh and I. B. Andreevoi.

[3] G. A. Grachev, "Theory of acoustic field invariants in layered waveguide", Acoust. Phys. **39(1)**, 33–35 (1993).

[4] L. M. Brekhovskikh and Y. P. Lysanov, *Fundamentals of Ocean Acoustics*, 3rd edition (Springer-Verlag, New York) (2003).

[5] F. B. Jensen, W. A. Kuperman, M. B. Porter, and H. Schmidt, *Computational Ocean Acoustics* (Springer, New York) (2011), Chaps. 2, 3, and 5.

[6] C. H. Harrison, "The relation between the waveguide invariant, multipath impulse response, and ray cycles", J. Acoust. Soc. Am. **129**, 2863–2877 (2011).

[7] H. C. Song, W. A. Kuperman, and W. S. Hodgkiss, "A time-reversal mirror with variable range focusing", J. Acoust. Soc. Am. **103**, 3234–3240 (1998).

[8] H. Tao and J. L. Krolik, "Waveguide invariant focusing for broadband beamforming in an oceanic waveguide", J. Acoust. Soc. Am. **123**, 1338–1346 (2008).

[9] S. Kim, W. A. Kuperman, W. S. Hodgkiss, H. C. Song, G. F. Edelmann, and T. Akal, "Robust time reversal focusing in the ocean", J. Acoust. Soc. Am. **114**, 145–157 (2003).

[10] T. C. Yang, "Beam intensity striations and applications", J. Acoust. Soc. Am. **113**, 1342–1352 (2003).

[11] P. Roux, W. A. Kuperman, B. Cornuell, F. Aulanier, W. S. Hodgkiss, and H. C. Song, "Analyzing sound speed fluctuations in shallow water from group-velocity versus phase-velocity data representation", J. Acoust. Soc. Am. **133**, 1945–1952 (2013).

[12] G. L. D'Spain and W. A. Kuperman, "Application of waveguide invariants to analysis of spectrograms from shallow water environments that vary in range and azimuth", J. Acoust.Soc. Am. **106**, 2454–2468 (1999).

[13] A. M. Thode, "Source ranging with minimal environmental information using a virtual receiver and waveguide invariant theory", J. Acoust. Soc. Am. **108**, 1582–1594 (2000).

[14] A. M. Thode, "Localization uisng bartlett matched-field processor sidelobes", J. Acoust. Soc. Am. **107**, 278–286 (2000).

[15] K. A. Sostrand, "Range localization of 10-100 km explosions by means of an endfire array and a waveguide invariant", IEEE J. Ocean. Eng. **30**, 207–212 (2005).

[16] K. L. Cockrell and H. Schmidt, "Robust passive ranging estimation using the waveguide invariant", J. Acoust. Soc. Am. **127**, 2780–2789 (2010).

[17] A. Turgut, M. Orr, and D. Rouseff, "Broadband source localization using horizontal-beam acoustic intensity striations", J. Acoust. Soc. Am. **127**, 73–83 (2010).

[18] S. Lee and N. C. Makris, "The array invariant", J. Acoust. Soc. Am. **119**, 336–351 (2006).

Chapter 3

Robust source-range estimation using the array/waveguide invariant and a vertical array

Authors:
Chomgun Cho
H.C. Song
W. S. Hodgkiss

3.1 Abstract

The array invariant based on beam-time migration has been proposed for source-range estimation using a horizontal or vertical array, with no need for forward model computations. The approach has been demonstrated successfully with experimental data in shallow water using a horizontal towed array. Recently the array invariant has been shown to be a special case of the waveguide invariant theory. In this paper, the unified array/waveguide invariant approach to source-range estimation is applied to a short-aperture vertical array in a fluctuating ocean environment over a one-day period. Specifically, the mean range estimates using a

12-m long vertical array in ∼100 m deep water are less than 8% relative error for a source (2–3 kHz) at 6-km range, demonstrating the robustness of this approach.

3.2 Introduction

This paper addresses the problem of passive source-range estimation using a short-aperture vertical array in shallow water, with no need for the forward model computations involved in matched field processing (MFP) [1]. The approach taken in this paper is a straightforward extension of the waveguide invariant concept first introduced by Chuprov [2] to the beam-time intensity domain, which is a generalization of the array invariant proposed by Lee and Makris [3,4]. The unified waveguide/array invariant approach is applied to both simulations and data to demonstrate the robustness of the proposed approach.

The waveguide invariant, denoted by β and based on the functional relationship between the group and phase speed in an acoustic waveguide (equivalently group and phase slowness) [5], describes the dispersive nature of waveguide propagation and characterizes the interference striations observed in the range-frequency plane. The isovelocity waveguide has a canonical value of $\beta = 1$, which also is applicable to many shallow water environments. For an arbitrary sound speed profile, however, the propagating modes that contribute to the wavefield can be divided into distinct groups of modes that behave similarly within each group with each group having a different value of β. The value of β also can be range-dependent if the waveguide has a range-dependent bathymetry and sound speed [6, 7] and internal waves [8]. Waveguide invariant theory has been exploited for various applications in the ocean, including time-reversal focusing [9,10], source localization [11–14], and sonar array processing [15].

On the other hand, the array invariant [3], denoted by χ, is derived in the beam-time intensity domain after plane-wave beamforming using either a horizontal or vertical array, presumably independent of the waveguide invariant. This approach provides a reasonable source-range estimate with little computational effort, the full array gain, and minimal knowledge of the environment, but is re-

stricted to bottom-interacting, shallow-water environments. The array invariant method was demonstrated using both simulations and data for source range estimation in shallow water using a towed horizontal array.

Motivated by the array invariant work, waveguide invariant theory recently has been reformulated in the beam-time domain since the phase and group speeds defined in β are associated with a local *beam* angle and a travel *time*, respectively [4]. It was found that the array invariant is a special case of $\beta = 1$, thus being extendable to waveguides with different values of β, i.e., a generalization of the array invariant. The implication is that the array invariant is fully supported by the waveguide invariant physics. In this paper, the unified waveguide/array invariant approach to source-range estimation is investigated using data collected on a 12-m long vertical array in ∼100-m deep water from a 2–3 kHz source at 6-km range.

The paper is organized as follows. Section 3.3 reviews the array invariant approach in conjunction with the waveguide invariant theory, with a major focus on vertical arrays. Section 3.4 describes the high-frequency experiment (HF97) [16] conducted in shallow water off San Diego, CA, in October 1997. In Sec. 3.5, range estimation based on the array/waveguide invariant theory is presented using simulations and HF97 data, followed by a summary in Sec. 3.6.

3.3 Unified array/waveguide invariant for vertical arrays

3.3.1 Array invariant

The array invariant [3] stems from the observation that in an ideal isovelocity waveguide the beam-time migration $s_h(t)$ for an endfire horizontal array, where $s_h(t) = \cos\theta(t)$ with a *grazing* angle θ, depends only on the source range r_0, independent of source frequency band, mode number, source/receiver depth, and waveguide depth (refer to Fig. 4 in Ref. [3]). This approach then was extended to many shallow-water waveguides by excluding so-called waterborne (refracted)

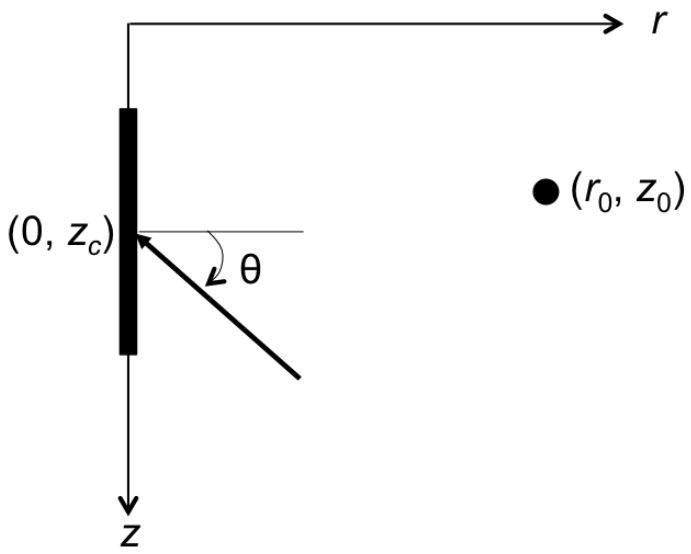

Figure 3.1: Coordinate system including the grazing angle θ and source range r_0.

modes. The array invariant can be applied to both horizontal and vertical arrays with the beam angle defined with respect to the broadside of the array, yielding two respective invariant parameters: χ_h (or χ_l) and χ_v. For a vertical array (see Fig. 3.1), the beam angle corresponds to the grazing angle $s_v = s = \sin\theta$ in the beam-time domain (s, t), whereas $s_h = \cos\theta$ for a horizontal array in (s_h, t). Conventional plane-wave beamforming requires appropriate element spacing to avoid spatial aliasing, adequate aperture which determines the beam resolution, and minimal sound speed variation across the array aperture.

The array invariant approach is summarized in the Appendix for a vertical array that enables source-range estimation directly from $r_0 = -c/\chi_v$, where c is the local (averaged) sound speed and χ_v is evaluated from data in the beam-time domain (s, t) after plane-wave beamforming. It should be pointed out that χ_v defined here is modified from the original but more consistent with χ_l in Eq. (16) of Ref. [3]. Further, the resulting beam-time migration curve $s(t)$ follows an identical elliptic equation in both the array invariant and waveguide invariant [4].

3.3.2 Waveguide invariant

In contrast with the array invariant theory which is restricted to isovelocity and similar shallow-water waveguides [3], waveguide invariant theory applies to general waveguides [5]. The waveguide invariant is based on the dependence of group speed V_g (or group slowness $S_g = 1/V_g$) on phase speed V_p (or $S_p = 1/V_p$), summarized by a scalar parameter β

$$\frac{1}{\beta} = -\frac{d(1/V_g)}{d(1/V_p)} = -\frac{d(S_g)}{d(S_p)}. \tag{3.1}$$

For a number of sound speed profiles, analytic expressions for β can be derived [17]. The ideal waveguide that led to the array invariant theory has $\beta = \cos^2\theta$, which is approximately $\beta \approx 1$ for low-order modes (e.g., $\theta < 20°$). Moreover, $\beta \approx 1$ remains valid for many shallow-water environments where surface/bottom reflected paths are dominant. On the other hand, an upward refracting profile has a negative $\beta = -3/(1 - \tan^2\theta)$, approximately $\beta \approx -3$ for small grazing angles. For an arbitrary sound speed profile, the modes contributing to the wavefield can be divided into different groups of modes [2] that behave similarly within each group having a different value of β. In other words, the waveguide invariant β can vary depending on the specific group of modes for a given waveguide.

The waveguide invariant defined in the (V_p, V_g) or (S_p, S_g) coordinate system can be transformed into the beam-time domain: (s, t) for a vertical array and (s_h, t) for a horizontal array. For a source-receiver distance r_0, the group speed is convertible to the travel time through $V_g = r_0/t$, whereas the phase speed is associated with the incident grazing angle θ of a mode (or ray) such that $V_p = c/\cos\theta$. Similar to the array invariant case, the coordinate transformation into the beam-time domain generates two invariant parameters [4]: (i) $b_v = (r_0/c)/\beta$ for a vertical array and (ii) $b_h = b_v/\sin\phi_0$ for a horizontal array with an azimuth angle of ϕ_0 (e.g., $\phi_0 = \pi/2$ for endfire). It is important to note that both parameters (b_v and b_h) contain β and have a dimension of time since β is a non-dimensional scalar. During this transformation, β is assumed constant, implying that the array/waveguide invariant is based on a single group of modes having the same value of β.

The two invariant parameters are inversely proportional to the array invariant parameters such that $b_v = -1/\chi_v$ and $b_h = -1/\chi_l$. For a vertical array, the range estimate based on the waveguide invariant theory now includes β:

$$r_0 = \beta\,(b_v c) = -\beta\,(c/\chi_v) \tag{3.2}$$

where χ_v is estimated from the beam-time intensity data (refer to the Appendix). This expression reduces to the array invariant case when $\beta = 1$, which is not surprising since the array invariant has been developed from the isovelocity waveguide with $\beta = 1$. In addition, $\beta \approx 1$ for most bottom-interacting shallow-water environments. A small deviation from $\beta = 1$ will map into range estimation errors in addition to errors resulting from uncertainty in the local sound speed c. The array invariant was demonstrated successfully with simulations and data in shallow water, without explicitly invoking waveguide invariant theory [3]. However, Eq. (3.2) is not restricted to shallow-water environments but applicable to general waveguides, provided that a group of modes having the same value of β are taken into account. Eq. (3.2) will be used for the unified array/waveguide invariant approach to source-range estimation in Sec. 3.5.

3.4 HF97 Experiment

The high frequency experiment (HF97) was conducted off San Diego, CA, during October 1997 [16, 18]. A schematic of the experiment is shown in Fig. 3.2 including the environmental and acoustic instrumentation in a mildly down-slope environment of ∼100 m depth. The goal of the experiment was to measure environmental variations in the water column and to relate the environmental effects with variations in the acoustic channel response. Thus both sources and receivers were moored near the bottom to minimize the impact of source/receiver motion. Time-evolving temperature structure over the 24-hour period on JD301 (October 28) measured by the thermistor string is displayed in Fig. 3.3a from the mixed layer through the main thermocline (10–70 m). In addition, sound speed profiles (SSPs) determined from concurrent CTD measurements at several times on JD301

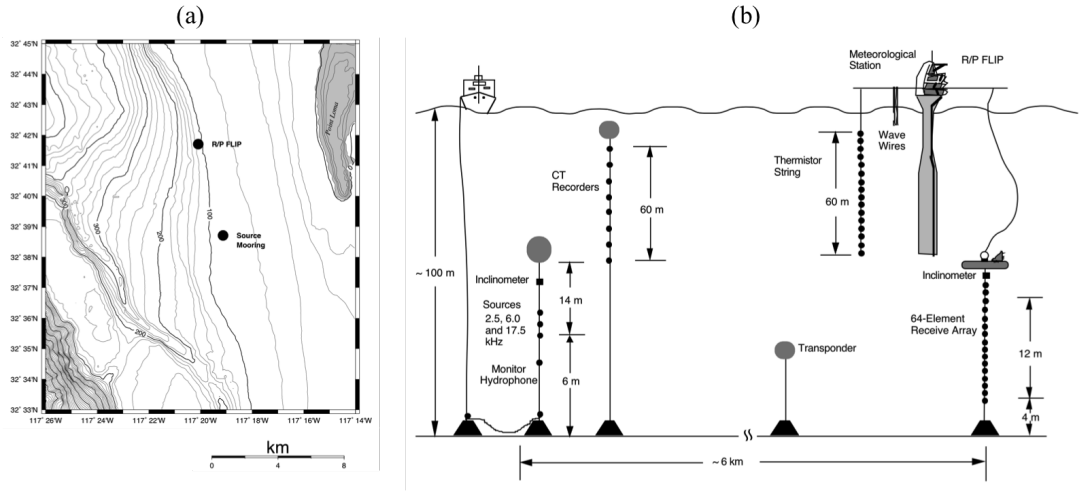

Figure 3.2: High Frequency 1997 experiment overview: (a) the source and receiver locations and bottom bathymetry off San Diego and (b) schematic of deployed hardware (not to scale)

are shown in Fig. 3.3b where the CTD data are offset by 4 m/s per cast for convenience. Note that the SSP contains two thermoclines, one near mid-water depth and another near the bottom. The presence of these two thermoclines induces a significantly downward refracting environment for acoustic energy propagation.

The three sources were operated in the 2.5-, 6.0-, and 18-kHz frequency bands. To investigate the unified array/waveguide invariant approach to source-range estimation, our analysis will focus on the 2.5-kHz source operated at a source level of 188 dB *re* 1 μPa at 1 m. Specifically, the 2.5 kHz source transmitted a 1-s, 2–3 kHz, linear frequency modulated (LFM) chirp continuously for 6 minutes beginning every hour for an extended period of time. The source transmissions were captured by a 64-element, 12-m long vertical array centered at 100-m and moored in 110-m water depth, approximately 6 km away from the source. The inter-element spacing of 0.1875 m corresponds to 0.3125 wavelength (λ) at 2.5 kHz, less than half the wavelength required to avoid spatial aliasing.

A typical example of the channel impulse response (CIR) along the vertical array is shown in Fig. 3.3c on JD301 17:07 UTC (marked by an arrow in Fig. 3.3a), estimated from the 1-s long, LFM chirp (2–3 kHz). The early arrivals (20–35 ms), group (i), are followed by a cluster of arrivals (40–55 ms), group (ii), that exhibit

a high-intensity energy. Then the late-arriving identifiable wavefronts, group (iii), are visible between 60–140 ms, which will be exploited for range estimation based on the array/waveguide invariant approach in Sec. 3.5.

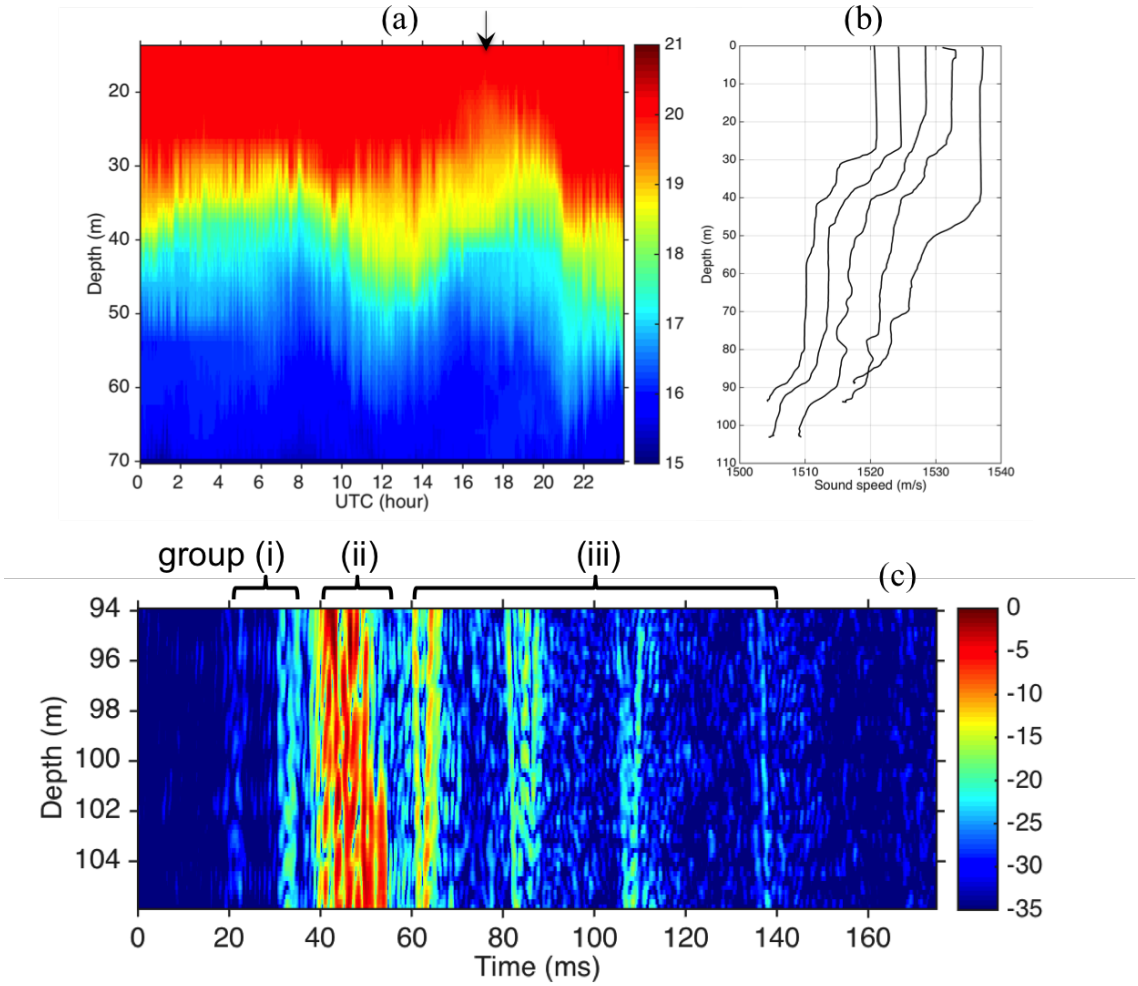

Figure 3.3: (a) Time-evolving temperature structure over the 24-hour period (JD301) measured by the thermistor string extending from the mixed layer through the main thermocline (10–70m). (b) Sound speed profiles determined from CTD measurements at several times on JD301. The profile contains two thermoclines, one near mid-water depth and another near the bottom. The CTD data are offset by 4 m/s per cast from the one on the far left. (c) Intensity of the channel impulse response as a function of delay and hydrophone depth on JD301 17:07 UTC denoted by a vertical arrow in (a). The early arrivals (20–35 ms), group (i), are followed by a cluster of arrivals (40–55 ms), group (ii), that exhibit a high-intensity energy. Then the late-arriving identifiable wavefronts, group (iii), are visible between 60–140 ms.

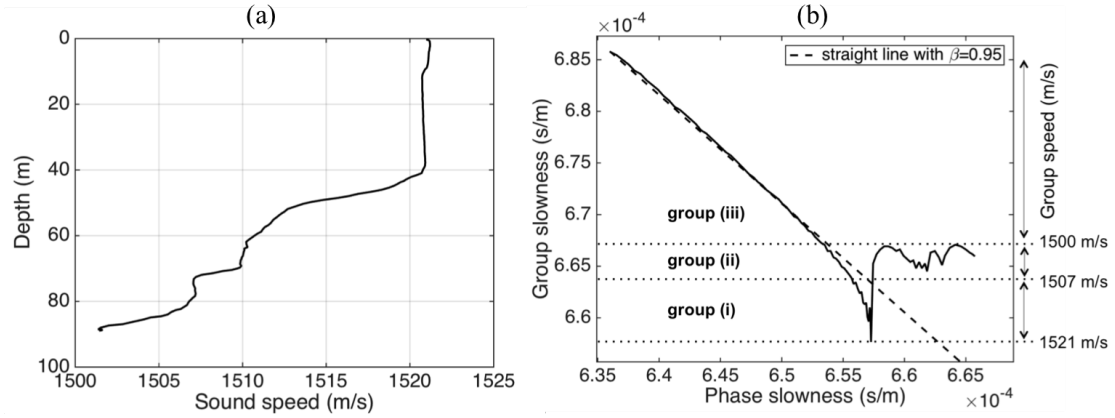

Figure 3.4: (a) Sound speed profile at 14:21 UTC on JD301 (October 28). (b) Group vs. phase slowness curve at 2.5 kHz. The modes are grouped into three different regions depending on the group speed (V_g): (i) early ($V_g > 1507$ m/s), (ii) intermediate ($1500 < V_g < 1507$ m/s), and (iii) later arrivals ($V_g < 1500$ m/s). The high-intensity of group (ii) is due to the contribution of several low-order modes which carry more energy than the high-order modes. The modes within group (iii) are lined up with a negative slope corresponding to $\beta = 0.95$ from Eq. (3.1), which can be exploited for the unified array/waveguide invariant for range estimation in Sec. 3.5.

3.5 Range estimation

3.5.1 Acoustic environment

For simulations and data analysis, a sound speed profile selected from the CTD casts is shown in Fig. 3.4a. The sound speed below 90 m to the bottom is assumed constant ($c = 1501.5$ m/s) where the vertical array is moored. The seafloor depth is ∼110 m at the receiver location, deeper than the source at ∼100 m, i.e., a mildly down-slope bathymetry over the 6-km distance. The ocean bottom can be modeled as a simple half-space for the high frequency source of interest (2–3 kHz) since the acoustic energy cannot penetrate deep into the bottom. The geoacoustic parameters in the area from previous experiments [19] are compressional wave speed $c_b = 1572$ m/s, density $\rho_b = 1.76$ g/cm^3, and attenuation $\alpha_b = 0.3$ dB/λ.

Assuming a range-independent environment with 110-m water depth, the group slowness (S_g) versus phase slowness (S_p) curve is presented in Fig. 3.4b using the normal mode program Kraken [20] at the center frequency of 2.5 kHz.

On the horizontal axis, the mode number increases from the right (i.e., first mode) towards the left. The modes can be grouped into three different regions depending on the group speed (V_g) or arrival time: (i) early ($V_g > 1507$ m/s), (ii) intermediate ($1500 < V_g < 1507$ m/s), and (iii) later arrivals ($V_g < 1500$ m/s).

The arrival structure based on the group speed can describe the observed CIR in Fig. 3.3c. The early arrivals (20–35 ms) are group (i) from relatively high-order modes, which are followed by the lower- and higher-order modes on both sides of group (i). The low-order modes generally carry more energy than high-order modes, especially when both the source and receiver are near the bottom in a downward-refracting environment. Consequently, the acoustic intensity increases significantly in group (ii) (40–55 ms). The later arrivals (60–140 ms) belong to group (iii) from much higher-order modes with large grazing angles. Note that modes within group (iii) are lined up with a negative slope corresponding to $\beta = 0.95$ from Eq. (3.1). Only those modes having the same value of β are used for the array/waveguide invariant approach to source-range estimation.

Although not included in the array invariant, group (i) contains a modal transition region around $V_g = 1521$ m/s where the nature of the mode changes (i.e., slope reversal), a case when a refracted mode changes to a reflected mode or vice versa [21]. It is where there is an abrupt change in SSP of Fig. 3.4a at $\sim$40 m depth and internal waves have a maximum amplitude. Since the transition region is most sensitive to the environmental fluctuations, the robustness of the array/waveguide invariant approach partly comes from not involving modes in group (i).

3.5.2 Simulation: Beam-time migration

Simulation of the beam-time migration curve based on Eq. (3.6) in the Appendix is shown in Fig. 3.5a for the range-independent environment described in Sec. 3.5.1 and the HF97 source/receiver geometry. The source signal is impulsive in the 2–3 kHz frequency band, and a spatial Hamming window is applied during plane-wave beamforming [3]. The vertical axis is relative time with respect to the high-intensity arrival.

As expected from Fig. 3.4b, the group (i) modes arrive first at the grazing

angle of $\sin\theta \approx 0.16$. Immediately follows the high-intensity group (ii) with a broad range of incident angles from the horizontal up to $\sin\theta = 0.25$. The higher-order modes of group (iii) arrive later at large grazing angles, whose intensity is 14 dB down from the peak. Both up-going and down-going waves can be resolved by a vertical array, but only the up-going component (i.e., positive θ) is shown in Fig. 3.5a. For source-range estimation, the array invariant parameter χ_v can be estimated from the curve (solid line) passing through the later arrivals of group (iii). The source-range estimate based on Eq. (3.2) incorporating the waveguide invariant $\beta = 0.95$ is 6.2 km with a relative error of 3% for the source at 6-km range.

3.5.3 HF97 data analysis

The HF97 data are analyzed over two separate periods on JD 301 (October 28), 00:00 – 3:20 and 16:00 – 23:20 UTC. The source signal was a 1-s, 2–3 kHz, LFM chirp, continuously transmitted for one minute (i.e., 60 chirp transmissions) and then repeated every hour over an extended period of time.

We begin with a representative example from 00:07 UTC of the beam-time migration shown in Fig. 3.5b after conventional plane-wave beamforming with a spatial Hamming window followed by matched filtering. The overall arrival structure is in good agreement with the simulation in Fig. 3.5a. Specifically, the early arrivals (i) come in at $\sin\theta = 0.13$, followed by the high-intensity arrivals (ii) with grazing angles ranging from the horizontal to $\sin\theta = 0.2$, and later arrivals (iii) whose intensity is 15 dB down from the peak. Based on the estimate of χ_v from the solid line passing through those modes within group (iii) and $\beta = 0.95$, an initial estimate of the source range of 6.5 km is obtained with an 8% error from the true source range of 6 km. The range error increases to about 13% if $\beta = 1$ is applied as would be the case using the original array invariant [3], indicating the benefit of the unified array/waveguide invariant approach with β incorporated (see Table 3.1).

A value of $\beta = 0.95$ was estimated using a range-independent environment assumed in Fig. 3.4a. The actual bottom, however, approximately has a constant

Table 3.1: Source-range estimation from beam-time migration of the HF97 data shown in Fig. 3.5b for various values of β

β	Source range estimate	relative range error	comments
1	6.8 km	13 %	array invariant
0.95	6.5 km	8 %	range-independent
0.9	6.1 km	2 %	down-slope bottom

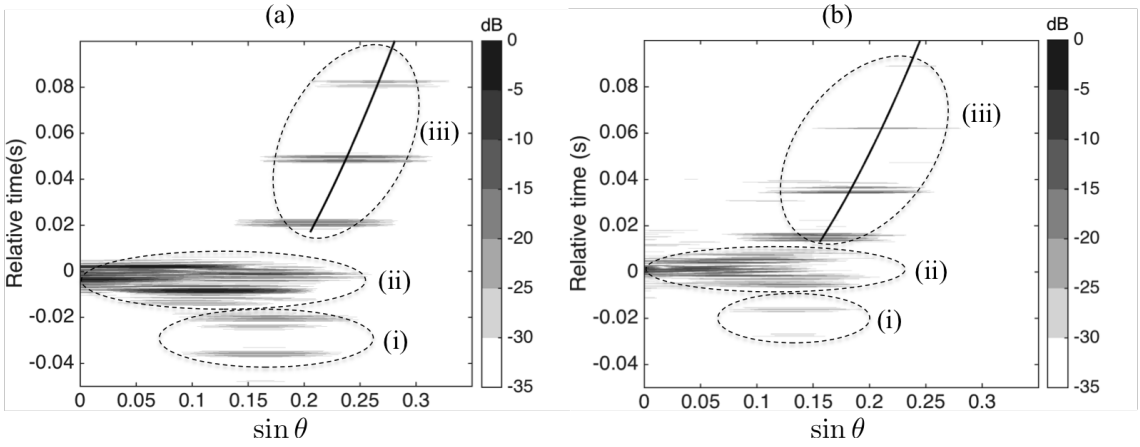

Figure 3.5: Beam-time migration after conventional plane-wave beamforming for the HF97 source/receiver geometry and 2–3 kHz broadband signal. (a) Simulation. The array invariant parameter χ_v can be estimated from the curve (solid line) passing through the modes within group (iii). The source-range estimate from Eq. (3.2) is 6.2 km with a 3% relative error using $\beta = 0.95$. (b) HF97 data at 00:07 UTC. The source range is estimated at 6.1 km with a 2% error using $\beta = 0.9$ incorporating the down-slope bottom bathymetry (see Table 3.1). Note that the vertical axis is relative time in both plots.

downward slope from about 100-m (source) to 110-m (receiver). If the waveguide has a range-varying bottom bathymetry, β also can depend on the range. D'Spain and Kuperman [7] have derived an expression for the range-dependent $\beta(r)$ for an isovelocity waveguide with a sloping bottom,

$$\beta \approx \frac{D(\text{source})}{D(\text{receiver})} \tag{3.3}$$

where D denotes the water depth at the source and receiver locations, respectively. The range-dependent β subsequently was applied to experimental data and provided excellent agreement between the data and model predictions in the anal-

ysis of spectrograms. With a new value of $\beta = 0.9$ incorporating the bathymetry change from Eq. (3.3), an improved estimate of the source range of 6.1 km is obtained with a 2% error, reduced from the 8% error when $\beta = 0.95$ (Table 3.1). In MFP, the effect of mismatch in bathymetry is to shift the peak of the match away from its correct position, resulting in a biased estimate of the source location. In a down-slope environment, the source appears deeper in depth and farther away from the true range, referred to as a mirage [19]. Thus the range-dependent β mitigates the offset in estimated range in MFP caused by neglecting the range dependence of the bottom bathymetry in a shallow water waveguide. We will use $\beta = 0.9$ for the analysis of the HF97 data.

A representative example of source-range estimation for a one-minute period (i.e., 60 chirp transmissions) is shown in Fig. 3.6 (01:07 UTC). The range estimates are distributed around the mean value of 6.09 km with a standard deviation of 0.77 km. Finally, the overall performance of range estimation over an extended period of time on JD301 is summarized in Fig. 3.7 with hourly means (rectangles) and standard deviations (vertical bars) based on the analysis of a 60 s transmission record per hour. The mean source-range estimates vary between 5.7 km and 6.5 km, which corresponds to less than 8 % relative error, with standard deviations about those means of less than 0.86 km. Note that there is a data gap between 3 and 16 hours, and results are not shown at 19 and 21 hours where the data are contaminated by noise. These results further demonstrate the robustness of the unified array/waveguide invariant approach under a fluctuating ocean environment as illustrated in Fig. 3.3a.

Since the angles of arrivals are less than 20° with respect to the broadside of the vertical array, we can use a much smaller number of array elements while maintaining its aperture and performance. The HF97 receive array had 64 elements with 0.3125 wavelength (λ) element separation at 2.5 kHz, and the critical angle of propagation is less than 20°. Therefore, the number of the elements can be reduced to 16 without concern for spatial aliasing.

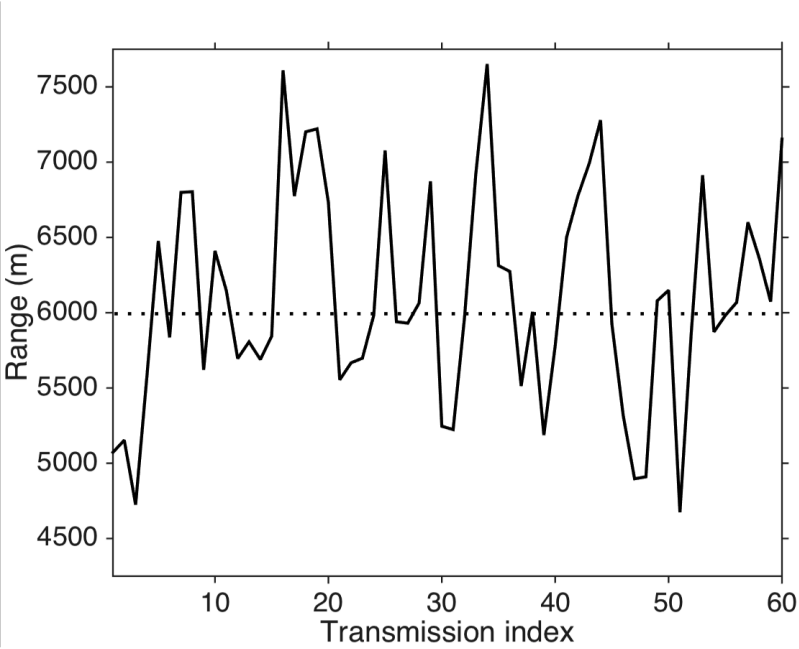

Figure 3.6: Range estimation of HF97 data for one-minute period (i.e., 60 chirp transmissions) at 01:07 UTC, using $\beta = 0.9$. The range estimates are distributed around the mean value of 6.09 km with a standard deviation of 0.77 km.

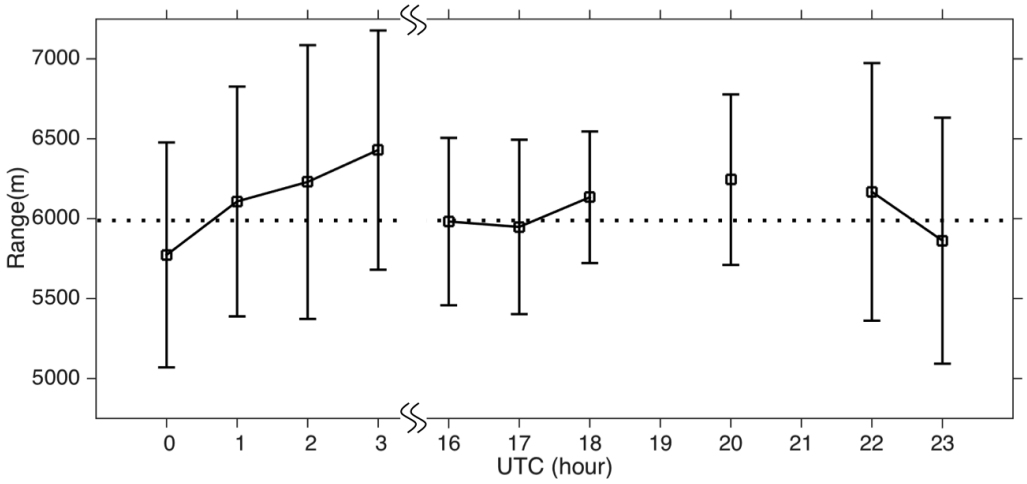

Figure 3.7: Overall performance of HF97 range estimation over an extended period of time on JD301 with hourly means (rectangles) and standard deviations (vertical bars) based on the analysis of a 60 s transmission record per hour. The mean source-range estimates vary between 5.7 and 6.5 km, corresponds to less than 8 % relative error, with standard deviations about those means of less than 0.86 km. Note that there is a data gap between 3 and 16 hours, and the results are not shown at 19 and 21 hours due to noise contamination.

3.6 Summary

The unified array/waveguide invariant approach based on beam-time migration was proposed for robust source-range estimation using a short-aperture vertical array. Rather than the forward model computations required for MFP, the approach involves conventional plane-wave beamforming and a single waveguide invariant parameter β which depends upon the acoustic waveguide. In many shallow-water environments, β can be assumed approximately equal to 1 and any deviation from $\beta = 1$ can be translated to range-estimation errors. With $\beta = 0.9$ incorporating the down-slope bottom bathymetry, the approach was applied successfully to HF97 data in a fluctuating shallow-water environment over a one-day period. Specifically, the mean range estimates using a 12-m long vertical array in $\sim$100 m deep water were less than 8% relative error for a source (2–3 kHz) at 6-km range, demonstrating the robustness of the proposed approach.

3.7 Appendix: Array invariant for vertical arrays χ_v

The array invariant approach in Ref. [3] is summarized with a focus on vertical arrays (VAs). The equations referred to here are from Ref. [3]. Acoustic propagation can be described in terms of normal modes in a range-independent environment. The acoustic pressure field at a receiver (r, z) and frequency f due to a source at (r_0, z_0) can be expressed as follows:

$$P(r, z, f) = 4\pi Q(f) \frac{i}{\sqrt{8\pi}\rho(z_0)} e^{-\frac{i\pi}{4}} \sum_n u_n(z_0) u_n(z) \frac{e^{ik_{rn}|r-r_0|}}{\sqrt{k_{rn}|r-r_0|}}, \tag{3.4}$$

where n is the mode number, k_{rn} the n^{th} horizontal wavenumber, ρ the density, $Q(f)$ the source spectrum, and the n^{th} mode shape $u_n(z)$ that satisfies the orthonormality condition of $\int_0^\infty u_m(z)u_n(z)/\rho(z)dz = \delta_{mn}$. For convenience, a VA is positioned at $r = 0$ with its center depth at z_c, and the horizontal distance between the source and receive array is r_0. (refer to Fig. 3.1).

Assuming that the sound speed variation is minimal across the array aperture [3], the output of conventional plane-wave beamforming in the frequency domain can be derived from Eq. (3.4)

$$P_B(s,f) = 4\pi Q(f)\frac{i}{\sqrt{8\pi}\rho(z_0)}e^{-\frac{i\pi}{4}}\sum_n u_n(z_0)\frac{e^{ik_{rn}r_0}}{\sqrt{k_{rn}r_0}} \times \left[N_n^+ B(s-s_n) + N_n^- B(s+s_n)\right], \tag{3.5}$$

where θ is a grazing angle defined from the horizontal axis (broadside of the array), $s = \sin\theta$, $s_n = \sin\theta_n$, $B(s)$ the beam pattern, and N_n^+ and N_n^- are the plane-wave amplitudes of the n^{th} mode in opposite directions. The n^{th} mode shape satisfies $u_n(z) = N_n^+ e^{ik_{zn}z} + N_n^- e^{-ik_{zn}z}$ with the n^{th} vertical wavenumber k_{zn}. Note that $\sin\theta$ corresponds to $\cos\phi$ in Ref. [3] where ϕ is defined as the elevation angle, i.e., $\phi = \pi/2 - \theta$.

The time-domain beamformer output $P_B(s,t)$ can be obtained simply by taking the inverse Fourier transform of Eq. (3.5),

$$P_B(s,t) = 2\ \mathrm{Re}\left\{\int_0^\infty P_B(s,f)e^{-i2\pi ft}df\right\}, \tag{3.6}$$

where $\mathrm{Re}\{\cdot\}$ represents the real part. Although not employed in this paper, the stationary phase approximation has been applied in Ref. [3] to further obtain analytical expressions when the source signals are transient (refer to Eq. (4) and Appendix A in Ref. [3]).

The array invariant parameter χ_v in Eq. (21) for a vertical array is estimated as follows: (a) multiple peaks are selected from $P_B(s,t)$ in the beam-time domain (s,t) and (b) then a least squares estimate of $\hat{\chi}_v$ is carried out using Eq. (30). Similar to χ_l in Eq. (16) for a horizontal array, we define a new χ_v from Eq. (18)

$$\chi_v \equiv \frac{d(\cos\theta)}{dt} \equiv \frac{d}{dt}\sqrt{1-\sin^2\theta} \simeq -\frac{c}{r_0}. \tag{3.7}$$

In this case, the least squares estimate of $\hat{\chi}_v$ can be obtained from $(1-s^2)^{1/2} = \chi_v t + d_v$ where d_v is a constant intercept. Note that Eq. (3.7) satisfies an elliptic equation in the (s,t) coordinate, consistent with the one derived from the waveguide invariant in Ref. [4].

Finally, the source-range can be estimated from $\hat{r}_0 = -c/\hat{\chi}_v$, where c is an average sound speed across the VA aperture used for conventional plane-wave beamforming $P_B(s, f)$.

Acknowledgment

This work was supported by the Office of Naval Research under grant N00014-13-1-0510.

Chapter 3, in full, is a reprint of the material as it appears in the Journal of Acoustical Society of Americas: Chomgun Cho, H.C. Song, and W. S. Hodgkiss, "Robust source-range estimation using the array/waveguide invariant and a vertical array," *J. Acoust. Soc. Am*, 139 (1), 63-69, 2016. The dissertation author was a primary investigator and author of this material.

Bibliography

[1] A. Tolstoy, *Matched field processing for underwater acoustics* (World Scientific Publishing Co.) (1993), Chap. 2.

[2] S. D. Chuprov, "Interference structure of a sound field in a layered ocean", in *Acoustics of the Ocean*, 71–91 (Nauka, Moscow) (1982), edited by L. M. Breakhovskikh and I. B. Andreevoi.

[3] S. Lee and N. C. Makris, "The array invariant", J. Acoust. Soc. Am. **119**, 336–351 (2006).

[4] H. C. Song and C. Cho, "The relation between the waveguide invariant and array invariant", J. Acoust. Soc. Am. **138**, 899–903 (2015).

[5] F. B. Jensen, W. A. Kuperman, M. B. Porter, and H. Schmidt, *Computational Ocean Acoustics* (Springer, New York) (2011), Chap. 5.

[6] S. V. Burenkov, "Distinctive features of the interference structure of sound field in a two-dimensionally inhomogeneous waveguide", Sov. Phys. Acoust. **35**, 465–467 (1989).

[7] G. L. D'Spain and W. A. Kuperman, "Application of waveguide invariants to analysis of spectrograms from shallow water environments that vary in range and azimuth", J. Acoust.Soc. Am. **106**, 2454–2468 (1999).

[8] D. Rouseff and R. C. Spindel, "Modeling the waveguide invariant as a distribution", Ocean Acoustic Interference Phenomena and Signal Processing **621**, 137–150 (2002).

[9] H. C. Song, W. A. Kuperman, and W. S. Hodgkiss, "A time-reversal mirror with variable range focusing", J. Acoust. Soc. Am. **103**, 3234–3240 (1998).

[10] S. Kim, W. A. Kuperman, W. S. Hodgkiss, H. C. Song, G. F. Edelmann, and T. Akal, "Robust time reversal focusing in the ocean", J. Acoust. Soc. Am. **114**, 145–157 (2003).

[11] A. M. Thode, "Localization uisng Bartlett matched-field processor sidelobes", J. Acoust. Soc. Am. **107**, 278–286 (2000).

[12] A. M. Thode, "Source ranging with minimal environmental information using a virtual receiver and waveguide invariant theory", J. Acoust. Soc. Am. **108**, 1582–1594 (2000).

[13] K. A. Sostrand, "Range localization of 10-100 km explosions by means of an endfire array and a waveguide invariant", IEEE J. Ocean. Eng. **30**, 207–212 (2005).

[14] A. Turgut, M. Orr, and D. Rouseff, "Broadband source localization using horizontal-beam acoustic intensity striations", J. Acoust. Soc. Am. **127**, 73–83 (2010).

[15] H. Tao and J. L. Krolik, "Waveguide invariant focusing for broadband beamforming in an oceanic waveguide", J. Acoust. Soc. Am. **123**, 1338–1346 (2008).

[16] N. M. Carbone and W. S. Hodgkiss, "Effects of tidally driven temperature fluctuations on shallow-water acoustic communications at 18 khz", IEEE J. Oceanic Eng. **25**, 84–94 (2000).

[17] C. H. Harrison, "The relation between the waveguide invariant, multipath impulse response, and ray cycles", J. Acoust. Soc. Am. **129**, 2863–2877 (2011).

[18] H. C. Song and W. S. Hodgkiss, "Self-synchronization and spatial diversity of passive time reversal communication (L)", J. Acoust. Soc. Am. **137**, 2974–2977 (2015).

[19] G. L. D'Spain, J. J. Murray, W. S. Hodgkiss, N. O. Booth, and P. W. Schey, "Mirages in shallow water matched filed processing", J. Acoust.Soc. Am. **105**, 3245–3265 (1999).

[20] M. B. Porter, *"The acoustics toolbox,"* Available: http://oalib.hlsresearch.com /Modes/AcousticsToolbox/ (Last viewed 12/28/2015).

[21] P. Roux, W. A. Kuperman, B. Cornuell, F. Aulanier, W. S. Hodgkiss, and H. C. Song, "Analyzing sound speed fluctuations in shallow water from group-velocity versus phase-velocity data representation", J. Acoust. Soc. Am. **133**, 1945–1952 (2013).

Chapter 4

Iterative range estimation in a sloping-bottom shallow-water waveguide using the generalized array invariant

Authors:
Chomgun Cho
H.C. Song
P. Hursky
S. M. Jesus

4.1 Abstract

The array invariant theory was generalized by incorporating the waveguide invariant β, referred to as the generalized array invariant. In this paper, the generalized array invariant is extended to mildly range-dependent environments with a sloping bottom where the waveguide invariant is variable in range. Assuming

knowledge of the bottom slope, the array invariant can be applied iteratively to estimate the source range starting with β=1 (i.e., range-independent), which converges toward the correct source range by updating β at the previously estimated range. The iterative array invariant approach is demonstrated using a short-aperture vertical array (2.8-m) in a sloping-bottom shallow-water waveguide from the Random Array of Drifting Acoustic Receivers 2007 experiment (RADAR07), where a high-frequency source (2–3.5 kHz) close to the surface (6-m) was towed between 0.5 to 5 km in range with the water depth varying from 80 to 50 m.

4.2 Introduction

The array invariant, first proposed by Lee and Makris [1], has been successful in achieving robust source-range estimation in shallow-water acoustic environments [2, 3]. The approach is based on the dispersion characteristics in ideal waveguides and involves conventional plane-wave beamforming, exploiting multiple arrivals separated in beam angle and travel time, i.e., beam-time migration. The array invariant [1] was extended to general waveguides by incorporating the waveguide invariant β, referred to as the generalized array invariant [3]. For ideal waveguides and reflection-dominated environments, the waveguide invariant is approximately unity ($\beta \approx 1$) for small grazing angles (e.g., $< 20°$). As a result, the original array invariant [1] was assumed to be independent of the waveguide invariant. Using a short- [2] or long-aperture [3] vertical array, the generalized array invariant for source-range estimation was demonstrated in shallow-water environments for relatively high-frequency sources (e.g., above 1 kHz), with minimal knowledge of the environment and computational efficiency.

The inclusion of the waveguide invariant β in the formulation [2–6] implies that the generalized array invariant can be extended to mildly range-dependent environments where mode propagation is adiabatic and thus the waveguide invariant is meaningful via the generalized waveguide invariant [7]. The objective of this paper is to demonstrate the array invariant-based source-range estimation in shallow-water environments with range-varying bottom bathymetry using at-sea

data.

The waveguide invariant for an ideal waveguide with a sloping bottom was derived by D'Spain and Kuperman using the adiabatic approximation [8], which is simply a ratio of the water depth at the source location to that at the receiver location. The main drawback for source range estimation is that an accurate value of β requires prior knowledge of the water depth at the source range (r_0) to be estimated. Assuming that the bottom slope is known to the receiver, we propose an iterative array invariant to estimate the source range starting with $\beta = 1$ (i.e., range-independent), which converges toward the correct source range by updating $\beta(\hat{r})$ at the previously estimated range ($\hat{r}$). The iterative array invariant approach will be experimentally verified using a short-aperture vertical array (2.8 m) in a sloping-bottom shallow-water waveguide, where a high-frequency source (2–3.5 kHz) near the surface (6-m) was towed between 0.5 to 5 km in range with the water depth varying from 80 to 50 m.

The paper is organized as follows. Section 4.3 reviews the generalized array invariant and generalized waveguide invariant for an ideal waveguide with a sloping bottom, including a high-order approximation that is derived in the Appendix. Then the iterative approach to range estimation is described in conjunction with the array invariant. Section 4.4 describes the Random Array of Drifting Acoustic Receivers 2007 (RADAR07) experiment [9], conducted off Setúbal, Portugal, in July 2007, with a major focus on the source-tow run in a sloping environment. In Sec. 4.5, the performance of tracking the towed source using the iterative array invariant is presented, followed by a summary in Sec. 4.6.

4.3 Generalized array invariant for a sloping bottom

The generalized array invariant that includes the waveguide invariant β is derived in the literature [3, 4]. The source range r_0 can be estimated simply from

$$r_0 = -\beta \left(\frac{c}{\chi} \right), \tag{4.1}$$

where c is the local sound speed used for beamforming. For an ideal waveguide with $\beta = 1$, this formula reduces to the original array invariant [1].

The array invariant parameter χ is defined as

$$\chi \equiv \frac{d}{dt}(\cos\theta) = \frac{d}{dt}\sqrt{1-\sin^2\theta} = \frac{d}{dt}\sqrt{1-s^2}, \tag{4.2}$$

where $s = \sin\theta$ with the grazing angle θ from the horizontal and t is the travel time. The above equation can be expressed as an elliptic curve in the beam-time (s, t) coordinate (see Fig. 4.3):

$$\left(\frac{t-t_0}{1/\chi}\right)^2 + \sin^2\theta = 1, \tag{4.3}$$

where $1/|\chi|$ is the horizontal semi-major axis and the center of ellipse is at $(0, t_0)$ [4]. The parameter χ can be estimated numerically from the beam-time migration data, e.g., using the least-squares (LS) approach as described in the Appendix of Ref. [3].

4.3.1 Generalized waveguide invariant for a sloping bottom

For an ideal waveguide with a sloping bottom, D'Spain and Kuperman [8] derived a generalized waveguide invariant such that

$$\frac{1}{\beta} = \frac{D_r}{D_s}, \tag{4.4}$$

where D_r and D_s are the water depth at the receiver and the source location, respectively. This simple expression was then experimentally verified to analyze the data collected in a bottom-slope shallow-water environment. For a range-independent environment, i.e., when $D_r = D_s$, Eq. (4.4) reduces to $\beta = 1$, which is also valid in many bottom-interacting shallow-water environments.

Since the source range (r_0) is proportional to β in Eq. (4.1), it is important to assess the accuracy of the simple expression Eq. (4.4). Thus, we have revisited the derivation in the Appendix where Eq. (4.4) corresponds to a zeroth-order approximation, Eq. (4.8). On the other hand, the first-order approximation derived in Eq. (4.10), which is almost identical to the analytic expression in Eq. (4.5), has an additional term that depends on the grazing angle (or mode number). For

an up-slope bottom similar to the RADAR07 environment, the zeroth-order approximation is estimated to be about 6% larger than the first-order approximation when averaged over up to the bottom critical angle of $\sin 24°$ (refer to Fig. 4.5). Consequently, the trade-off of using the simple expression Eq. (4.4) with the array invariant would be over-estimation of the source range, as will be confirmed in Sec. 4.5.

4.3.2 Iterative array invariant

The array invariant-based source-range estimation using Eq. (4.1) includes β, which is approximately unity in many shallow-water environments [7]. For range-dependent sloping bottom, however, an accurate value of β in Eq. (4.4) requires prior knowledge of the water depth (D_s) at the source range (r_0) to be estimated. Assuming the bottom slope is known to the receiver, the array invariant approach can be employed iteratively as follows:

1. Estimation of the array invariant parameter χ from the beam-time migration data

2. Initial range estimate of $\hat{r}_0 = -c/\chi$, assuming $\beta_0 = 1$ (i.e., $D_s = D_r$) and $c = 1500\ m/s$

3. Iterative range estimate of $\hat{r}_k = \beta_k \hat{r}_0$ with an updated $\beta_k = D(\hat{r}_{k-1})/D_r$, where $D(x)$ is the water depth at the estimated source range x in the previous iteration.

4. Convergence check: $|\hat{r}_k - \hat{r}_{k-1}| \leq R_c$ (e.g., 100 m), a radius of convergence (threshold)

4.4 RADAR07 experiment

The RADAR07 experiment was performed in 9-15 July 2007 on the continental shelf off the west coast of Portugal, roughly 23 km south of Setúbal [9]. This

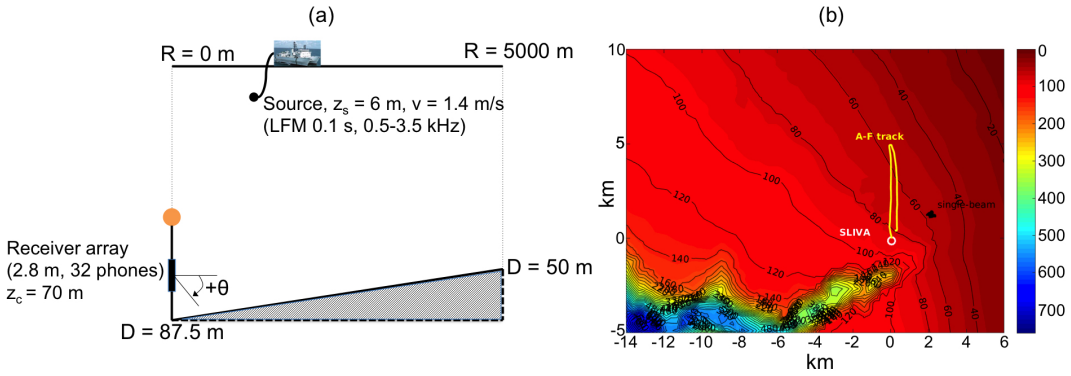

Figure 4.1: (Color online) RADAR07 source-tow experiment overview: (a) schematic of the deployed hardware in a simplified sloping environment and (b) complex bottom bathymetry off Setúbal, Portugal, along with the ship track (yellow line), first in the up-slope and then down-slope direction. The open circle (○) denotes the receiver array location (SLIVA). The water depth is in meters.

is a dynamic site with significant internal tide activity due to the complex bathymetric features, including a canyon, seamounts, and a narrow continental shelf. The experiment was a multi-institutional effort between University of Algarve's SiPLAB, Nato Undersea Research Centre (NURC), the Hydrographic Institute (of the Portuguese Navy), Naval Research Laboratory (NRL), and Heat, Light and Sound (HLS) Research Inc. The experiment was designed to support research in several areas, including matched field tomography and underwater communications. Two research vessels from the Hydrographic Institute of Portugal were used, NRP Don Carlos I and NRP Auriga. Active acoustic signals were transmitted from NRP D. Carlos I towing three different acoustic sources covering 0.5–20 kHz and were received by multiple receive arrays, drifting or moored.

To investigate the proposed iterative array invariant approach, our analysis will focus on the source-tow run carried out on JD 194 (July 13), from 16:38 to 18:19 UTC (about 2 hours). The schematic of the experiment is illustrated in Fig. 4.1 along with the bathymetry. A broadband low-frequency source (0.5–3.5 kHz) was deployed to about 6-m depth and towed mostly at a speed of about 3 knots (1.4 m/s) by the NRP D. Carlos I along the specified A-F source-tow track in a sloping environment, first in the up-slope and then down-slope direction. The white circle (○) in Fig. 4.1b indicates the location of NURC's SLIVA (SLIm Vertical

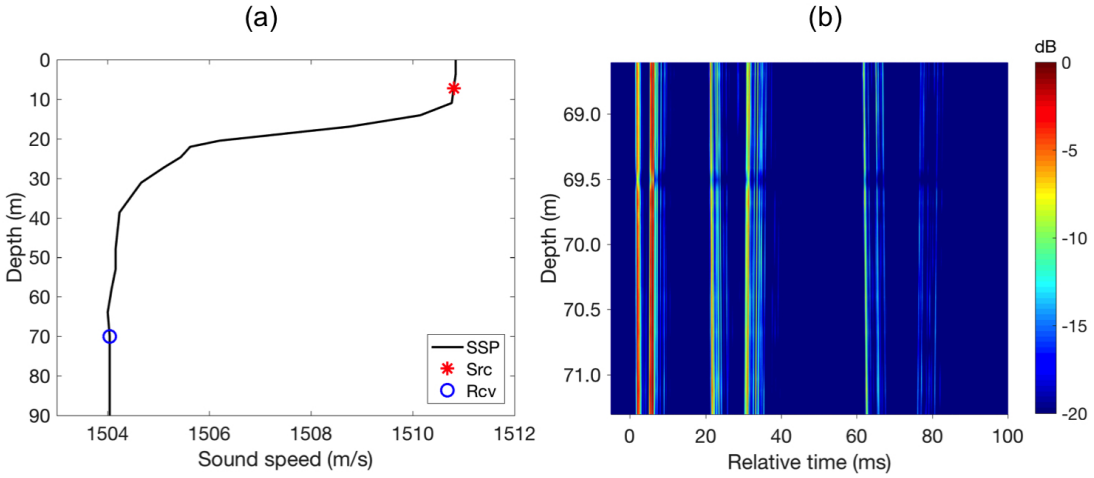

Figure 4.2: (Color online) (a) A representative sound speed profile during the source-tow run on JD 194. The source at 6-m depth (∗) is in the surface mixed layer, while the receiver at 70-m depth (∘) is well below the thermocline in a downward-refracting environment. (b) Channel impulse response (CIR) measured at a range of 0.7 km, indicating a delay spread of about 80 ms with 6 distinct arrivals. The plot is normalized by the maximum intensity and displayed in dB. Few hydrophones (e.g., at 68.6 and 69.5 m) were not working properly and thus excluded for conventional plane-wave beamforming.

Array) moored in about 87.5-m water depth, consisting of three nested subsets of hydrophones spaced for various frequency bands of interest. In this paper, we will use a subset of 32-element line array with a 2.8-m aperture centered around 70-m depth. Note that the bottom bathymetry is approximated by a simple sloping bottom in Fig. 4.1a, facilitating the iterative approach based on the knowledge of the slope. This work utilizes 100-ms, 0.5–3.5 kHz linear frequency modulated (LFM) chirp channel probe transmitted at various ranges (0.5–5 km) during the source-tow run.

Environmental data included water-column sound-speed profiles (SSPs) using CTD (conductivity, temperature, and depth) and thermistor strings. Two SSPs measured prior to the source-tow run were averaged out in Fig. 4.2a, which is a downward-refracting environment with the mixed layer depth down to 10 m. The towed source at 6-m depth (∗) is in the mixed layer, while the receiver array (∘) is well below the thermocline at 70-m depth. The source near the surface can excite high-order modes that interact with surface and bottom; thus, these modes

behave like ones in an ideal waveguide from which the array invariant originated. As a result, all the high-order modes (i.e., ray arrivals) can be used to estimate the source range based on the array invariant.

An example of channel impulse response (CIR) at 0.7 km range is displayed in Fig. 4.2b, indicating six distinct arrivals with a delay spread of about 80 ms. The plot is normalized by the maximum intensity and displayed in dB. Few hydrophones (e.g., at at 68.6 and 69.5 m) were not working properly; thus, they are excluded for plane-wave beamforming.

4.5 Source tracking in a sloping environment

The RADAR07 data collected during the source-tow run (16:38–18:19 UTC) are analyzed to track the source traveling in a sloping environment as depicted in Fig. 4.1. The source signal was a 100-ms, 0.5–3.5 kHz, LFM chirp transmitted at 0.2-s intervals for 4 s (i.e., 20 chirp transmissions) and then repeatedly every 30 s at various ranges from 0.5 km up to 5 km. To improve the beam resolution given the aperture of the array (2.8 m), only the upper-half frequency band (i.e., 50-ms, 2–3.5 kHz) is utilized for matched-filtering and beamforming.

4.5.1 Beam-time migration

The beam-time migration (s, t) is presented in Fig. 4.3 for three representative source ranges: (a) 0.7 km, (b) 2.8 km, and (c) 4.9 km. The water depth at the corresponding range is 75 m, 62 m, and 55 m, respectively. The vertical axis denotes the beam ($s = \sin\theta$) with a positive angle θ defined for an up-going paths (red circles), and the horizontal axis is the relative travel time (t). A varying number of arrivals were identified at different ranges, determined by a threshold set to find peaks (e.g., -10 dB) [3]. For instance, there are two up-going (circles) and three down-going (squares) arrivals at 0.7 km, whereas many more arrivals up to 11 are captured at 2.8 km.

Following the steps in Sec. 4.3.2, an elliptic curve (solid line) that best fits the identified arrivals (circles and squares) in the least-squares (LS) sense [3] can

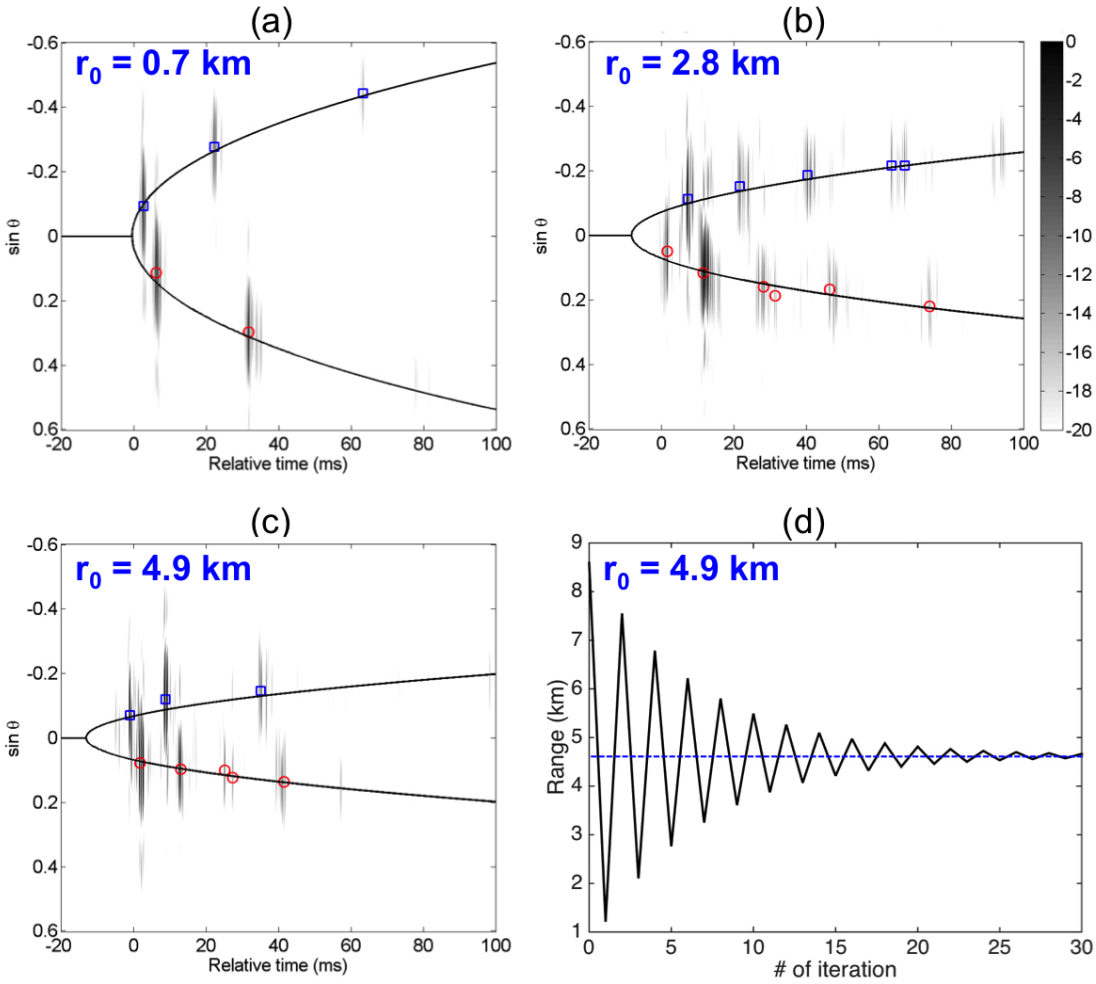

Figure 4.3: (Color online) Beam-time migration at three representative ranges: (a) 0.7 km (16:41), (b) 2.8 km (17:06), and (c) 4.9 km (17:29 UTC). The water depth at the corresponding range is 75, 62, and 55 m. A positive beam angle represents an up-going path (red circles), and the dynamic range is 20 dB. Note that the curvature of the elliptic curve increases with range. A different number of distinct arrivals (circles and squares) is used to estimate the array invariant parameter χ at different ranges. (d) Iterative range estimation in a sloping environment for a source at 4.9 km range corresponding to (c). The range estimate is initially 8.6 km assuming $\beta = 1$ (range-independent) and c = 1500 m/s, but gradually converges toward 4.6 km in a zig-zag fashion with a relative range error of -6%. The performance of iterative range estimation is summarized in Table 4.1.

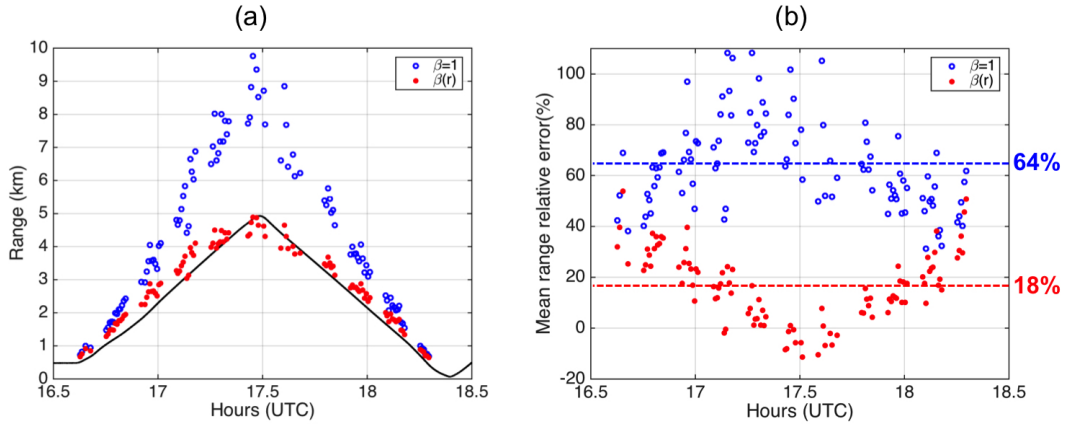

Figure 4.4: (Color online) (a) Source-range estimation during the source-tow run for about 2 hours (16:38–18:19): assuming $\beta = 1$ (open circles, blue) and using the iterative approach with $\beta(r)$ (solid circles, red). The solid line is based on the ship GPS. (b) Corresponding relative range errors (%). The mean relative range error with the iterative approach is about 18%.

be drawn with an appropriate array invariant parameter χ (refer to Table 4.1). It is noticeable that the curvature of the ellipses increases as the range increases. The iterative array invariant approach to range estimation is illustrated in Fig. 4.3d for the source at 4.9 km range. The range estimate is initially 8.6 km assuming $\beta = 1$ and $c = 1500\ m/s$, but gradually converges over the iteration toward 4.6 km in a zig-zag fashion, with a relative range error of -6%. The performance of iterative range estimation for the above three ranges is summarized in Table 4.1.

Table 4.1: Iterative source-range estimation from beam-time migration shown in Fig. 4.3 at various ranges.

Source range (r_0)	Water depth (D_s)	$\beta(r_0) = D_s/D_r$	χ	Initial estimate with $\beta = 1$	Range estimate ($\hat{r}_0$)	Relative range error
(a) 0.7 km	75 m	0.86	-1.60	0.9 km	0.9 km	25%
(b) 2.8 km	62 m	0.71	-0.31	4.8 km	3.3 km	17%
(c) 4.9 km	55 m	0.63	-0.17	8.6 km	4.6 km	-6%

4.5.2 Source-range tracking

During the source-tow run, the LFM chirp signal was transmitted continuously at 0.2-s intervals for 4 s (i.e., 20 chirp transmissions) and then repeated every 30 s over almost two hours. Thus, for each range, the mean range estimate was obtained from 20 transmissions. The overall performance of range estimate is presented in Fig. 4.4 over the entire source-tow run. The solid line is based on the ship GPS data where the towed source was assumed to be about 70 m behind the actual GPS location, although the offset is relevant only at close ranges (e.g., < 1 km).

The open circles ($\circ$) obtained with $\beta = 1$ do not take into account the variability of $\beta(r)$ in a sloping range-dependent environment. As a result, the range error increases significantly with range such that the relative range error exceeds 100% at about 5 km range. On the other hand, the iterative array invariant approach ($\bullet$) even with a simplified sloping bottom in Fig. 4.1a provides good performance over the entire source track with the relative range error of about 18%. As described in the Appendix, the source range is mostly over-predicted because the simple expression for the waveguide invariant in Eq. (4.4) is always larger than the exact value. A few exceptions of under-prediction at around 5 km (e.g., -6%) are likely due to the mismatch between the simplified sloping bottom and the actual bottom bathymetry. Additional uncertainty is attributed to the fact that the derivation of β is based on a two-dimensional sloping bottom, neglecting the three-dimensional propagation effect in the RADAR07 environment.

4.6 Summary

The generalized array invariant that includes the waveguide invariant β has been successful for source range estimation with minimal environmental information and using a short-aperture vertical array in shallow water. In this paper, the array invariant was extended to a range-dependent environment with a sloping bottom where β requires prior knowledge of the water depth at the source range to be estimated. To get around the problem, an iterative approach was proposed,

which starts with $\beta = 1$ but gradually converges toward the correct source range by updating β at the previously estimated source range. The iterative array invariant approach was demonstrated using a short-aperture vertical array (2.8 m) in a sloping-bottom shallow-water environment, where a high-frequency source (2–3.5 kHz) near the surface (6-m) was towed between 0.5 to 5 km in range with the water depth varying from 80 to 50 m. The mean absolute relative range error was about 18% during the entire source-tow run.

4.7 Appendix: Waveguide invariant for an ideal waveguide with a sloping bottom

The starting point is the expression for the waveguide invariant $\beta(r_0)$ derived in Ref. [8] for an ideal waveguide with range-varying bottom bathymetry where mode propagation is adiabatic (refer to Eq. (22) of Ref. [8])

$$\frac{1}{\beta(r_0)} = \frac{(1-\gamma_n^2(0)/k^2)^{1/2}}{\gamma_n^2(0)} \frac{1}{r_0} \int_0^{r_0} \frac{\gamma_n^2(x)}{(1-\gamma_n^2(x)/k^2)^{3/2}} dx, \tag{4.5}$$

where $\gamma_n(x)$ is the nth-mode vertical wave number, k is the medium wave number, and r_0 is the source range from the receiver at $r = 0$. For the low-order modes where $\gamma_n^2/k^2 \ll 1$, we can apply the first-order Taylor approximation [10] to each of the two power functions containing γ_n^2/k^2, and Eq. (4.5) thus becomes

$$\frac{1}{\beta(r_0)} \approx \left(\frac{1}{\gamma_n^2(0)} - \frac{1}{2k^2} \right) \frac{1}{r_0} \int_0^{r_0} \left(\gamma_n^2(x) + \frac{3\gamma_n^4(x)}{2k^2} \right) dx. \tag{4.6}$$

Neglecting the product of the two first-order terms (i.e., $\frac{1}{2k^2} \times \int_0^{r_0} \frac{3\gamma_n^4(x)}{2k^2} dx$), we obtain

$$\frac{1}{\beta(r_0)} \approx \frac{1}{\gamma_n^2(0)} \frac{1}{r_0} \int_0^{r_0} \gamma_n^2(x) dx + \frac{1}{\gamma_n^2(0)} \frac{1}{r_0} \int_0^{r_0} \frac{3\gamma_n^4(x)}{2k^2} dx - \frac{1}{2k^2} \frac{1}{r_0} \int_0^{r_0} \gamma_n^2(x) dx. \tag{4.7}$$

The first term on the right-hand side, corresponding to a zeroth-order approximation, can be simplified for an ideal waveguide with a sloping bottom

$$\frac{1}{\gamma_n^2(0)} \frac{1}{r_0} \int_0^{r_0} \gamma_n^2(x) dx = \frac{D_r^2}{r_0} \int_0^{r_0} \frac{1}{d_n^2(x)} dx = \left(\frac{D_r}{D_s} \right), \tag{4.8}$$

where $\gamma_n(x) = n\pi/d(x)$, $\gamma_n(0) = n\pi/d(0)$, $d(x) = D_r + Ax$ with A representing the bottom slope. The water depths at the receiver and the source locations are D_r and $D_s = D_r + Ar_0$, respectively. D'Spain and Kuperman [8] used this formula for the analysis of data collected in a sloping shallow-water environment. For a range-independent case (i.e., $D_r = D_s$), the zeroth-order waveguide invariant becomes equal to one ($\beta = 1$).

The second and third terms on the right-hand side of Eq. (4.7), corresponding to the first-order approximation, can be combined into a simple expression

$$\begin{aligned}
&\frac{1}{\gamma_n^2(0)}\frac{1}{r_0}\int_0^{r_0}\frac{3\gamma_n^4(x)}{2k^2}dx - \frac{1}{2k^2}\frac{1}{r_0}\int_0^{r_0}\gamma_n^2(x)dx \\
&= \frac{3n^2\pi^2 D_r^2}{2k^2}\frac{1}{r_0}\int_0^{r_0}\frac{1}{d^4(x)}dx - \frac{n^2\pi^2}{2k^2}\frac{1}{r_0}\int_0^{r_0}\frac{1}{d^2(x)}dx \\
&= \frac{n^2\pi^2}{D_r^2k^2}\frac{D_r^2}{D_s^2}\left(\frac{D_r + D_s}{2D_s}\right) = \sin^2\theta_n\left(\frac{D_r}{D_s}\right)^2\left(\frac{D_{avg}}{D_s}\right),
\end{aligned} \tag{4.9}$$

where $D_{avg} = (D_r + D_s)/2$ is the averaged water depth and θ_n is the grazing angle of nth mode at the receiver. From Eqs. (4.8) and (4.9), we obtain an expression for the waveguide invariant $\beta(r_0)$ in an ideal waveguide with a sloping bottom that includes up to the first-order terms

$$\frac{1}{\beta(r_0)} \approx \left(\frac{D_r}{D_s}\right) + \left(\frac{D_{avg}}{D_s}\right)\left(\frac{D_r}{D_s}\right)^2 \sin^2\theta_n. \tag{4.10}$$

Besides the water depth at the source and receiver locations, the first-order waveguide invariant $\beta(r_0)$ depends on the grazing angle θ_n at the receiver. For a range-independent case ($D_r = D_s$), the above expression reduces to $\beta = 1/(1+\sin^2\theta_n) \approx \cos^2\theta_n$ for small angles (e.g., $\sin\theta < 0.4$), which is the analytic expression for the waveguide invariant in ideal waveguide suppressing the modal index ($\beta = \cos^2\theta$) [7]. It should be mentioned that Burenkov [11] also provided a similar first-order approximation where the factor (D_{avg}/D_s) was missing in the second term.

To investigate the accuracy of the above approximations, the waveguide invariant $\beta(r_0)$ is evaluated at 2 km range for an upslope bottom similar to the RADAR07 and is displayed in Fig. 4.5 as a function of grazing angle (or mode number). The water depths at the receiver and source location are 87.5 m and 72.5

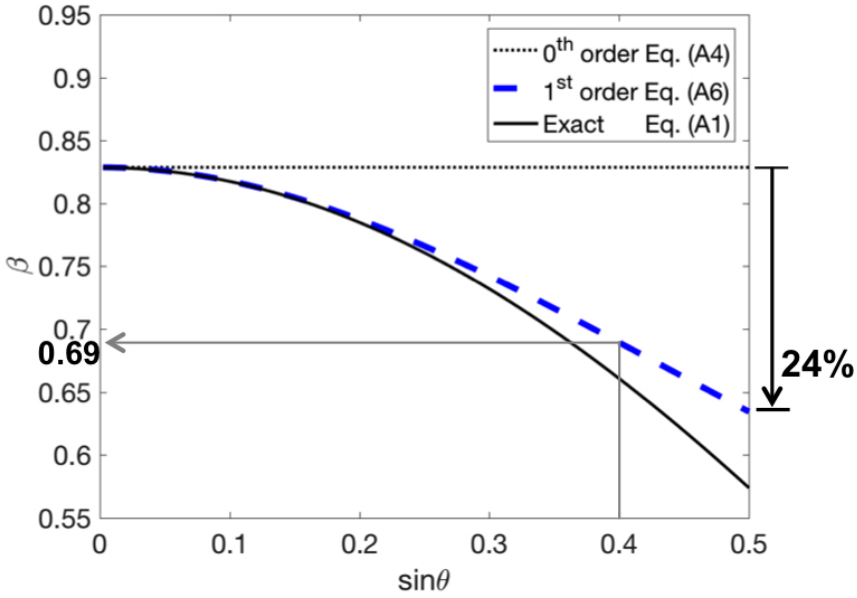

Figure 4.5: (Color online) The waveguide invariant $\beta(r_0)$ evaluated at 2-km range for an upslope bottom as a function of grazing angle (or mode number). The water depth at the receiver and source location is 87.5 m and 72.5 m, respectively, and the bottom critical angle for the RADAR07 environment is about $\sin\theta = 0.4$. The zeroth order approximation (dotted horizontal line) is 24% higher than the first-order approximation (dashed blue line) at $\sin\theta = 0.5$.

m, respectively. While the first-order approximation (dashed line) of Eq. (4.10) gradually decreases with an increase in the grazing angle (i.e., high-order modes), it is almost identical to the exact solution of Eq. (4.5) (solid line) up to $\sin\theta = 0.2$ and the deviation at $\sin\theta = 0.5$ is less than 10%. On the other hand, the zeroth-order approximation of Eq. (4.8) (dotted horizontal line) has a constant value of $\beta = 0.83$, which is about 24% higher than the first-order approximation at $\sin\theta = 0.5$. Although not shown here, similar results were obtained at other ranges. The bottom critical angle for the RADAR07 environment was about $\sin 24^\circ = 0.4$.

The source-range estimation based on the generalized array invariant is directly affected by the accuracy of β via Eq. (4.1). The average value of β from the horizontal up to the critical angle is about 0.78, which is 6% less than the zeroth-order approximation of 0.83. Thus, the range estimate based on the generalized array invariant using $\beta = 0.83$ is larger than the actual source range. This is

evident in Fig. 4.4 where the majority of the data indicates an over-prediction in source-range estimates with a few exceptions at around 5 km ranges.

Acknowledgment

Chomgun Cho and Hee-chun Song were supported by the Office of Naval Research under Grant No. N00014-13-1-0510. The authors gratefully acknowledge the captains and crew of NRP Don Carlos I and NRP Auriga from the Portuguese Navy, the engineering staff from NURC, and the graduate students from the University of Algarve, who helped perform the RADAR07 experiment. The participation of HLS Research Inc. in the RADAR07 experiment was funded through a Phase 2 STTR, Topic N05-T022, titled Acoustic Communications Modem Using MIMO Technology, performed for Bob Headrick and the ONR Ocean Acoustics program.

Chapter 4, in full, is a reprint of the material as it appears in the Journal of Acoustical Society of Americas: Chomgun Cho and H.C. Song, P. Hursky, and S. M. Jesus, "Iterative range estimation in a sloping-bottom shallow-water waveguide using the generalized array invariant," *J. Acoust. Soc. Am*, 142 (1), 55-60, 2017. The dissertation author was a primary investigator and author of this material.

Bibliography

[1] S. Lee and N. C. Makris, "The array invariant," J. Acoust. Soc. Am. **119**, 336–351 (2006).

[2] C. Cho, H. C. Song, and W. S. Hodgkiss, "Robust source-range estimation using the array/waveguide invariant and a vertical array," J. Acoust. Soc. Am. **139**, 63–69 (2016).

[3] H. C. Song and C. Cho, "Array invariant-based source localization in shallow water using a sparse vertical array," J. Acoust. Soc. Am. **141**, 183–188 (2017).

[4] H. C. Song and C. Cho, "The relation between the waveguide invariant and array invariant (L)," J. Acoust. Soc. Am. **138**, 899–903 (2015).

[5] C. Cho and H. C. Song, "Impact of array tilt on source-range estimation in shallow water using the array invariant," J. Acoust. Soc. Am. **141**, 2849–2856 (2017).

[6] H. C. Song, C. Cho, G. Byun, and J. S. Kim, "Cascade of blind deconvolution and array invariant for robust source-range estimation (L)," J. Acoust. Soc. Am. **141**, 3270–3273 (2017).

[7] F. B. Jensen, W. A. Kuperman, M. B. Porter, and H. Schmidt, *Computational Ocean Acoustics* (Springer, New York) (2011), Chap. 2, pp. 133–139.

[8] G. L. D'Spain and W. A. Kuperman, "Application of waveguide invariants to analysis of spectrograms from shallow water environments that vary in range and azimuth," J. Acoust. Soc. Am. **106**, 2454–2468 (1999).

[9] C. Soares, S. M. Jesus, P. Hursky, T. Folegot, C. Martins, F. Zabel, L. Quaresma, D.-S. Ko, E. F. Coelho, "Random Array of Drifting Acoustic Receivers (RADAR'07)," available at: http://sapientia.ualg.pt/handle/10400.1/5277/ (Last viewed 6/28/2017).

[10] K. F. Riley, M. P. Hobson, and S. J. Bence, *Mathematical methods for physics and engineering: a comprehensive guide* (Cambridge University Press) (2006), Chap. 4, pp. 139–140.

[11] S. V. Burenkov, "Distinctive features of the interference structure of a sound field in a two-dimensionally inhomogeneous waveguide," Sov. Phys. Acoust. **35**, 465–467 (1989).

Chapter 5

Array invariant-based source localization in shallow water using a sparse vertical array

Authors:
H.C. Song
Chomgun Cho

5.1 Abstract

The array invariant proposed for robust source localization in shallow water exploits the beam-time migration of broadband signals. The approach requires minimal knowledge of the environment, but involves plane wave beamforming using a short-aperture vertical array in stratified acoustic waveguides. In this paper, the array invariant approach is extended to a large-aperture vertical array that is sparse with significant variation of the sound speed across the aperture for conventional beamforming. The extension is feasible because the array invariant in shallow water utilizes surface/bottom-reflected arrivals that behave like those in ideal waveguides.

Robust source-range estimation is demonstrated using data from a 16-element, 56-m long vertical array at various ranges (1.5–3.5 km) from a broadband source (0.5–2 kHz) in approximately 100-m deep shallow water.

5.2 Introduction

The array invariant [1], denoted by χ, was proposed for robust source-range estimation in shallow-water environments, which involves conventional plane wave beamforming using a vertical or horizontal array. The approach is based on the dispersion characteristics in ideal waveguides and utilizes multiple arrivals separated in beam angle and travel time. The benefit of the approach is that no forward model computations are required, thus avoiding the potential environmental mismatch inherent in matched-field processing (MFP), especially for source frequencies above 1 kHz [2] [3] [4]. The method was first demonstrated using simulations and experimental data collected from a towed horizontal array [1]. Despite its robustness and computational simplicity, the array invariant has not received much attention.

Recently it was revealed [5] that the array invariant based on the beam-time migration can be derived directly from the well-known waveguide invariant theory [6]. Specifically, the array invariant is a special case of the waveguide invariant parameter $\beta = 1$, which is not only a canonical value for ideal waveguides from which the array invariant originated, but is also applicable to many shallow-water environments involving surface/bottom-interacting ray paths. As a result, the array invariant [1] was successfully applied without explicitly invoking the waveguide invariant. The implication is that the array invariant can be extended to general waveguides with different values of β, fully supported by the physics of the waveguide invariant. Subsequently, the unified array/waveguide invariant approach to source-range estimation was demonstrated using a short-aperture vertical array (12-m) for a broadband source (2–3 kHz) at 6-km range in approximately 100-m deep shallow water [7].

The array invariant requires broadband signals for multipath separation in

beam angle and travel time, where the resolution in beam and time depends on the array aperture, center frequency, and signal bandwidth. An important and practical question is whether the array invariant approach is applicable to a large aperture vertical array employed for MFP in stratified acoustic waveguides where (i) the array is sparse and (ii) the sound speed varies significantly across the array aperture for conventional plane wave beamforming. The contribution of this paper is two-fold. First, the array invariant is reformulated into a generalized array invariant that formally incorporates the waveguide invariant in the derivation. Second, it is demonstrated using experimental data that indeed a sparse vertical array can be utilized for the array invariant-based source-range estimation in shallow water.

The rest of the paper is organized as follows. Section 5.3 discusses the generalized array invariant and range estimation, with a detailed derivation provided in the Appendix. Then a recent shallow water experiment conducted in the northeastern East China Sea is briefly described in Sec. 5.4. A representative channel impulse response (CIR) captured by a vertical array from a modest broadband source (0.5–2 kHz) is analyzed and compared to a simulated CIR using a normal mode propagation model. Section 5.5 presents the beam-time migration and source-range estimation at various ranges (1.5–3.5 km), followed by a summary in Sec. 5.6.

5.3 Generalized array invariant

The generalized array invariant χ that includes the waveguide invariant β is derived in the Appendix. From Eq. (5.9), the source range r_0 can be estimated simply from

$$r_0 = -\beta \left(\frac{c}{\chi} \right), \tag{5.1}$$

where c is the local sound speed used for beamforming. For an ideal waveguide with $\beta = 1$, this formula reduces to the expression in the array invariant [1].

The array invariant parameter χ should be estimated numerically from the beam-time migration data [7], e.g., using the least-squares approach described in

the Appendix. For a vertical array denoted by a subscript v, the measured beam angle is $s_v = \sin\theta$ with the grazing angle θ defined in Fig. 5.5b, and χ_v can be calculated from Eq. (5.8)

$$\chi_v \equiv \frac{d}{dt}\sqrt{1 - s_v^2}. \tag{5.2}$$

The above equation leads to an elliptic curve in (s_v, t) coordinate, as will be illustrated in Sec. 5.5 (see Figs. 5.3 and 5.4).

5.4 SAVEX15 Experiment

A Shallow-water Acoustic Variability EXperiment (SAVEX15) was conducted in the northeastern East China Sea during May 2015. The goal of SAVEX15 was to obtain acoustic and environmental data appropriate for studying the coupling of oceanography, acoustics, and underwater communications in the region. The experimental site had a nearly flat sandy bottom and water depth of approximately 100 m. Both fixed and towed source transmissions were carried out to two moored vertical line arrays (VLAs) over ranges of 1–10 km. The acoustic transmissions were in various frequency bands covering 0.5 to 32 kHz and included both channel probing waveforms as well as communication transmissions. Environmental data included water column sound speed structure, sea surface directional wave field, and local wind speed and direction.

To examine array invariant-based source-range estimation, a segment of data is analyzed during a source-tow run conducted on JD 146 (May 26), from 16:40 to 16:55 UTC. The schematic of the source-tow run is illustrated in Fig. 5.1a. A broadband source (0.5–2 kHz) called SeaNos was deployed to about 50-m depth and towed by the R/V Onnuri mostly at a speed of 4 knots (2 m/s) along a specified ship track. The SeaNos source level (SL) was 165 dB re μPa @ 1 m. The VLA consisted of 16 elements spanning a 56.25-m aperture with 3.75-m element spacing, covering about half the water column (from 25 to 81 m) in about 100-m deep water. This work utilizes a 100-ms, 0.5–2 kHz linear frequency modulated (LFM) chirp channel probe transmitted at various ranges (1.5–3.5 km) from the VLA.

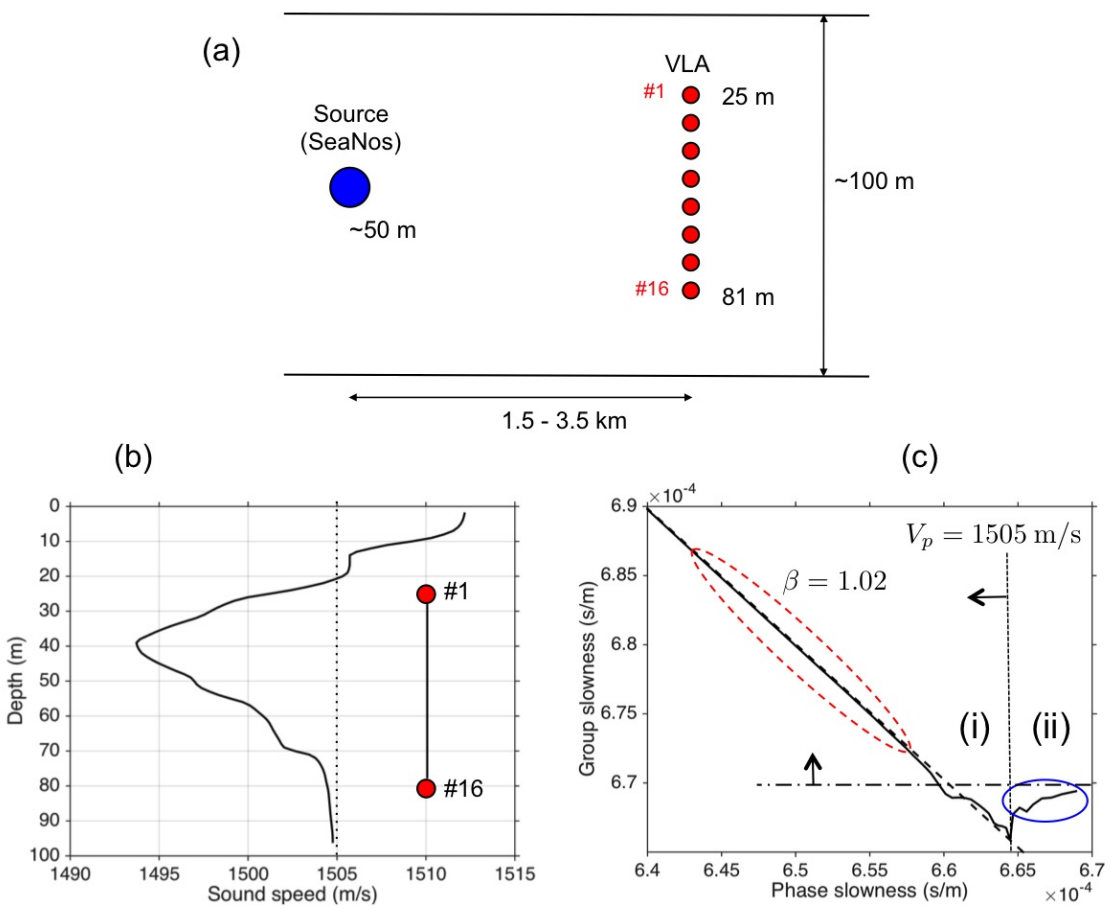

Figure 5.1: (Color online) (a) Schematic of a source-tow run on JD 146 (May 26). A 16-element vertical line array (VLA) was moored in 100-m deep water. A broadband source (0.5–2 kHz) deployed to 50-m depth was towed at a radial speed of approximately 2 m/s at various ranges (1.5–3.5 km). (b) SSP averaged from 3 CTD profiles collected around JD 146, featuring an asymmetrical underwater sound channel (USC) with the channel axis at 40 m. The vertical line (dotted) at 1505 m/s corresponds to the lower edge of the USC. (c) Group slowness (S_g) versus phase slowness (S_p) curve at the center frequency of 1.25 kHz. The modes are grouped into two regions depending on the phase speed $V_p = 1/S_p$: (i) high-order modes with $V_p > 1505$ m/s and (ii) low-order modes with $V_p < 1505$ m/s (blue circle). The dashed line is an approximate slope of the group (i) modes associated with the waveguide invariant $\beta = 1.02$. The high-order, late-arriving modes within the slanted ellipse (above the horizontal line) will be exploited for array invariant-based range estimation in Sec. 5.5.

A sound speed profile (SSP) averaged from three CTD (conductivity, temperature, and depth) casts conducted before and after the source-tow run is shown in Fig. 5.1b. Surprisingly, the SSP indicates an underwater sound channel (USC) that is typical for deep water, although a similar USC is also observed during the summer in the shallow southern Baltic Sea [8]. The USC is asymmetric with respect to the channel axis at 40 m close to the source depth (50 m), and the sound speed of 1505 m/s corresponds to the bounding region of the USC (vertical dotted line). While the maximum sound speed difference between the sound channel and surface/seafloor amounts to 20 m/s, the variation of the sound speed across the VLA (Fig. 5.1b) is about 12 m/s. In a companion paper to follow, the USC will be discussed in more detail.

5.4.1 Measured CIR

The CIR estimated at 2.8-km range using the LFM channel probe is shown in Fig. 5.2a along the VLA depth after matched-filtering (JD146164500). The horizontal axis is a relative time of arrival (ms) with the high-intensity arrivals at around $t = 20$ ms. The arrival structure appears complicated with many distinct paths and a delay spread of up to 140 ms. The modest source level (165 dB) is compensated for by the pulse compression gain of about 22 dB (i.e., the time-bandwidth-product of the LFM chirp).

To understand the channel characteristics, the group slowness (S_g) versus phase slowness (S_p) curve corresponding to the SSP in Fig. 5.1b, or equivalently the group speed ($V_g = 1/S_g$) versus phase speed ($V_p = 1/S_p$), is illustrated in Fig. 5.1c at the carrier frequency of 1.25 kHz. On the horizontal axis, the mode number (or phase speed) increases from the right towards the left. The modes can be divided into two groups based on the phase speed V_p: (i) high-order modes ($V_p > 1505$ m/s) and (ii) low-order modes ($V_p < 1505$ m/s). For group (i) high-order modes, the waveguide invariant parameter β is defined by [9]

$$\frac{1}{\beta} = -\frac{d(1/V_g)}{d(1/V_p)} = -\frac{d(S_g)}{d(S_p)}. \tag{5.3}$$

The inverse of the negative slope (dashed line) for group (i) modes in Fig. 5.1c is

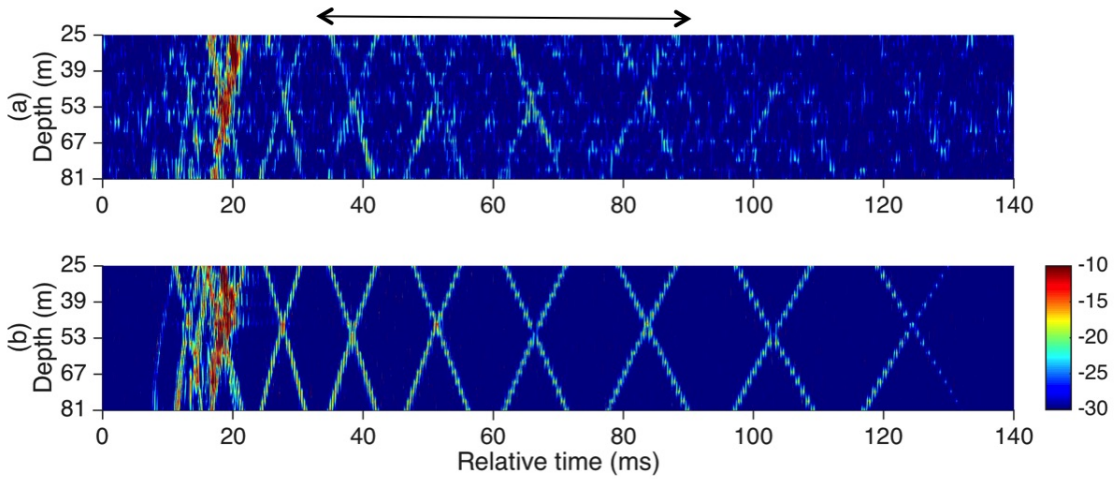

Figure 5.2: (Color online) Channel impulse response (CIR) at 2.8 km range using the LFM channel probe after matched-filtering (JD146164500): (a) data and (b) model. The simulated CIR (b) is based on a normal mode propagation model and the SSP displayed in Fig. 5.1b, assuming a range-independent environment with a simple half-space bottom. The eight distinct arrivals captured between 30 and 90 ms (indicated by the top arrow) are from the group (i) high-order reflected modes, which are exploited for source-range estimation based on the array invariant in Sec. 5.5.

estimated as about $\beta = 1.02$, being close to the ideal waveguide of $\beta = 1$. Thus the group (i) modes are surface/bottom-reflected paths that behave like those in ideal waveguides, which can be exploited for source-range estimation based on the array invariant [5]. The delay spread of the channel (e.g., 140-ms) is determined by the group speeds of the lowest and highest modes (along the dashed line in Fig. 5.1c) contributing to the field.

On the other hand, the low-order modes in group (ii) are refracted (waterborne) paths with a similar group speed (blue circle), whose acoustic energy is trapped mostly around the channel axis. Within group (ii), high-order modes propagate faster than do low-order modes with a negative value of β. The high-intensity arrivals at around $t = 20$ ms in Fig. 5.2a correspond to the group (ii) modes with a delay spread of less than 10 ms, which are embedded in the early reflected arrivals from the group (i) modes along the dashed line, but below the horizontal line (dash-dot).

5.4.2 Simulated CIR

For comparison purposes, a model-based CIR is presented in Fig. 5.2b using a normal mode propagation model, assuming a range-independent environment with a simple half-space bottom. With the SSP in Fig. 5.1b, the geoacoustic properties of the sea floor [10] are typical of sand: density $\rho_b = 1.97$ g/cm^3, compressional sound speed $c_b = 1800$ m/s, and compressional wave attenuation $\alpha_b = 0.94$ dB/wavelength. The simulated CIR shows a good agreement with the data (Fig. 5.2a) in terms of its arrival structure, as will be confirmed in the beam-time migration presented in Sec. 5.5 (Fig. 5.3). In particular, several pairs of up and down-going, X-shaped arrivals that are well separated in travel time are aligned closely with the data counterparts after the high-intensity arrivals up to $t = 90$ ms.

There are some notable differences, too. The simulated arrivals in Fig. 5.2b remain strong vis-a-vis the data counterparts in Fig. 5.2a, which gradually diminish over time and are barely visible around 100 ms. This can be attributed to the fact that the higher-order modes of group (i) with steeper propagation angles and slower group speeds (within the dashed ellipse in Fig. 5.1c) are significantly attenuated due to the many interactions with rough boundaries, coupled with uncertainties in the bottom attenuation. In addition, the averaged SSP used for modeling may not capture the details of the actual SSP present during data collection, which resulted in some difference in the early strong refracted arrivals from group (ii) at around $t = 20$ ms.

5.5 Beam-time migration and range estimation

For source-range estimation, the beam-time migration (s_v, t) is presented in Fig. 5.3 (gray scale): (a) data and (b) model, each corresponding to Fig. 5.2, respectively. The vertical axis represents the beam angle $s_v = \sin\theta$ with a positive value defined for an up-going path (e.g., red circles), and the horizontal axis is the relative travel time t (ms). The VLA is positioned around the channel axis with significant variation of the sound speed up to 12 m/s (refer to Fig. 5.1b) and thus

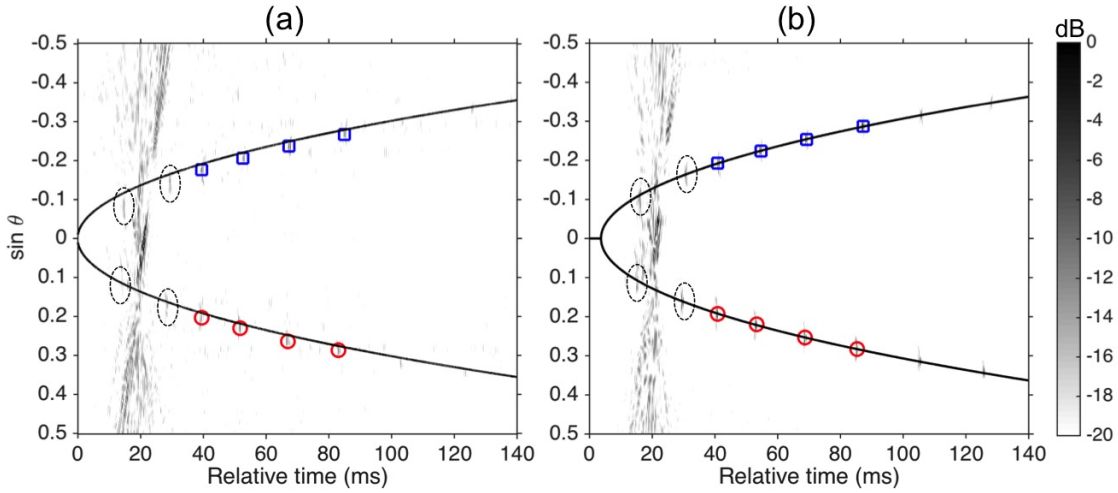

Figure 5.3: (Color online) Beam-time migration at 2.8 km range: (a) data and (b) model, each corresponding to Fig. 5.2. A positive beam angle represents an up-going ray path (e.g., red circles) and the dynamic range is 20 dB, showing an excellent agreement between data and model. The high-intensity arrivals around $t = 20$ ms are from refracted low-order modes with low grazing angles that are confined to the broadside (e.g., $|\sin\theta| < 0.1$), whereas the similar structure appearing on both sides at higher angles ($|\sin\theta| > 0.2$) is due to spatial aliasing. The eight reflected arrivals from group (i), marked by circles and squares between 30 and 90 ms, constitute an elliptic curve (solid line) from which the array invariant parameter χ_v can be obtained for source-range estimation. There are additional early reflected arrivals detected around $t = 20$ ms (dotted circles) that are not used for the array invariant-based range estimation. The estimated source range is 3.2 km with a 15% relative error for (a) data and 3.0 km with a 7% relative error for (b) model.

an averaged sound speed of $c = 1500$ m/s is used for plane-wave beamforming. Although the design frequency for the VLA is 200 Hz with the element spacing of 3.75 m, the spatial aliasing in beam angle (i.e., grating lobes) is expected to be mitigated over the broad frequency band (0.5–2 kHz) [11]. The dynamic range is 20 dB.

A few interesting observations can be made. First, there is an excellent agreement between the data and model in Fig. 5.3, indicating that modeling can be used as a powerful tool for simulations and analysis despite some uncertainties in the environment. Second, the early high-intensity arrivals around $t = 20$ ms are spread around the broadside (i.e., $|s_v| < 0.1$), which are from the group (ii)

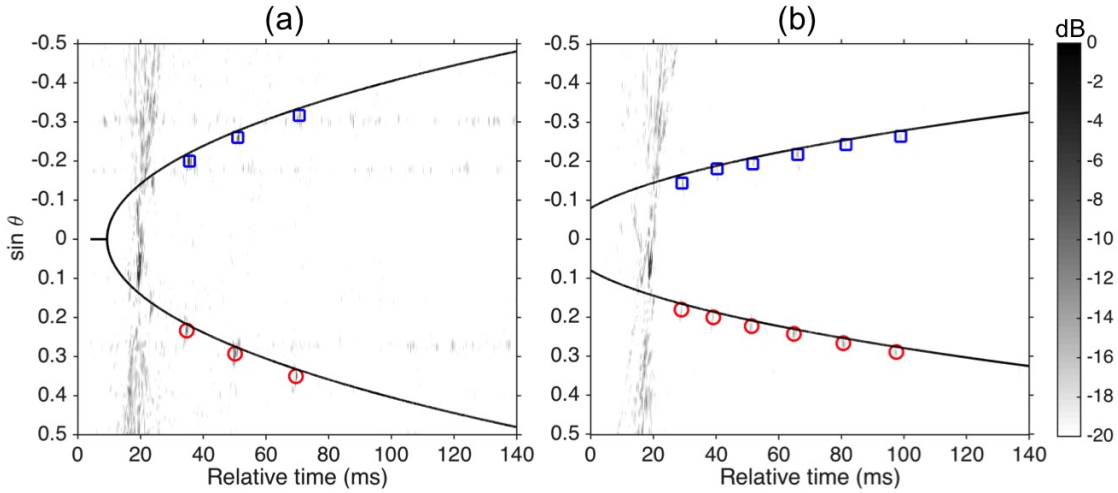

Figure 5.4: (Color online) Same as Fig. 5.3 but for other ranges using data: (a) 1.5 km (JD146165500) and (b) 3.5 km (JD14616400). The structure is similar to Fig. 5.3, and a different number of reflected arrivals (circles and squares) is used for the array invariant analysis. The estimated source range is 1.6 km with a 6% relative error for (a) and 4.1 km with a 17% relative error for (b) (see Table 5.1).

refracted low-order modes with smaller grazing angles (blue curve in Fig. 5.1c). The similar, less-intense (e.g., 7 dB below) structure appearing on both sides at higher angles ($|s_v| > 0.2$) is due to spatial aliasing with the sparse VLA. Third, many reflected arrivals at higher angles ($0.1 < |s_v| < 0.3$) are visible, albeit weak, marked by circles and squares. For array invariant-based range estimation, a total of eight distinct arrivals of up- (circles) and down-going (squares) rays captured between 30 and 90 ms will be utilized, as depicted in Fig. 5.2 (top arrow).

Finally, an elliptic curve (solid line) corresponding to Eq. (5.2) that best fits the eight reflected arrivals (circles and squares) in the least-squares sense is obtained with an appropriate array invariant parameter χ_v, enabling the source-range estimation based on Eq. (5.1). Note that the distinct arrivals in Fig. 5.3a (data) are a little offset from the elliptic curve by approximately 0.7° likely due to an array tilt, which is neglected in this paper. However, the impact of array tilt on the array invariant is analyzed in a separate paper. For the source at 2.8-km range in Fig. 5.3, the estimated source range is 3.2 km with a relative error of 15% for (a) data and 3.0 km with a relative error of 7% for (b) model, respectively. Similarly, the beam-time migration for two other source ranges is presented in Fig. 5.4 using

experimental data: (a) 1.5 km (JD146165500) and (b) 3.5 km (JD14616400). The beam-time migration structure is similar to Fig. 5.3, and a different number of reflected arrivals (circles and squares) is selected for the array invariant analysis. The estimated source range is 1.6 km with a 6% relative error for (a) and 4.1 km with a 17% relative error for (b), which are summarized in Table 5.1.

Table 5.1: Source-range estimation from beam-time migration of the SAVEX15 data at various ranges using $\beta = 1$.

Source range	Estimated range	Relative range error	Beam-time migration
1.5 km	1.6 km	6%	Fig. 5.4a
2.8 km	3.2 km	15%	Fig. 5.3a
3.5 km	4.1 km	17%	Fig. 5.4b

5.6 Summary

The array invariant approach for robust source-range estimation in shallow water utilizes multiple arrivals separated in beam angle and travel time, which behave like those in ideal waveguides. While the approach requires minimal knowledge of the environment, it involves plane wave beamforming using a short-aperture vertical array in stratified acoustic waveguides. In this work, the array invariant approach was extended to a large-aperture vertical array that was sparse with significant variation of the sound speed across the aperture for conventional beamforming. Robust source-range estimation was confirmed using experimental data from a 16-element, 56-m long vertical array at various ranges (1.5–3.5 km) from a broadband source (0.5–2 kHz) in approximately 100-m deep shallow water.

5.7 Appendix: Generalized array invariant

The array invariant proposed by Lee and Makris [1] is revisited to formally connect the array invariant and waveguide invariant such that the waveguide invariant parameter β is embedded in the array invariant χ, referred to as a generalized

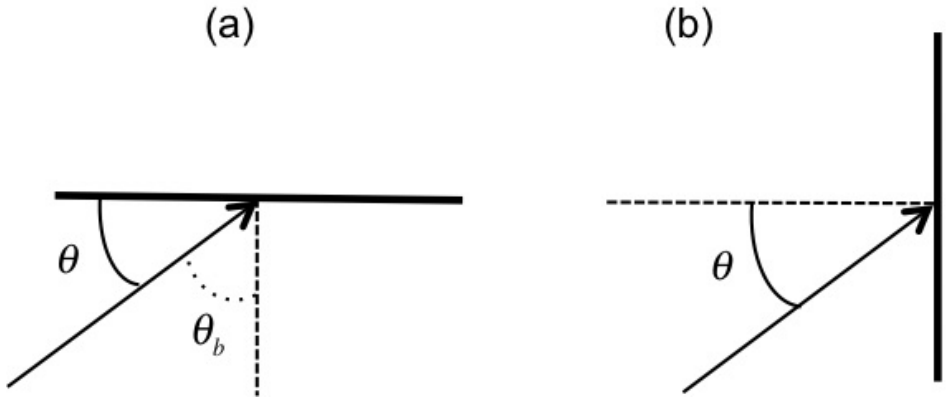

Figure 5.5: The geometry of two arrays (thick lines): (a) endfire horizontal array and (b) vertical array. θ is the grazing angle of each ray/mode arrival. In general, the horizontal array will have an azimuth angle ϕ_0 in the horizontal plane from the source (i.e., source bearing) while $\phi_0 = \pi/2$ corresponds to the endfire array in (a).

array invariant. Two common arrays in acoustic waveguides are considered: (a) horizontal and (b) vertical, as depicted in Fig. 5.5. The horizontal array is aligned with a source (i.e., endfire) that can be easily extended to the case with an azimuth angle ϕ_0 in the horizontal plane [5].

5.7.1 Horizontal array

Consider an ideal waveguide with the water depth of 100 m and the sound speed of $c = 1500$ m/s, whose dispersion characteristics are illustrated in Fig. 5.6a. The modal group speed $V_{g,n}$ is related to the modal propagation angle θ_n defined as a grazing angle in Fig. 5.5a

$$V_g = c \cos\ \theta. \tag{5.4}$$

This equation is the basic building block of the array invariant approach where the mode number n is dropped for convenience [1].

The group speed V_g is simply replaced with the source range r_0 divided by the travel time t, i.e., $V_g = r_0/t$, whereas $\cos\theta$ is the beam angle measured by a horizontal array, denoted by s_h. Then we have

$$s_h \equiv \cos\theta = \frac{V_g}{c} = \left(\frac{r_0}{c}\right)\frac{1}{t}. \tag{5.5}$$

For a given source range r_0 and sound speed c, the beam angle s_h and the travel time t are inversely proportional in (s_h, t) coordinate, as shown in Fig. 5.6b.

The horizontal array invariant parameter χ_h is defined as the derivative of the horizontal beam angle s_h with respect to the travel time t, i.e., the slope in (s_h, t) coordinate

$$\chi_h \equiv \frac{ds_h}{dt} = -\left(\frac{r_0}{c}\right)\frac{1}{t^2} = -\left(\frac{c}{r_0}\right)\cos^2\theta, \tag{5.6}$$

where $t = r_0/(c\cos\theta)$ from Eq. (5.5) is substituted. In general, χ_h (or slope) varies depending on the grazing angle θ (or mode), as evident in Fig. 5.6b. By constraining the range of the grazing angle, however, χ_h can be treated as approximately constant or invariant over those modes or angles.

The analytical expression for the waveguide invariant in ideal waveguides is $\beta = \cos^2\theta$ [9]. Then the array invariant parameter χ_h in Eq. (5.6) reveals the waveguide invariant parameter β, formally connecting the two invariants

$$\chi_h = -\left(\frac{c}{r_0}\right)\beta. \tag{5.7}$$

Previously the above relationship was derived from the waveguide invariant theory where the array invariant was a special case of $\beta = 1$ [5]. Here, the array invariant is transformed to a generalized array invariant that contains the waveguide invariant parameter β, closing the loop. On the flip side, the analytic expression for the waveguide invariant in ideal waveguides is derived indirectly, $\beta = \cos^2\theta$. For low-order modes with small grazing angles (i.e., $\theta < 20°$), $\beta \approx 1$ and thus $\chi_h \approx -(c/r_0)$, which is applicable to many shallow-water environments where surface/bottom reflected paths are captured [7] [9].

When the horizontal array is not in the endfire with an azimuth angle of ϕ_0 in the horizontal plane from the source, the process of rotating the horizontal array to the endfire is equivalent to replacing the local sound speed c with a virtual sound speed, $(c\ \sin\phi_0)$. The endfire horizontal array corresponds to $\phi_0 = \pi/2$.

5.7.2 Vertical array

The only difference between a vertical and a horizontal (endfire) array is the beam angle measured by the respective array. For a vertical array depicted

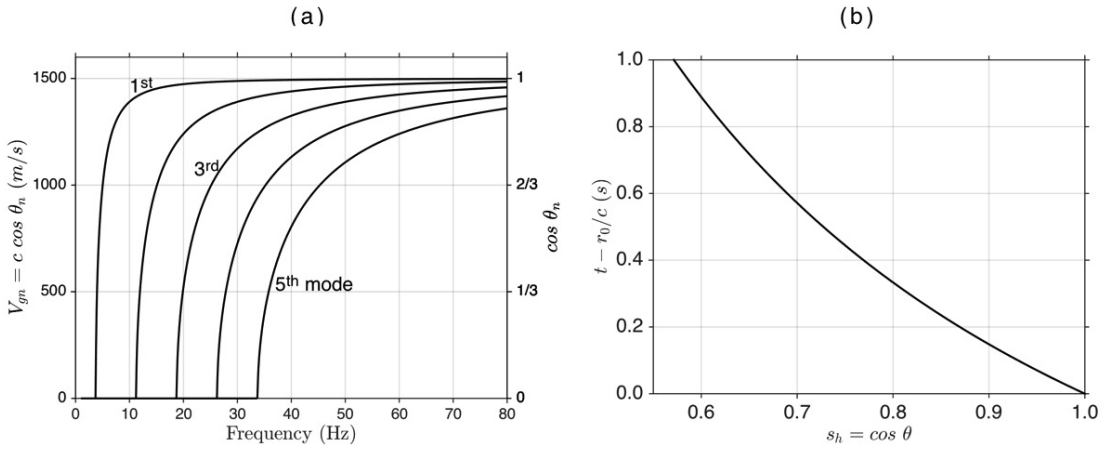

Figure 5.6: (a) Group speed V_g and propagation angle θ as a function of frequency in an ideal waveguide. The water depth and the sound speed are 100 m and 1500 m/s, respectively. The first 5 modes are displayed starting from the left. (b) The beam-time migration curve as a function of reduced travel time $(t - r_0/c)$ and array beam angle $s_h = \cos\theta$ when the source azimuth angle $\phi_0 = \pi/2$ and the source range $r_0 = 2$ km.

in Fig. 5.5b, the measured beam angle is $\sin\theta$, denoted by $s_v = \sin\theta$. While the vertical array invariant parameter χ_v is defined in (s_v, t) domain, it provides the same result as χ_h in Eq. (5.6)

$$\chi_v \equiv \frac{d}{dt}(\cos\theta) \equiv \frac{d}{dt}\sqrt{1 - s_v^2} = -\left(\frac{c}{r_0}\right)\cos^2\theta = -\left(\frac{c}{r_0}\right)\beta. \tag{5.8}$$

The array invariant parameter χ_v can be evaluated numerically from the beam-time migration in (s_v, t) coordinate, which satisfies an elliptic equation [5]. On the other hand, the horizontal array invariant parameter χ_h is deduced from the beam-time migration in (s_h, t) coordinate, which is linear. Once χ_v or χ_h is calculated from beam-time migration data, the source range r_0 can be simply estimated from

$$r_0 = -\beta\left(\frac{c}{\chi}\right). \tag{5.9}$$

For stratified waveguides, the local sound speed c can be replaced by an average sound speed across the array aperture for plane wave beamforming.

5.7.3 A least-squares estimate of χ_v

The array invariant parameter χ_v in Eq. (5.8) can be estimated as follows: (a) find peaks above a threshold (e.g., -10 dB) in (s_v, t) domain, (b) cluster the peaks with similar arrival times while the clusters are separated when the minimal time difference between them is larger than a specified time-interval (e.g., 1-ms), and (c) identify the maximum peak in each cluster, $\{s_{max}(t_1), \cdots, s_{max}(t_N)\}$. This process can be done automatically for various choices of the parameters (threshold and time-interval).

A least-squares estimate of $\hat{\chi}_v$ then can be obtained from Eq. (5.8) approximated by $\sqrt{1-s_v^2} = \chi_v t + d_v$, with d_v being a constant intercept [1]:

$$[\hat{\chi}_v \quad d_v]^T = (\boldsymbol{T}^T\boldsymbol{T})^{-1}\boldsymbol{T}^T\boldsymbol{S}, \tag{5.10}$$

where $\boldsymbol{S} = [(1-s_{max}(t_1))^{1/2}, (1-s_{max}(t_2))^{1/2}, \cdots, (1-s_{max}(t_N))^{1/2}]^T$, $\boldsymbol{T} = [(t_1, t_2, \cdots, t_N)^T\mathbf{1}^T]$, and $\mathbf{1}$ is an $1 \times N$ vector given by $\mathbf{1} = [1, 1, \cdots, 1]$.

Acknowledgment

This research was supported by the US Office of Naval Research.

Chapter 5, in full, is a reprint of the material as it appears in the Journal of Acoustical Society of Americas: H.C. Song and Chomgun Cho, "Array invariant-based source localization in shallow water using a sparse vertical array," *J. Acoust. Soc. Am*, 141 (1), 183-188, 2017. The dissertation author was a primary investigator and author of this material.

Bibliography

[1] S. Lee and N. C. Makris, "The array invariant", J. Acoust. Soc. Am. **119**, 336–351 (2006).

[2] A. B. Baggeroer, W. A. Kuperman, and P. N. Mikhalevsky, "An overview of matched field methods in ocean acoustics", IEEE J. Oceanic Eng. **18**, 401–424 (1993).

[3] P. Hursky, M. Porter, M. Siderius, and V. McDonald, "High-frequency (8-16 kHz) model-based source localization", J. Acoust. Soc. Am. **115**, 3021–3032 (2004).

[4] B. M. Worthmann, H. C. Song, and D. R. Dowling, "High-frequency source localization in a shallow water sound channel using frequency difference matched field processing", J. Acoust. Soc. Am. **138**, 3549–3562 (2004).

[5] H. C. Song and C. Cho, "The relation between the waveguide invariant and array invariant", J. Acoust. Soc. Am. **138**, 899–903 (2015).

[6] S. D. Chuprov, "Interference structure of a sound field in a layered ocean", in *Acoustics of the Ocean*, 71–91 (Nauka, Moscow) (1982), edited by L. M. Breakhovskikh and I. B. Andreevoi.

[7] C. Cho, H. C. Song, and W. S. Hodgkiss, "Robust source-range estimation using the array/waveguide invariant and a vertical array", J. Acoust. Soc. Am. **139**, 63–69 (2016).

[8] G. Grelowska, "Prevaling patterns of the sound speed distributions in the environment of the southern Baltic", Archives of acoustics **25**, 359–368 (2000).

[9] F. B. Jensen, W. A. Kuperman, M. B. Porter, and H. Schmidt, *Computational Ocean Acoustics* (Springer, New York) (2011). Chs. 3 and 5.

[10] W. Ryang, S. Kim, S. Kim, and D.-C. Kim, "Geoacoustic model of the transverse acoustic variability experiment area in the northern East China Sea", Geosciences Journal **17**, 267–278 (2013).

[11] J. Dmochowski, J. Benesty, and S. Affes, "On spatial aliasing in microphone arrays", IEEE Trans. Signal Process. **57**, 1383–1395 (2009).

Chapter 6

Impact of array tilt on source-range estimation in shallow water using the array invariant

Authors:
Chomgun Cho
H.C. Song

6.1 Abstract

The array invariant proposed for robust source-range estimation in shallow water is based on the dispersion characteristics in ideal waveguides for broadband signals. With minimal knowledge of the environment, the approach involves plane-wave beamforming using a vertical array, utilizing multiple arrivals (i.e., eigenrays) separated in beam angle and travel time. In the presence of array tilt, however, the beam angle estimates are shifted, which potentially affects the range estimation based on the array invariant. Conversely, the array tilt could be estimated for a known source range. In this paper, the sensitivity to array tilt is analyzed theoretically and examined using simulations and data. It is found that even a

small tilt angle (e.g., $< 2°$) of a 1.2-m long vertical array near the surface, if not compensated for, can result in a relative range error of 20% or more, for a high-frequency source (7–19 kHz) at 3-km range in approximately 100-m deep shallow water. Moreover, the power spectrum of the time-evolving array tilt estimated for 9 min shows a dominant period of 5.6 s, which is consistent with the surface wave period concurrently measured from a waverider buoy.

6.2 Introduction

Since first introduced by Bucker in 1976 [1], matched field processing (MFP) has been extensively studied for passive source localization in oceanic waveguides typically using a vertical array [2–4]. MFP is a generalization of plane-wave beamforming wherein the "steering vectors," or replicas, are not plane waves but solutions of the wave equation (i.e., Green's function) descriptive of the ocean environment at array elements for all possible source locations [3]. This computationally intensive array processing requires accurate knowledge of the environment in order to exploit the unique spatial structure of the field (i.e., complexity) for source localization (range and depth). The localization resolution and uniqueness (ambiguity) depend upon the waveguide and the source frequency, and the localization performance depends on spatial sampling that improves with a large aperture array and an appropriate element spacing. The main drawback of MFP is its sensitivity to mismatch in the acoustic environment (sound speed, bottom attenuation, etc.) and/or geometry (e.g., array position and tilt), and variants of MFP have been developed for robustness since its introduction, including a recent frequency-difference MFP [5]. For broadband signals, MFP can be applied at each Fourier component and then incoherently averaged across the frequency band. In practice, MFP has been successful mostly at low frequencies below 1 kHz [4].

On the other hand, the array invariant [6], denoted by χ, has been proposed for robust source-range estimation in shallow-water environments. The approach is based on the dispersion characteristics in ideal waveguides for broadband signals. In a complete reversal to MFP, this approach involves plane-wave beamforming,

utilizing coherent multiple arrivals (i.e., eigenrays) separated in beam angle and travel time, referred to as "beam-time migration" (e.g., Fig. 6.1b). The resolution of the beam angle and travel time depends on the array aperture, center frequency, and signal bandwidth. The source-range information is contained in the beam-time migration pattern, either linear for a horizontal array or elliptic for a vertical array [7]. With no forward model computations required, the approach is robust and efficient, especially in the high-frequency regime (e.g., > 1 kHz) where MFP performs poorly with a lack of robustness to environmental mismatch. The method was first demonstrated using simulations and experimental data collected from a towed horizontal array [6].

Recently it was revealed [7] that the array invariant can be derived directly from the well-known waveguide invariant theory [8–11] in the beam-time coordinate. Specifically, the array invariant is a special case of the waveguide invariant corresponding to $\beta = 1$. This value is not only a canonical value for ideal waveguides from which the array invariant originated, but it is also applicable to many shallow-water environments involving surface/bottom-interacting ray paths [4, 12]. As a result, the array invariant [6] was successfully applied without explicitly invoking the waveguide invariant. The implication is that the array invariant can be extended to general waveguides with different values of β, including mildly range-dependent environments, and is fully supported by the physics of the waveguide invariant. Subsequently, the unified array/waveguide invariant approach to source-range estimation was demonstrated using a short-aperture vertical array (12-m) moored near the seafloor and a broadband source (2–3 kHz) at 6-km range in approximately 100-m deep shallow water [13].

Despite the robustness and computational simplicity, the array invariant approach has a potential weakness. The array invariant relies entirely on plane-wave beamforming to estimate the beam angles under the assumption that the vertical array involved is vertical. In the presence of array tilt, however, the estimated beam angles are shifted, which in turn will affect the beam-time migration and ultimately the source-range estimation. On the other hand, the array tilt angle could be estimated inversely for a known source range. The objective of this paper

is to investigate the impact of array tilt on the array invariant and range estimation using both simulations and data collected in a shallow-water environment. In this paper, the array tilt will be confined to a two-dimensional plane containing the source and receiver.

The paper combines results from theoretical analysis, simulated data analysis, and experimental data analysis. In Sec. 6.3, a modified array invariant is derived that accounts for the array tilt. Section 6.4 begins with a description of a shallow-water experiment where a 1.2-m long vertical array deployed near the surface was used to measure the channel impulse response (CIR) from a moored broadband source (7–19 kHz) at 3-km range in approximately 100-m deep water. A geometric ray model is employed to identify several distinct ray paths (eigenrays), which are displayed in the arrival angle and (relative) travel time domain. Then plane-wave beamforming is applied to simulated data generated by a normal mode propagation model, providing a theoretical beam-time migration. Section 6.5 analyzes the beam-time migration of experiment data without compensation for array tilt, and its impact on range estimation. Finally, the power spectrum of a time-varying array tilt over one minute is presented to confirm the correlation between the array tilt and surface wave movement, followed by a summary in Sec. 6.6.

6.3 Array invariant with array tilt

For a general acoustic waveguide with the waveguide invariant parameter β, the source range r_0 based on the array invariant parameter χ is estimated using

$$r_0 = -\beta \left(\frac{c}{\chi} \right), \tag{6.1}$$

where c is the local sound speed. For an ideal waveguide with $\beta = 1$, this formula reduces to the expression in the array invariant [11, 13].

The array invariant parameter χ should be estimated numerically from the beam-time migration. For a vertical array of interest, χ_0 with no array tilt is defined as

$$\chi_0 \equiv \frac{d}{dt}(\cos\theta) = \frac{d}{dt}\sqrt{1 - \sin^2\theta}, \tag{6.2}$$

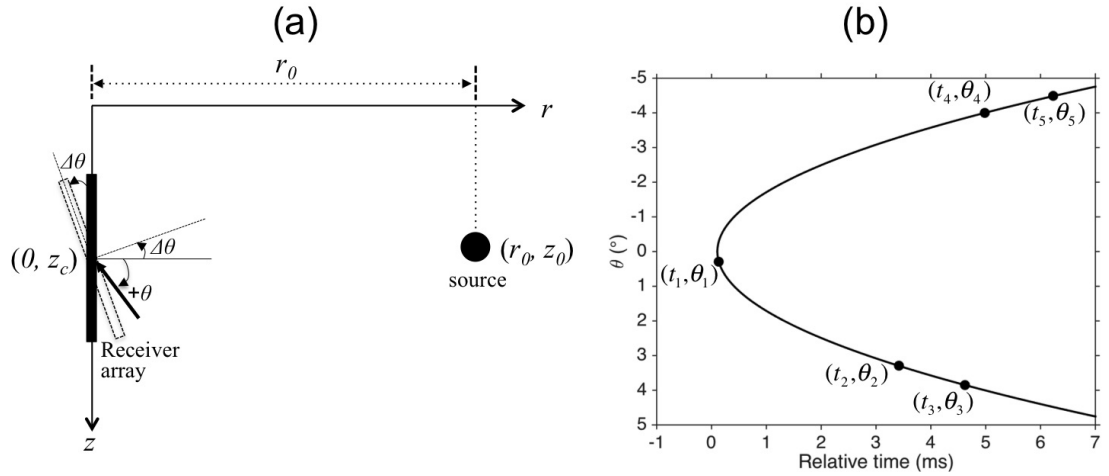

Figure 6.1: (Color online) (a) Coordinate system including a vertical line array and a point source at range r_0. A positive grazing angle of θ is assigned to an up-going ray path, and the tilt angle $\Delta\theta$ is defined as positive for counter-clockwise rotation in the source-receiver plane. (b) An ideal beam-time migration for a shallow-water environment corresponding to the KAM11 experiment in Sec. 6.4. The migration curve passing through the distinct arrivals (dots) is elliptic for a vertical array.

where $\sin\theta$ is the beam angle measured by a vertical array with the grazing angle θ defined in Fig. 6.1a. A positive θ is assigned to an up-going ray path. The above equation leads to an elliptic curve in $(t, \sin\theta)$ coordinate or approximately in (t, θ) coordinate for small grazing angles (e.g., $|\theta| < 10°$) [7], which is a reasonable assumption for a far-field source. An ideal beam-time migration is illustrated in Fig. 6.1b for a shallow-water environment corresponding to the KAM11 experiment described in Sec. 6.4.

In theory, χ_0 can be calculated from a pair of distinct arrivals in the beam-time domain, (t_1, θ_1) and (t_2, θ_2):

$$\chi_0 = \frac{1}{t_2 - t_1}\left(\sqrt{1-\sin^2\theta_2} - \sqrt{1-\sin^2\theta_1}\,\right) \cong \frac{1}{2\Delta t_{1,2}}(\sin^2\theta_1 - \sin^2\theta_2), \quad (6.3)$$

where $\Delta t_{1,2} \triangleq t_2 - t_1$ and the beam angles are assumed small (e.g., $|\sin\theta| < 0.2$). For typical shallow-water environments with a positive β, $|\theta_1| < |\theta_2|$ for $t_1 < t_2$. When there are multiple arrivals available, χ_0 can be estimated using the least-squares approach [13].

6.3.1 Tilted array invariant

In the presence of array tilt, $\Delta\theta$, the arrival angles after plane-wave beamforming are shifted by the same amount, and instead we obtain a tilted array invariant parameter χ_t

$$\chi_t \equiv \frac{d}{dt}\left(\cos(\theta + \Delta\theta)\right) \cong \frac{1}{2\Delta t_{1,2}}\left(\sin^2(\theta_1 + \Delta\theta) - \sin^2(\theta_2 + \Delta\theta)\right), \tag{6.4}$$

from a pair of shifted arrivals, $(t_1, \theta_1' = \theta_1 + \Delta\theta)$ and $(t_2, \theta_2' = \theta_2 + \Delta\theta)$. A positive tilt angle $\Delta\theta$ is assigned to counter-clockwise rotation in Fig. 6.1a. Applying a Taylor series expansion of Eq. (6.4) to the first order around zero for θ_1, θ_2, and $\Delta\theta$ [14], i.e., a small angle approximation, we can represent χ_t as a sum of two terms including χ_0:

$$\chi_t \cong \frac{1}{2\Delta t_{1,2}}(\sin^2\theta_1 - \sin^2\theta_2) + \frac{\sin\Delta\theta}{\Delta t_{1,2}}(\sin\theta_1 - \sin\theta_2) = \chi_0 + \Delta\chi. \tag{6.5}$$

The additional second term $\Delta\chi$ is due to the array tilt, which vanishes when $\Delta\theta = 0$. If the tilt angle $\Delta\theta$ is available (i.e., measured), we can recover χ_0 from Eq. (6.5), and the source range can be estimated correctly using Eq. (6.1).

The impact of array tilt on the range estimation error can be described by the change in the array invariant parameter $\Delta\chi$ from Eqs. (6.1) and (6.5) such that

$$\frac{r_t - r_0}{r_0} = \left(\frac{r_t}{r_0}\right) - 1 = \left(\frac{\chi_0}{\chi_t}\right) - 1 = -\frac{\chi_t - \chi_0}{\chi_t} = -\frac{\Delta\chi}{\chi_t}, \tag{6.6}$$

where r_t denotes the range estimate in the presence of an array tilt. For a pair of arrivals, the relative range error will be affected by both the angle of arrivals (θ_1, θ_2) and tilt angle $\Delta\theta$.

6.3.2 Estimation of array tilt

For a known source range r_0, the array tilt angle $\Delta\theta$ can be inversely estimated from the shifted beam-time migration. Using Eqs. (6.1) and (6.5), the tilt angle $\Delta\theta_{1,2}$ is derived for a pair of angle-shifted arrivals, $(t_1, \theta_1' = \theta_1 + \Delta\theta)$ and $(t_2, \theta_2' = \theta_2 + \Delta\theta)$:

$$\Delta\theta_{1,2} = \sin^{-1}\left(\frac{(\beta c/r_0)\Delta t_{1,2}}{\sin(\theta_1') - \sin(\theta_2')} + \frac{\sin(\theta_1') + \sin(\theta_2')}{2}\right). \tag{6.7}$$

In shallow-water environments, the surface/bottom reflected arrivals are exploited for the array invariant [13], which behave like those in ideal waveguides. Thus, we can simply use $\beta = 1$ and $c = 1500$ m/s in Eq. (6.7) with minimal knowledge of the environment.

When there are more than two arrivals (i.e., $N > 2$), the array tilt angle can be estimated by averaging all possible combinations of pairs, i.e., ${}_NC_2$:

$$\overline{\Delta\theta} = \frac{2}{N(N-1)} \sum_{n=1}^{N-1} \sum_{m>n}^{N} \Delta\theta_{n,m}. \tag{6.8}$$

6.4 KAM11 experiment

The Kauai Acomms MURI 2011 (KAM11) experiment was conducted in shallow water off the western side of Kauai, Hawaii, in the summer of 2011 [15]. The goal of KAM11 was to collect acoustic and environmental data appropriate for studying the coupling of oceanography, acoustics, and underwater communications. A number of acoustic sources and receivers were deployed along the approximately 100-m deep isobath. The acoustic transmissions were in three bands covering 3.5 to 35 kHz, which included both channel probing waveforms as well as communication transmissions. Environmental data collected included water-column sound-speed profiles (SSPs) using CTDs (conductivity, temperature, and depth) and thermistor strings, sea surface directional wave field from a waverider buoy, and local wind speed and direction from the R/V Kilo Moana. The acoustic environment was downward refracting with the mixed layer depth varying between 20 m to 60 m.

Figure 6.2 shows the wind speed and direction along with waverider-derived sea surface wave spectrum during the first deployment of the waverider buoy, from June 24 (JD 175) to July 1 (JD 182). The wind speed and sea surface conditions exhibited a daily pattern, similar to the substantial daily oceanographic variability in the region. The peak surface wave direction in Fig. 6.2c was northeastern (about 45°) almost parallel to the 100-m isobath (i.e., acoustic transmission path). The dominant surface wave period (ocean swell, red curve) in Fig. 6.2d was about 4–6 s, with the corresponding wavelength (λ) of 25–55 m.

For the array invariant analysis in conjunction with array tilt, we focus on

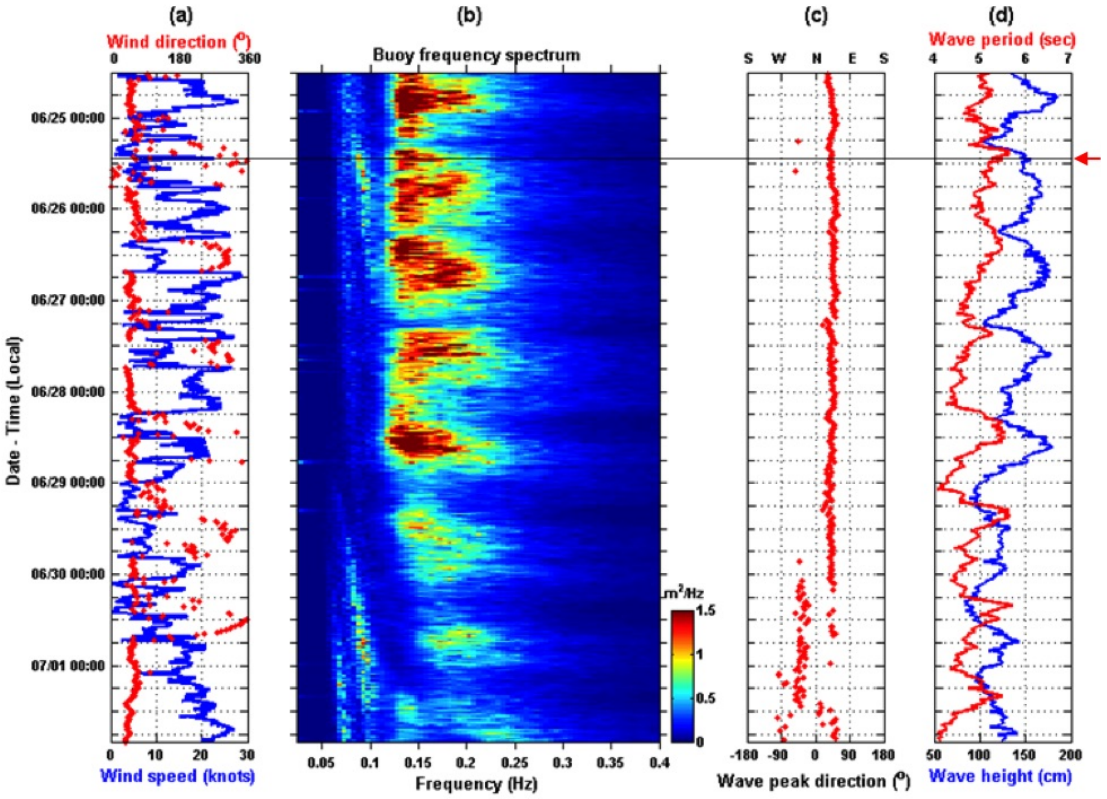

Figure 6.2: (Color online) KAM11 environmental data: (a) wind speed and direction, (b) sea surface wave spectrum, (c) peak surface wave direction, and (d) significant wave height and wave period. The data were collected during the first deployment of the waverider buoy, from June 24 (JD 175) to July 1 (JD 182), and (a) was collected from the R/V Kilo Moana. The wind speed and sea surface conditions exhibited a daily pattern, similar to the daily oceanographic variability in the area. The horizontal line with the red arrow on panel (d) indicates the sea surface condition corresponding to the time period (i.e., 20:55 UTC) when the acoustic data analyzed in Sec. 6.5 were transmitted. Specifically, the surface wave period in (d) (red curve) was about 5.5 s. Local time is 10-hour earlier than UTC, i.e., UTC = Local time + 10 hours.

the acoustic transmissions carried out on June 25 (JD 176) with the schematic shown in Fig. 6.3a. The source on the right side, called WHOI-Tx1, was actually a 4-element source array with 0.5-m element spacing, whose center depth was about 15 m. Since the elements are closely spaced and the array invariant is to estimate the source range without knowledge of the source depth (i.e., source depth-blind), the short-aperture source array is represented by a single source moored at 15-m

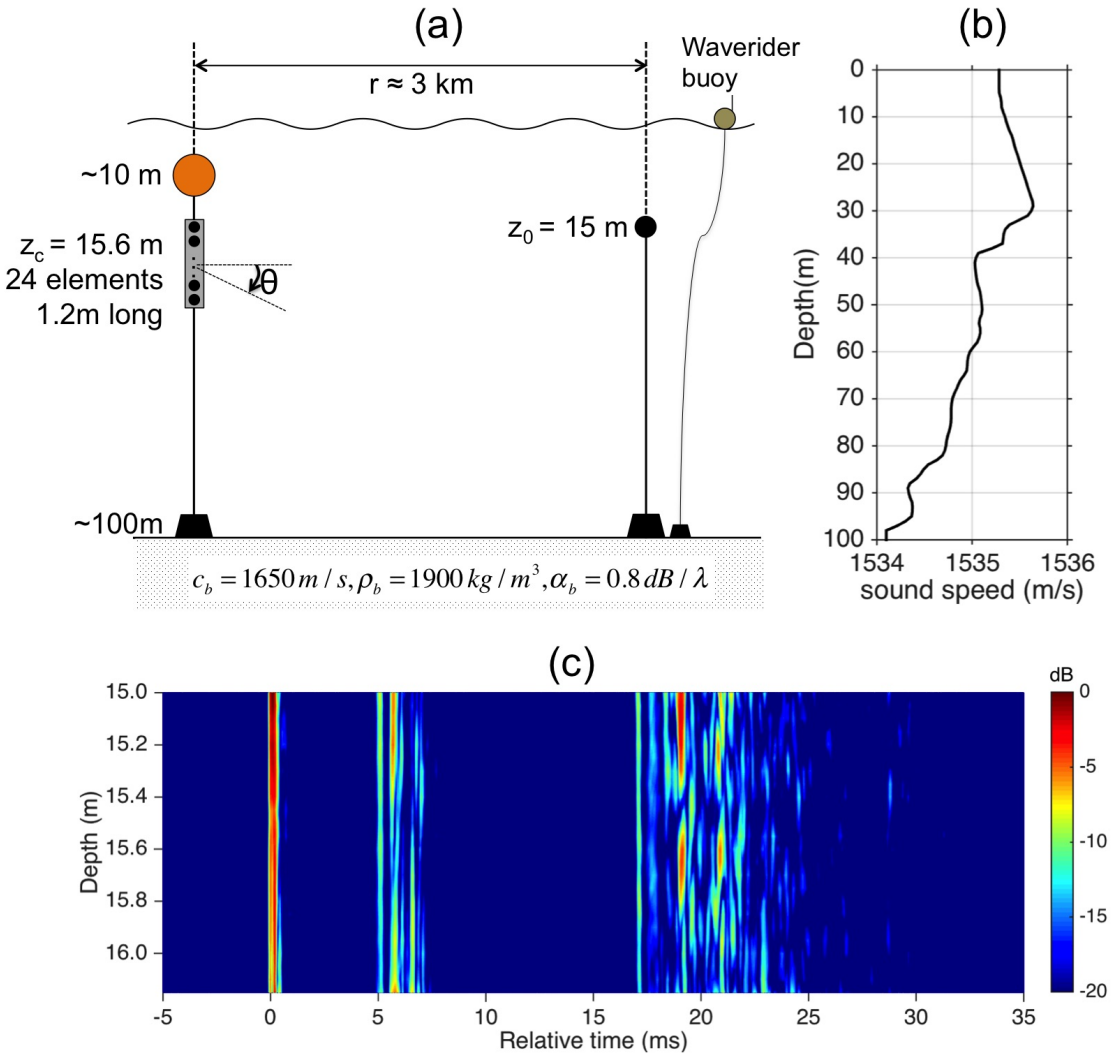

Figure 6.3: (Color online) (a) Schematic of KAM11 experiment (JD 176). The source at approximately 15-m depth (WHOI-Tx1) represents a short-aperture, 4-element source array with inter-element spacing of 0.5-m. The transmitted signal was 48-ms long, 9–17 kHz LFM chirp waveforms every 96 ms for 9 min. The receiver (WHOI-Rx1) was a 1.2-m long, 24-element vertical array with 5-cm element spacing, with all the elements embedded in polyurethane forming a single line array. The short vertical array with no inclinometer was moored at 3-km range and about 16-m depth. The 32″ subsurface float (orange ball) above the array at about 10-m depth was intended to keep the vertical array straight, but it was subject to horizontal movement due to its proximity to the ocean surface, resulting in the array tilt. (b) Sound speed profile measured from a CTD cast (19:22:14 UTC) about an hour prior to the source transmissions. (c) A representative channel impulse response (CIR) along the receiver depth after matched-filtering (20:51:13 UTC). The dynamic range is 20 dB.

depth in Fig. 6.3a. The source (WHOI-Tx1) transmitted 48-ms, 9–17 kHz linear frequency modulation (LFM) chirp waveforms, every 96 ms for 9 min. The receiver approximately at 3-km range from the source, called WHOI-Rx1, was a 1.2-m long, 24-element vertical array with 5-cm element spacing, with all the elements embedded in polyurethane forming a single line array, tilted or not. The short vertical array (WHOI-Rx1) was deployed to 15.6-m depth with a 32″ subsurface float (orange ball) above the array at about 10-m depth. The float was intended to keep the vertical array straight with enough buoyancy, but its proximity to the ocean surface (i.e., $< \lambda/2$, λ is a surface wavelength, e.g., $\lambda = 40$ m) subjected it to horizontal movement, thus resulting in the array tilt. Unfortunately, no inclinometer was attached to the receiver array to monitor the array tilt during the deployment. The array invariant with a known source range, however, provides an opportunity to inversely estimate the array tilt angle over the duration of 9 min, as will be presented in Sec. 6.5.

A representative channel impulse response (CIR) is displayed in Fig. 6.3c after matched-filtering (20:51:13 UTC). The horizontal axis is delay time in milliseconds and the vertical axis is depth in meters. There appear three separate groups of arrivals spread over 30 ms: (i) early, strong arrivals around $t = 0$, (ii) intermediate, several distinct arrivals packed over 5 ms ($5 < t < 10$ ms), and (iii) later, weak, diffused arrivals ($t > 15$ ms). Plane-wave beamforming using the vertical array (WHOI-Rx1) will translate the data into a beam-time migration in Sec. 6.5 (see Fig. 6.5b).

6.4.1 Acoustic propagation with ray tracing

To understand the arrival structure, a geometric ray-tracing model [16] is applied with the sound speed profile shown in Fig. 6.3b, which was measured from a CTD cast (19:22:14 UTC) about an hour prior to the source transmissions. After a slight increase from the surface down to 30 m (i.e., upward-refracting surface channel), the sound speed tends to decrease toward the bottom, i.e., downward refracting. Nevertheless, the sound speed variation in the water column is minimal with less than 2 m/s, and the local sound speed around the receiver depth (16 m)

is 1535.4 m/s.

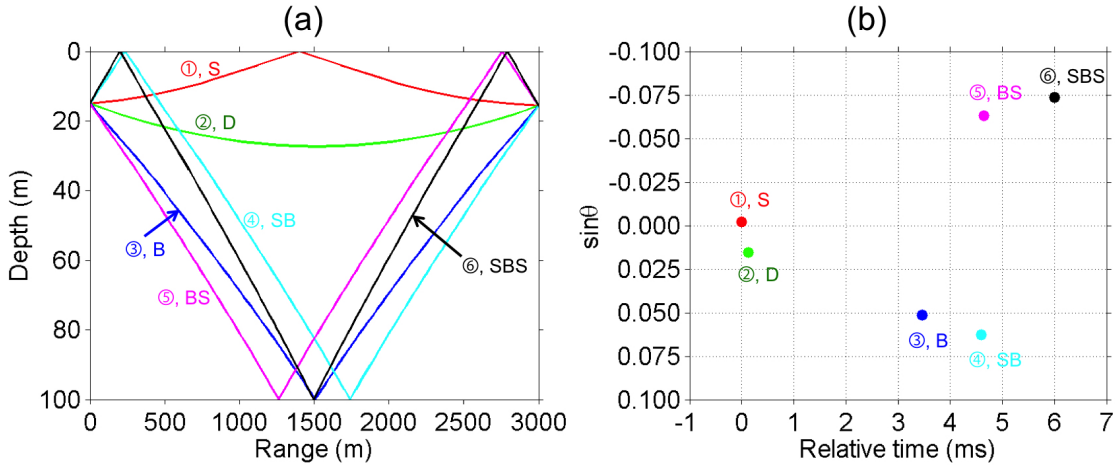

Figure 6.4: (Color online) (a) Ray path diagram, showing the first six paths (eigenrays) for the source/receiver geometry depicted in Fig. 6.3a. (b) Corresponding six eigenrays (color-matched) are displayed in terms of the arrival angle ($\sin\theta$) and delay time (t), similar to a beam-time migration. The arrivals, in order from left to right with the number increasing (①–⑥), are labeled as S (surface bounce, red), D (direct, green), B (bottom bounce, blue), SB (surface-bottom, cyan), BS (bottom-surface, magenta), and SBS (surface-bottom-surface, black). Note that S and D both are trapped in the surface channel, arriving almost simultaneously around $t = 0$ with the angle of arrivals being close to the horizontal ($\sin\theta \approx 0$).

Assuming a range-independent environment with a flat surface and bottom, a ray path diagram is illustrated in Fig. 6.4a for the source/receiver geometry depicted in Fig. 6.3a. The first six arrivals (eigenrays) are presented in Fig. 6.4b in terms of the arrival angle and delay time with respect to the first arrival at $t = 0$, equivalent to a beam-time migration. The arrivals, in order from left to right with the number increasing (①–⑥), are labeled as S (surface bounce, red), D (direct, green), B (bottom bounce, blue), SB (surface-bottom, cyan), BS (bottom-surface, magenta), and SBS (surface-bottom-surface, black).

Notably, S and D both are trapped in the surface channel (down to 30 m depth), arriving almost simultaneously around $t = 0$ with the angle of arrivals being close to the horizontal ($\sin\theta \approx 0$). The two arrivals often merge into one that usually becomes the strongest one due to minimal interactions with boundaries, corresponding to the first group (i) shown in Fig. 6.3c. As a result, the angle of

the early high-intensity arrivals is an indication of array tilt, providing an initial estimate of the tilt angle when it occurs. Subsequently followed are four distinct arrivals between 3–6 ms consisting of two up-going (B and SB) and then two down-going paths (BS and SBS), which correspond to the intermediate group (ii) between 5–8 ms in Fig. 6.3c. The 2-ms difference in delay time between the model and the data is likely due to the uncertainty in sound speed and water depth between the source and receiver.

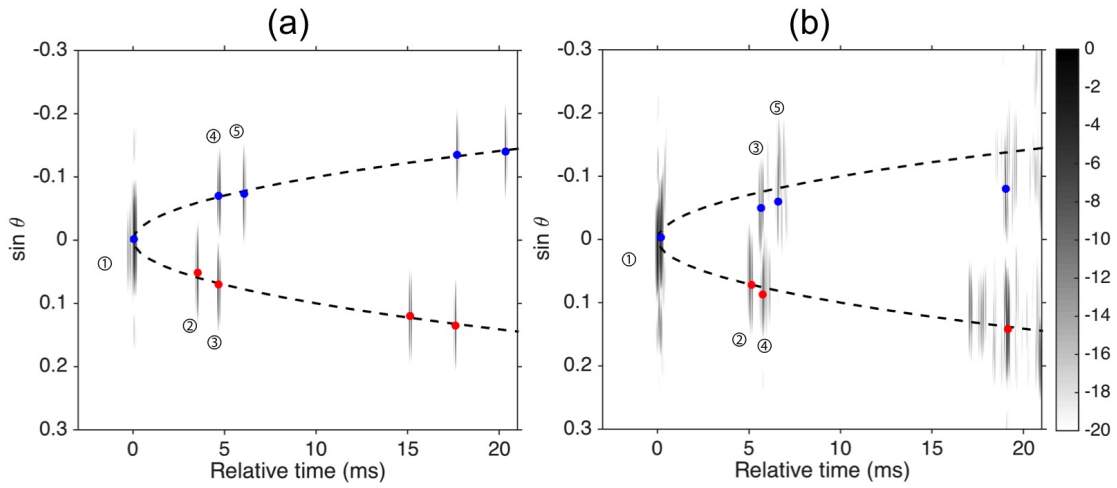

Figure 6.5: (Color online) Beam-time migration. (a) Simulation with no array tilt. A total of nine arrivals are identified, consisting of five down-going paths (blue dots) and four up-going paths (red dots). For the source range of $r_0 = 3$ km and using a generic value of $\beta = 1$ and $c = 1500$ m/s, the expected migration (dashed line) is derived and superimposed, which passes through the nine distinct arrivals. (b) KAM11 data corresponding to Fig. 6.3c (20:51:13 UTC). Similar to (a), the angle of the first arrival at $t = 0$ (blue dot) is almost horizontal, thus indicating no array tilt. While the up-going ray paths (red dots) remain close to or on the expected migration curve (dashed), the down-going ray paths (blue dots) excluding the first arrival ① are significantly off from the migration curve, which is likely due to the interaction with dynamic ocean surface waves prior to reaching the array.

6.4.2 Beam-time migration with normal mode

For simulations of beam-time migration, a normal mode propagation model [17] is used to generate the acoustic field along the receiver aperture. In addition

to the sound speed profile within the water column (Fig. 6.3b), the geo-acoustic parameters in the areas [18] are assumed typical of sand: density = 1900 kg/m^3, compressional sound speed = 1650 m/s, and compressional wave attenuation = 0.8 dB/wavelength. The broadband source signal is a 48-ms, 9–17 kHz LFM chirp waveform. The beam-time migration with no array tilt is obtained after conventional plane-wave beamforming with no spatial window applied, followed by matched filtering for pulse compression.

The beam-time migration for the simulated data is shown in Fig. 6.5a with a 20-dB dynamic range in gray scale. A total of nine distinct arrivals (eigenrays) within 22 ms are identified from the peaks which occur approximately at mid-points in the angle direction, and they consist of five down-going paths (blue dots) and four up-going paths (red dots). The arrival structure up to 7 ms is similar to Fig. 6.4b based on a ray model, except that the first group of arrivals are merged into a single, near-horizontal, strong one around $t = 0$. Using the nine distinct arrivals and least-square approach [13], the array invariant parameter is estimated at $\chi_0 = -0.5065$ with no array tilt. The corresponding source-range estimate is then $\hat{r}_0 = 2.96$ km with a -1.3% relative error. Assuming an ideal waveguide ($\beta = 1$ and c = 1500 m/s), the expected migration curve for the source range of 3 km (dashed line) is derived and superimposed in Fig. 6.5a, which passes through all nine distinct arrivals.

6.5 Experimental results

In this section, we analyze the beam-time migration for the KAM11 data collected over 9 minutes (20:51–20:59 UTC) on JD 176 (June 25), with the schematic shown in Fig. 6.3a. Recall that the subsurface buoy (orange ball) above the array at about 10-m depth was to keep the vertical array straight with sufficient buoyancy. Due to its proximity to the ocean surface, however, the buoy moved in the horizontal direction, which dragged the array and resulted in the array tilt. No inclinometer was attached to the receiver array to measure the tilt angle. Therefore, we will use the first arrival with maximum intensity as an initial estimate

of the array tilt, and then apply the array invariant method to estimate the tilt angle more precisely for the known source range. Since the dominant surface wave direction (i.e., ocean swell) was almost parallel to the acoustic transmission path, the motion of the buoy induced by the wave is also expected to be parallel to the acoustic transmission path. Hence, the estimated tilt angle is considered the actual tilt angle of the vertical array.

To investigate the impact of array tilt on source-range estimation, three representative examples are analyzed: no array tilt (20:51:13 UTC, Fig. 6.5b), counter-clockwise tilt (20:51:06 UTC, Fig. 6.6a), and clockwise tilt (20:57:55 UTC, Fig. 6.6b), respectively. Then we will examine the temporal variation of the array tilt to validate the connection between the array tilt and surface wave movement.

6.5.1 No array tilt

The first example is presented in Fig. 6.5b where seven distinct arrivals are selected consisting of four down-going (blue dots) and three up-going paths (red dots), with the first five arrivals denoted by circled numbers (①–⑤). The first arrival at $t = 0$ (blue dot, ①) is the strongest and almost horizontal, thus indicating a minimal array tilt. The overall arrival structure up to 10 ms is similar to the simulation result shown in Fig. 6.5a. However, the second group of arrivals (②–⑤) are delayed about 2 ms as discussed in Sec. 6.4.1, and the third and fourth arrivals are reversed in time. For the known source range of $r_0 = 3$ km and a generic value of $\beta = 1$ and c = 1500 m/s, the expected migration curve (dashed line) is elliptic and symmetric with respect to the travel time. Interestingly, the up-going ray paths (red dots) remain close to or on the migration curve (dashed), whereas the down-going ray paths (blue dots) excluding the first arrival ① are significantly off from the migration curve. The deviation of the down-going paths (blue dots) may be due to the interaction with the dynamic ocean surface waves prior to reaching the receiver array.

For array invariant-based source-range estimation with no array tilt, we tested with three different sets of distinct arrivals: (i) three up-going (red dots) plus the first arrival (blue dot,①), (ii) four down-going (blue dots), and (iii) all

seven arrivals (red and blue dots). Not surprisingly, case (i) that closely follows the migration curve provides the best estimate of $\hat{r}_0 = 2.86$ km with a -5% relative error. On the other hand, case (ii) leads to the worst performance of 11.38 km with a 280% relative error. With all seven paths of case (iii), the source range is estimated at 4.37 km with a 45% relative error. The results clearly indicate that the up-going ray paths and the first arrival ① are more reliable than the down-going ones, and thus we will utilize the up-going paths plus the first arrival (blue or red) for the estimation of range and array tilt hereafter. As a cross-check, the array tilt is estimated at 0.22° using Eq. (6.8) and the three up-going arrivals (red dots) plus the first arrival.

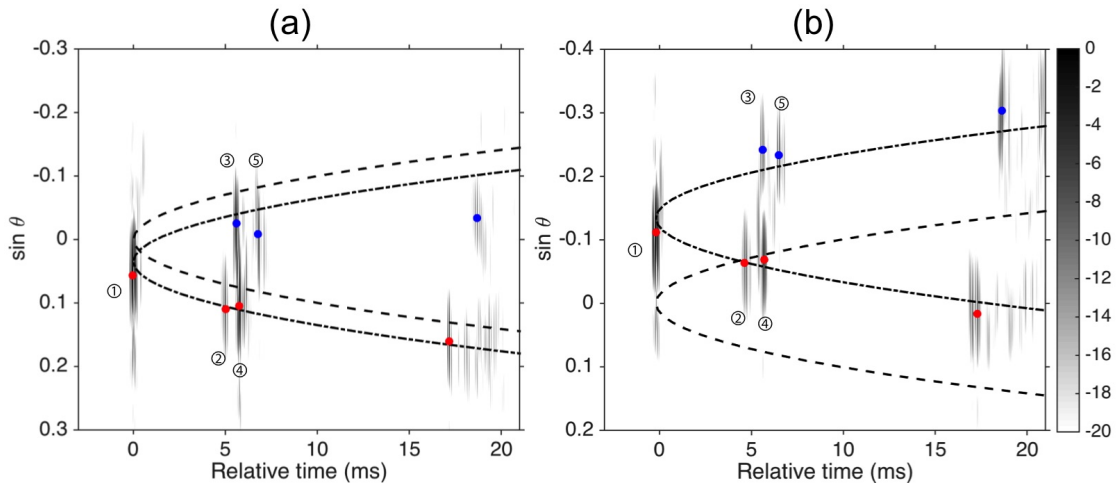

Figure 6.6: (Color online) Beam-time migration for KAM11 data. (a) Case with a positive (counter-clockwise) array tilt (20:51:06 UTC). The expected migration curve in the absence of array tilt (dashed line) is shifted down by $\sin\theta = +0.035$ (dash-dot) to match the four distinct up-going arrivals (red dots) by visual inspection. (b) Case with a negative (clockwise) array tilt (20:57:55 UTC). The expected migration curve (dashed) is shifted up by $\sin\theta = -0.134$ (dash-dot) to match the four distinct up-going arrivals (red dots) by visual inspection. Note that the vertical-axis range in (b) is shifted by -0.1 to accommodate the large tilt.

6.5.2 Array tilt

The second example is shown in Fig. 6.6a for a positive (counter-clockwise) array tilt where seven distinct arrivals (dots) are identified with the first five ar-

rivals denoted by circled numbers (①–⑤). The dashed line is identical to the migration curve shown in Fig. 6.5 with no array tilt. Clearly, all the arrivals are biased downward (i.e., positive angle), evident in the strong first arrival ① that is supposed to be near-horizontal. The migration curve then can be shifted down by approximately $\sin\theta = +0.035$ (dash-dot) to match the four up-going arrivals (red dots) by visual inspection. Without compensation of the array tilt, the estimated source range is 2.34 km with a -22% relative error using the up-going arrivals (red dots). Here, the impact of the array tilt is exacerbated by the use of the reliable up-going paths alone. For the known source range with the four up-going arrivals (red dots), the array tilt is estimated at 1.4°, which is close to the down-shifted angle of 2°.

The third example shown in Fig. 6.6b is for a negative (clockwise) array tilt where seven distinct arrivals (dots) are identified and the overall arrival structure remains similar to Fig. 6.6a. However, all the arrivals are biased upward (i.e., negative angle), including the first arrival ①. Thus the migration curve (dashed) is shifted up by $\sin\theta = -0.134$ (dash-dot) to match the four up-going arrivals (red dots) by visual inspection. Note that the vertical-axis range is moved by -0.1 to accommodate the large angle shift. The array tilt is estimated at 7° using the four up-going arrivals (red dots). If the array tilt is not compensated for, the source range is estimated at an absurd range of negative 5 km due to the large array tilt.

6.5.3 Time-varying array tilt

The vertical array tilt was attributed to horizontal movement of the subsurface buoy near the surface, which was induced by dynamic ocean surface waves (see Fig. 6.3a). In this section, we examine the time-evolving array tilt from multiple LFM chirps transmitted over an extend period of time. Specifically, a 1-min sequence consisted of 48-ms LFM chirps at 96-ms intervals for 54 s with the remaining 6 s of silence (i.e., 558 LFMs), and the 1-min sequence was repeatedly transmitted for 9 min.

An example of the time-varying array tilt is illustrated in Fig. 6.7a, sampled at 96-ms intervals over 54 s, starting 20:59 UTC on JD 176, where two different

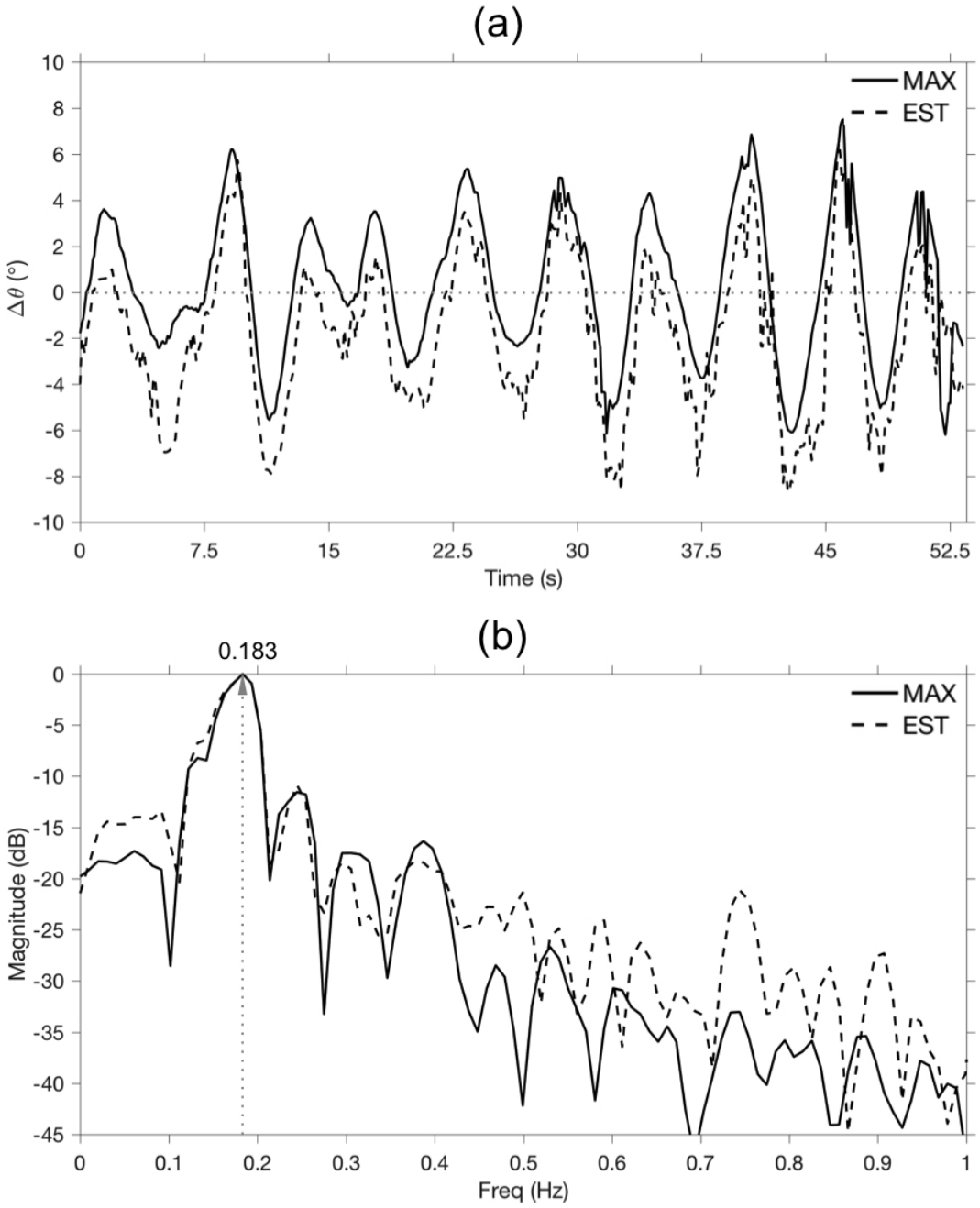

Figure 6.7: (Color online) (a) Temporal variation of the array tilt (dashed) inversely estimated using the array invariant for the known source range, over a duration of about 1 min at 96-ms intervals starting 20:59 UTC on JD 176 (560 samples). The angle of the maximum-intensity arrival (solid) that mostly coincides with the first arrival indicates a high correlation between the two. (b) Normalized power spectrum of (a). The dominant spectral frequency occurs at $f = 0.183$ Hz, or equivalently a period of 5.5 s, which is consistent with the surface wave period measured from a waverider buoy shown in Fig. 6.2d.

methods are applied. The dashed curve is tilt angle estimated using the array invariant with up-going ray paths plus the first arrival, as demonstrated in the previous three examples. There were some outliers in the estimation, which were removed and filled in by linear interpolation. On the other hand, the solid curve is the angle of the maximum-intensity arrival that mostly coincides with the first arrival, a robust indicator of the array tilt. As expected, the two curves exhibit a high correlation with a mean difference of $-2.3°$, both oscillating like a sinusoidal wave with a maximum amplitude of about $8°$. A normalized power spectrum of Fig. 6.7a using the Fourier transform is shown in Fig. 6.7b. The dominant frequency is at $f = 0.183$ Hz, or equivalently a period of 5.5 s. Although not shown, the dominant period of the array tilt ranged from 4.5 to 8.2 s for 9 min, with an average value of 5.6 s. Not surprisingly, the surface wave period measured from a waverider buoy was 5.5 s in Fig. 6.2d, confirming the link between the array tilt and ocean surface wave movement.

6.6 Conclusions

The array invariant proposed for robust source-range estimation in shallow water is based on the dispersion characteristics in ideal waveguides for broadband signals. The approach involves plane-wave beamforming using a vertical array, utilizing multiple arrivals separated in beam angle and travel time. In the presence of array tilt, however, the estimated beam angles are shifted, and the range estimation based on the array invariant can be significantly affected. Inversely, the array tilt can be estimated for a known source range. In this paper, its sensitivity to array tilt was analyzed by deriving a modified array invariant incorporating the array tilt, and then applying the formulation to both simulations and KAM11 data. It was found that even a small tilt angle (e.g., $< 2°$) of a 1.2-m long vertical array near the surface, if not compensated for, can result in a relative range error of 20% or more, for a high-frequency source (7–19 kHz) at 3-km range in approximately 100-m deep shallow water. Here, the impact of the array tilt was exacerbated by the use of reliable up-going ray paths alone. Moreover, the power spectrum of the

time-evolving array tilt estimated for 9 min showed a dominant period of 5.6 s, which was consistent with the surface wave period concurrently measured from a waverider buoy.

Acknowledgment

This work was supported by the Office of Naval Research under Grant No. N00014-13-1-0510.

Chapter 6, in full, is a reprint of the material as it appears in the Journal of Acoustical Society of Americas: Chomgun Cho and H.C. Song, "Impact of array tilt on source-range estimation in shallow water using the array invariant," *J. Acoust. Soc. Am*, 141 (4), 2849-2856, 2017. The dissertation author was a primary investigator and author of this material.

Bibliography

[1] H. P. Bucker, "Use of calculated sound fields and matched-field detection to locate sound sources in shallow water," J. Acoust.Soc. Am. **59**, 368–373 (1976).

[2] A. Tolstoy, *Matched field processing for underwater acoustics* (World Scientific Publishing Co.) (1993), Chap. 2.

[3] A. B. Baggeroer, W. A. Kuperman, and P. N. Mikhalevsky, "An overview of matched field methods in ocean acoustics," IEEE J. Oceanic Eng. **18**, 401–424 (1993).

[4] F. B. Jensen, W. A. Kuperman, M. B. Porter, and H. Schmidt, *Computational Ocean Acoustics* (Springer, New York) (2011), Chs. 2 and 10.

[5] B. M. Worthmann, H. C. Song, and D. R. Dowling, "High frequency source localization in a shallow ocean sound channel using frequency difference matched field processing," J. Acoust. Soc. Am. **138**, 3549–3562 (2015).

[6] S. Lee and N. C. Makris, "The array invariant," J. Acoust. Soc. Am. **119**, 336–351 (2006).

[7] H. C. Song and C. Cho, "The relation between the waveguide invariant and array invariant (L)," J. Acoust. Soc. Am. **138**, 899–903 (2015).

[8] S. D. Chuprov, "Interference structure of a sound field in a layered ocean," in *Acoustics of the Ocean*, 71–91 (Nauka, Moscow) (1982), edited by L. M. Breakhovskikh and I. B. Andreevoi.

[9] K. A. Sostrand, "Range localization of 10–100 km explosions by means of an endfire array and a waveguide invariant," IEEE J. Ocean. Eng. **30**, 207–212 (2005).

[10] K. L. Cockrell and H. Schmidt, "Robust passive ranging estimation using the waveguide invariant," J. Acoust. Soc. Am. **127**, 2780–2789 (2010).

[11] H. C. Song and C. Cho, "Array invariant-based source localization in shallow water using a sparse vertical array," J. Acoust. Soc. Am. **141**, 183–188 (2017).

[12] K. L. Cockrell and H. Schmidt, "A modal Wentzel-Kramers-Brillouin approach to calculating the waveguide invariant for non-ideal waveguides," J. Acoust. Soc. Am. **130**, 72–83 (2011).

[13] C. Cho, H. C. Song, and W. S. Hodgkiss, "Robust source-range estimation using the array/waveguide invariant and a vertical array," J. Acoust. Soc. Am. **139**, 63–69 (2016).

[14] K. F. Riley, M. P. Hobson, and S. J. Bence, *Mathematical methods for physics and engineering: a comprehensive guide* (Cambridge University Press) (2006), Chap. 4.

[15] W. S. Hodgkiss and J. C. Preisig, "Kauai Acomms MURI 2011 (KAM11) experiment," in *Proc. of ECUA'12*, 993–1000 (Edinburgh, UK) (2012).

[16] Y. Choo, W. Seong, and H. C. Song, "Emergence of striation patterns in acoustic signals reflected from dynamic surface waves," J. Acoust. Soc. Am. **136**, 1046–1053 (2014).

[17] M. B. Porter, "The acoustics toolbox," available at: http://oalib.hlsresearch.com/Modes/AcousticsToolbox/ (Last viewed April 17, 2017).

[18] C. Tiemann, M. Porter, and L. Frazer, "Localization of marine mammals near Hawaii using an acoustic propagation model," J. Acoust. Soc. Am. **115 (6)**, 2834–2843 (2004).

Chapter 7

Conclusions and future work

7.1 Conclusions

This dissertation presented the relationship between the waveguide invariant and array invariant, the impact of array tilt on source range estimation, and the several applications using the generalized array invariant for a short- or long-aperture vertical array in shallow water environments.

The array invariant approach for passive localization is essentially equivalent to the waveguide invariant based on the dispersion between the group and phase speeds when $\beta = 1$. Specifically, the functional relationship between the group and phase speeds in the waveguide invariant can be converted into the relationship between the travel time and beam angle in the array invariant. The array invariant approach could be applied without knowing the value of the waveguide invariant parameter due to $\beta \approx 1$ for many shallow-water environments. Also, the generalized array invariant approach can be potentially utilized for an upward-refracting environment with $\beta = -3$. It was shown that the beam-time migration follows ellipses for vertical arrays and lines for horizontal arrays.

The array invariant utilizes multiple arrivals in beam angle and travel time to estimate the source-range, and it does not require knowledge of the environment and an acoustic propagation model. At high frequencies, the arrivals can be interpreted as ray arrivals, so the array invariant approach is comparable to the ray tracing that incorporates relative time of arrival information in the aspect of range

estimation for only reflected modes. The main advantages of the array invariant are no requirement of an acoustic propagation model and no ambiguities of estimated range. However, in the presence of array tilt, the beam angle estimates are shifted by the array tilt, which potentially affects the range estimation based on the array invariant. Inversely, the array tilt could be estimated for a known source range. Even a small tilt angle (e.g., $< 2^{\circ}$) of a 1.2-m long vertical array near the surface can cause a relative range error of 20% or more, for a high-frequency source (7–19 kHz) at 3-km range in ∼100-m deep water for the KAM11 experiment. Here, the impact of the array tilt was exacerbated by the use of reliable up-going ray paths alone.

There are several applications using the generalized array invariant for a short- or long-aperture vertical array.

Firstly, the array invariant approach in this dissertation is applied to a bottom-mounted short-aperture vertical array for the HF97 experiment in a fluctuating ocean environment over a one-day period. The result showed that the mean range estimates using a 12-m long vertical array in ∼100-m deep water are less than 8% relative error for a source (2–3 kHz) at 6-km range, demonstrating the robustness of this approach.

Secondly, the generalized array invariant is extended to mildly range dependent environments with a sloping bottom where the waveguide invariant is variable in range. Assuming knowledge of the bottom slope, the generalized array invariant can be applied iteratively to estimate the source range starting with β=1 (i.e., range-independent), which converges toward the correct source range by updating β at the previously estimated range. The iterative array invariant approach is demonstrated using a short vertical array (2.8-m) from the RADAR07 experiment, where a high-frequency source (2–3.5 kHz) close to the surface (6-m) was towed between 0.5 to 5 km in range with the water depth varying from 80 to 50 m.

Lastly, the array invariant also can be useful to a large-aperture vertical array that is sparse with significant sound speed variation (12 m/s) across the array in the SAVEX15 experiment. This approach showed that robust source-range estimation is demonstrated using data from a 16-element, 56-m long vertical

array at various ranges (1.5–3.5 km) from a broadband source (0.5–2 kHz) in $\sim$ 100-m deep shallow water.

7.2 Future work

In this dissertation, the generalized array invariant has demonstrated robust source localization performances for either a range-independent or a range-dependent environment in shallow water, involving surface-and-bottom-interacting paths, i.e., reflected modes, or high order modes. The reflected modes are not sensitive to a sound speed profile because they propagate at averaged sound speed in the water column, indicating the waveguide invariant parameter close to 1 for range-independent environment or the ratio of the water depths of the source to the receiver in sloping-bottom for range-dependent environment. However, applying the array invariant approach to deep water environments encounters big challenges in several aspects.

- First of all, the generalized array invariant requires to find a group of modes which behave similar and to know a value of the waveguide invariant of that group in deep water environment, which means that the environmental knowledge is required for deep-water environments, for example, sound speed profiles (SSPs). To make it more difficult, the value of the waveguide invariant in deep water fundamentally changes over mode and varies a lot from less than -100 to about 0; as a result, this large variation of β can cause the generalized array invariant approach to be suffered from a very high relative range error that can be more than 100 % unless we do know the exact value of β.

- Second, in deep water environment, the refractive modes dominantly propagate and are very sensitive to SSPs. Thus, arrivals to the receiver array can be varied over depth. To capture many arrivals, a large aperture array can be more beneficial since it can increase chance to have more arrivals.

- Lastly, using a large-aperture vertical array to receive many arrivals, the

generalized array invariant needs to use non-isovelocity beamforming, i.e., the turning point filter, due to sound speed variation in order to correctly estimate beam angles, which makes the processing more complicated and required of the SSP.